Studies of Flow Modification and Polymer Conformation in Extensional Flows of Dilute Polymer Solutions

Thesis by

Paul N. Dunlap

in Partial Fulfillment of the Requirements

for the Degree of

Doctor of Philosophy

California Institute of Technology

Pasadena, California

1986

(Submitted October 24, 1985)

Dedicated:

To Karen, who gave up more than a husband has a right to ask.

To Jennifer, Matthew and Emily, who missed more
than a father can ever make up.

To my God, who can turn the hearts of fathers to their children
and the hearts of children to their fathers,[1]
who can join two and make them one flesh,[2]
who longs to save and restore![3]

[1] Malachi 3:13–4:6 [2] Matthew 19:5–6 [3] John 11:35–44

Abstract

This is a study of the coil-stretch transition of macromolecules in dilute solutions which are subjected to extensional flows and of the effects of the polymer molecules on the flow fields. The flow fields are produced in a four-roll mill, two-roll mills of several different gap width to roller radius ratios, and a cylindrical Couette device. These flows are laminar, and approximately two-dimensional linear flows covering the range of flow types with different amounts of extension and vorticity from pure extension to simple shear flow. The two-roll mills were constructed to extend the previously accessible range of flow types to those with only slightly more extension than vorticity, *i.e.*, much nearer to simple shear flow. The flows are characterized by using homodyne light scattering spectroscopy to directly measure velocity gradients fields. The degree of polymer extension is monitored using flow birefringence measurements.

Studies using 100 ppm polystyrene in viscous solvents show that the flow birefringence data for all the different strong flows (simple shear is a weak flow) correlate with the eigenvalue of the velocity gradient tensor. Extensional flow birefringence data for the same polymer in different solvents correlate with the Zimm relaxation time based on the intrinsic viscosity. When the polymers are sufficiently extended there is a distinct onset of measurable decreases in the velocity gradients. A necessary condition for this to occur is a very high level of domain overlap between the extended molecules. If we estimate this by the volume concentration of circumscribed spheres, ϕ_{eff} (*i.e.*, the sphere diameter equals the extended length of the polymer), the onset of an effect of polymer on the flow does not occur until $\phi_{eff} \sim$ 4000–6000. Nevertheless, our measurements show that dilute polymer solutions do inhibit the development of large strain rates in regions of persistent extensional flow.

Studies using sodium polystyrenesulfonate in glycerol with various amounts

of added sodium chloride show the range of coil-stretch behavior that can occur as a function of the equilibrium conformation of the polyelectrolyte. With high ionic strength solutions, the polyelectrolyte behavior is the same as that of nonionic polymers. As the ionic strength decreases and the equilibrium dimensions increase, the onset of the coil-stretch transition shifts to much lower shear rates. With no added salt, the expanded coil approaches free-draining behavior with a monotonic increase of flow birefringence with increasing shear rate instead of the distinct onset point usually observed. These low ionic-strength solutions also exhibit overshoots in the birefringence on startup of simple shear flow.

The flow birefringence data have been compared with predictions of the nonlinear elastic dumbbell model with various combinations of constant or conformation-dependent friction laws, internal viscosity, strain-inefficient rotation, and Coulombic charges on the beads. It seems that *all* of the models studied work well in pure extension where the coil-stretch process largely governed by the limited amount of total strain (or finite residence time) in the flow. However, in flows with considerable vorticity, the details of the hydrodynamic interaction between beads and solvent and the rotational motion of the deforming dumbbell become very important in determining the behavior of the model. Thus the birefringence data in the flows near simple shear flow provide more stringent tests of the models than flows with no vorticity. In flows slightly more extensional than simple shear flow, none of the more advanced models gives entirely satisfactory comparisons with the data. In this flow regime, the best comparisons with data are obtained with the simple FENE dumbbell. Some evidence that the current modeling approach (and conformation-dependent hydrodynamic friction) is basically sound was found. The charged dumbbell model is able to describe the large difference in behavior between highly charged polyelectrolytes and those with excess added salt only if a conformation-dependent friction law is included.

Contents Page

INTRODUCTION

Several well-known and dramatic flow phenomena are observed in dilute polymer solutions, including drag reduction in turbulent pipe flow, abrupt increases in pressure drop in laminar porous media flows, and reduction of jet breakup and mist formation. The solutions involved are often so dilute that they exhibit no measurable non-Newtonian flow behavior in simple shear flow. These important effects are all believed to occur only when the solution is transformed by the flow to an effectively much more concentrated solution as the polymer undergoes a transition from the coiled equilibrium configuration to a greatly extended and oriented configuration. In order to fully understand the flow effects, one must understand both the behavior of the polymer in the flow and the effect of polymer conformation changes on the flow field.

In Chapter I, the flow birefringence technique is applied to measure polymer conformation in laminar two-dimensional extensional flows with different amounts of vorticity as produced in four- and two-roll mills. At the same time flow fields are characterized by measuring velocity gradients via homodyne light scattering spectroscopy, a technique sensitive enough to detect the highly localized effects on the flow due to the extended polymers in very dilute solutions. The results are used to estimate the degree of polymer stretching necessary for flow modification. This information is best reported in terms of an effective concentration based upon the volume concentration of spheres with diameter equal to the extended polymer length.

The results of Chapter I are applicable to any flexible, linear, high-molecular weight polymer in poor to fairly good solvents. In Chapter III the behavior of polyelectrolytes is investigated in extensional flows and also in simple shear flow. Polyelectrolytes exhibit a wide range of equilibrium conformations as a function of pH, ionic strength and charge density. By varying the ionic strength, the equilibrium

coil dimensions of sodium polystyrenesulfonate in glycerol was found to vary by as much as a factor of 5, with an accompanying change in behavior from non-free-draining at high ionic strengths to nearly free-draining with no added salt. The behavior of these solutions in extensional flows contributes to an understanding of the coil-stretch transition in a wide range of polymer/solvent systems including good solvent systems and semi-rigid or semi-flexible polymers.

The flow birefringence data are very useful for testing molecular models for polymer dynamics in dilute solutions. The dumbbell model is applied throughout. In Chapter II, the charged dumbbell model is developed specifically for polyelectrolytes in extensional flows. It is then compared with the data obtained in Chapter III. Various other forms of the dumbbell model are also compared with the data in Chapters I and III including features such as internal viscosity, anisotropic, conformation-dependent friction, and strain-inefficient rotation.

CHAPTER I.

Dilute Polystyrene Solutions in Extensional Flows: Birefringence and Flow Modification

Dilute Polystyrene Solutions in Extensional Flows: Birefringence and Flow Modification

by

P. N. Dunlap and L. G. Leal

Department of Chemical Engineering
California Institute of Technology
Pasadena, California 91125

Abstract: The coil-stretch transition in dilute polymer solutions has been studied using four- and two-roll mills to generate two-dimensional extensional flows. Flow birefringence measurements give the polymer conformation in the flow, while velocity gradient measurements using homodyne light scattering reveal the effects of the polymer on the flow field. When the polymers become sufficiently extended there is a distinct onset of measurable decreases in the velocity gradients. A necessary condition for this to occur is a very high level of domain overlap between the extended molecules. If we estimate this by the volume concentration of circumscribed spheres, ϕ_{eff} (*i.e.*, the sphere diameter equals the extended length of the polymer), the onset of an effect of polymer on the flow does not occur until $\phi_{eff} \sim$ 4000–6000. Nevertheless, our measurements show that dilute polymer solutions do inhibit the development of large strain rates in regions of persistent extensional flow. The present flow birefringence measurements also extend previous studies to a wider range of flow types, thus providing new information that can be used in the evaluation of molecular models for polymer flow dynamics. In the present paper, we compare experimental data with predictions from the elastic dumbbell model with various combinations of a nonlinear spring, conformation-dependent anisotropic friction (including strain-inefficient rotation), and internal viscosity.

1. INTRODUCTION

In dilute solutions, flexible polymers have the unique capability of existing either in a coiled configuration in which there is little if any effect of the polymer on the rheological properties of the solution, or in an extended configuration which can result in strong, measurable modifications of a flow. The coiled configuration is the equilibrium shape, and it takes a flow with sufficient elongational content to extend the polymer significantly. The abrupt onset process is commonly called the coil-stretch transition and is believed to be associated with several dilute solution flow effects. Among these are: an abrupt increase in the pressure drop for laminar porous media flows,[1] capillary entrance flows,[2] and converging flows;[3,4] drag reduction in turbulent pipe flows;[5,6] flow birefringence in stagnation flows of various geometries;[6-11] mass transfer effects in flow around cylinders;[12] and reduction of jet breakup and mist formation.[13]

In order to fully understand these effects, it is apparent that one must understand both the effect of the flow on the polymer, and, conversely, the effect of the polymer on the flow. Most of the examples cited above involve complex flows, and we thus have only macroscopic indications of the flow modification by polymers, such as changes in the pressure drop, rather than a detailed analysis of the flow structure. The birefringence studies, on the other hand, provide a direct indication of polymer extension, but only in relatively simpler flows.[14] At the present time, these two sets of studies experiments can be interrelated[1,6,12] only by theories of polymer behavior in flow.[15,16] Polymer conformation cannot be easily determined in the flows with the largest and most easily measured macroscopic flow effects (drag reduction, porous media, mist reduction, *etc.*). These are also flows whose detailed structure is least well understood or documented, and which are not accessible at the present time to theoretical prediction even for a Newtonian fluid. On the other hand, in simpler stagnation flows where polymer conformation can

be determined, and theoretical prediction is conceivable, no significant effects of the polymer on the flow have yet been measured in truly dilute solutions. In this work, we combine the standard flow birefringence measurements in laminar, two-dimensional stagnation flows produced in four- and two-roll mills with sensitive flow field measurements using homodyne light scattering (HLS).[17] Thus we produce the first direct and simultaneous experimental measurement of both a flow field modification and polymer extension in a dilute polymer solution. This data not only allows better understanding of polymer-flow interactions in a dilute solution, but should also provide an excellent basis for comparison with theoretical attempts to predict the flow via constitutive equations derived from "molecular" models such as the nonlinear dumbbell.

There have been several previous attempts to measure flow modification effects in laminar two-dimensional flows of dilute polymer solutions, and these provide some background and useful insight for the present study. In the earliest attempts in well-defined flows, streamline photography was used to characterize the flow fields,[6,8,18–20] while birefringence was used to characterize the degree of macromolecular extension and orientation. These latter measurements typically indicated very localized regions containing highly stretched polymers, located along outgoing streamlines emanating from the stagnation points of the flow. In general, however, the streamline *pattern* is not much changed in two-dimensional extensional flows, even for concentrated polymer solutions. For example, earlier workers using visual observation[6,8] in both a four-roll mill and a cross-slot device could detect no flow modification due to the presence of the polymer, even for a 1% solution of Polyox in water. Flow visualization studies showed an effect of polymer only in flows with appreciable vorticity,[18–20] and then only in concentrated solutions (1–2% Polyox in water).

Since streamlines are essentially an integral property of the velocity fields, they

are relatively *insensitive* to small or localized changes in a flow field. Furthermore, in flows with a high degree of symmetry, such as the pure extensional flow in a four-roll mill, the streamline pattern tends to be preserved even if velocity gradients in the streamwise direction are changed. A more sensitive approach to study flow modification in dilute polymer solutions is therefore direct velocity measurements using the technique of laser Doppler velocimetry (LDV). Such a study has been carried out by Gardner *et al.*,[21] using a cross-slot flow device which simulates two-dimensional extension near the center stagnation point (as does our four-roll mill). The polymer conformation was monitored using flow birefringence. These investigators reported that the flow was affected when the polymers were stretched, but only if the concentration exceeded the critical concentration, c^*, where molecular interactions are present even in the rest state. In this case, velocities were significantly decreased along the outgoing streamline when flow rates were sufficiently high to extend the polymers. These results suggest that intermolecular interactions are necessary for flow modification, but also that a truly dilute solution will not exhibit flow modification. This latter fact is difficult to understand in view of the strong flow effects that are observed in such solutions for drag reduction, flow in porous media, *etc.* Possibly, the lack of any measurable effect in the velocity field for dilute solutions in laminar flow is a consequence of the extreme localization of the effect in that case. Apparently, if we are to verify the modification of selected laminar flows by dilute polymer solutions, an even more sensitive flow characterization technique than LDV has to be used.

Therefore, in the present study we have turned to the homodyne light-scattering technique of Fuller *et al.*[17] (HLS) for direct measurement of *velocity gradient* fields. Since the velocity gradients are first derivatives of the velocity field (and second derivatives of the streamlines), small or localized velocity changes should show up as much more dramatic velocity gradient changes. Furthermore, it is the velocity

gradients which produce polymer extension, and are therefore of greatest interest to our studies. Fuller and Leal[11] did attempt such a study. They reported no flow modification in a 100 ppm solution of 8×10^6 M_w polystyrene in the four-roll mill. As we will see, such solutions *do* exhibit significant flow effects. Looking back at their data, one can see a slight effect that is very similar to what we have measured. Improvements in the experiment since Fuller and Leal's original work have made the measurements much more accurate and reproducible. Fuller and Leal[11] also filtered their polystyrene solutions several times, removing an unknown amount of polymer (and thus yielding a true concentration less than the initial 100 ppm value). Their solution may also have degraded during shearing and filtering before the HLS experiments were performed.

In the following sections we will present the major result of the HLS theory worked out by Fuller *et al.*,[17] our specific application of it in four- and two-roll mills, and detailed results of the flow birefringence and velocity gradient measurements in dilute polystyrene solutions. Our results show a distinct onset for flow modification. From this onset point, and the corresponding birefringence level relative to the saturation birefringence for full extension, one can estimate the degree of polymer extension that is necessary for each particular solution to change the flow. It is convenient to report the polymer extension data in terms of an "effective" volume concentration of spheres that are circumscribed around the polymer molecule, since this provides a measure of the level of polymer-polymer interaction that exists at the onset of a measurable effect on the flow. The flow birefringence results reported here extend significantly the measurements of Fuller and Leal[11] and thus provide a more stringent and accurate basis for testing theoretical models for dilute polymer solutions. We compare our results with theoretical predictions of the elastic dumbbell model, in order to evaluate the importance of such proposed effects as internal viscosity, conformation-dependent friction, and strain-inefficiency of rotation.[22–24]

2. EXPERIMENTAL DETAILS

2.1 Materials

The two polystyrene samples used in this study were used in previous work.[11] One (PS8) was from Toyo Soda with a molecular weight, $M_w = 8.42 \times 10^6$ and polydispersity index of 1.17. The other (PS2) was from Pressure Chemical with $M_w = 2 \times 10^6$ and polydispersity 1.3. The concentrations used were all around 100 ppm which is well below the critical concentration, c^*, which is 700 ppm for PS8 and even larger for PS2.

The solvent used for most of the experiments was Chlorowax LV (LV), a chlorinated paraffin from Diamond Shamrock. In addition, some birefringence measurements were done in tricresylphosphate (TCP) from Fisher Chemical. We also refer to previous work in Pyralene 4000 (PCB), a chlorinated biphenyl from Prodelec, France.[11] The viscosity (η_s), density (ρ), refractive index (n), and Maxwell constant (M_c) for each solvent are presented in Table I.

TABLE I. Solvent Properties[a]

Solvent	η_s (poise)	ρ (gm/cc)	n	$M_c = \frac{\Delta n_s}{\gamma(1+\lambda)}$ $\times 10^{10}(s)$
LV	11.2	1.12	1.52	13
TCP[b]	2.75	1.18	1.56	10
PCB	6.62	1.46	1.63	40

[a] 20.0°C [b] 7.5°C

Characteristic relaxation times, τ, for the polymer solutions were estimated from measurements of intrinsic viscosities, $\tau = [\eta]\eta_s M_w/RT$, with R the gas constant and T the temperature. It will be seen that this parameter will correlate our extensional flow data in the three solvents. The values of $[\eta]$ and τ are given in Table II. The intrinsic viscosities in LV were very difficult to measure. LV seems

to be a rather poor solvent for PS. Dissolution was very slow and phase separation occurs if solutions are warmed to approximately 40°C. The dilute solutions used showed negligible viscosity increases, and we were unable to make homogeneous solutions of sufficiently high concentration in LV for accurate determination of the intrinsic viscosity. The values reported in Table II for PS in LV were instead obtained by measuring the hydrodynamic radius, R_h, of dilute PS in LV and in TCP using standard dynamic light-scattering methods,[26] and then estimating the intrinsic viscosity in LV from the measured value in TCP, assuming $[\eta] \propto R_h^3$.[25]

TABLE II. Solution Properties[a]

Solvent	$[\eta]$ (cc/gm)		τ (s)		R_h (Å)
	PS2	PS8	PS2	PS8	PS8
LV	229	472	0.21	1.83	780
TCP	292	600[b]	0.058[b]	0.60[b]	855
PCB	271	612	0.15	1.40	–

[a] 20.0°C [b] 7.5°C

2.2 Homodyne Light Scattering

The measurement of velocity gradients using homodyne light-scattering spectroscopy is described by Fuller *et al.*[17] We used 0.091 micron PS latex spheres to seed the solutions. The solvents were carefully filtered to improve the correlations, which were taken on a Brookhaven Instruments BI2030 correlator. The incident light was from a Spectra-Physics 165 Argon ion laser at 488 nm.

Figure 1 shows the orientation of the incoming light $\mathbf{k}_i$, the scattered light $\mathbf{k}_s$, and the scattering vector $\mathbf{q} = \mathbf{k}_i - \mathbf{k}_s$. The flow is in the xy-plane, and ϕ denotes the angle between the scattering vector and the x-axis. Thus $\mathbf{q} = q(\cos\phi, \sin\phi)$, where $q = \frac{4\pi n}{\lambda_0} \sin\frac{\theta}{2}$, with λ_0 being the incident wavelength and θ the scattering angle. The homodyne correlation function in an arbitrary linear flow, according to

the theory of Fuller *et al.*,[17] is

$$F_2(\mathbf{q},t) = \left| \iiint d^3\mathbf{x}\; I(\mathbf{x}) \exp\{-i\,\mathbf{q}\cdot\boldsymbol{\Gamma}\cdot\mathbf{x}\,t\} \right|^2, \tag{1}$$

where $I(\mathbf{x})$ is the intensity distribution of the incident laser light, and $\boldsymbol{\Gamma}$ is the transpose of the velocity gradient tensor for a velocity field $\mathbf{v} = \boldsymbol{\Gamma}\cdot\mathbf{x}$. We have applied equation (1) to the general two-dimensional linear flow with

$$\boldsymbol{\Gamma} = \gamma \begin{pmatrix} 0 & 1 \\ \lambda & 0 \end{pmatrix} \tag{2}$$

where γ is the magnitude of the velocity gradient, and λ is the flow type parameter which ranges from -1 to 1. Pure rotational flow corresponds to λ=-1, simple shear flow to λ=0, and pure extensional flow to λ=1. Figure 2 shows the streamlines of these limiting, theoretical flows and how they can be obtained in our flow devices, in principle.

We assume the same Gaussian intensity distribution as Fuller *et al.*,[17] namely

$$I(x',y',z') = \exp\{-(x'^2+y'^2)/L^2 - z'^2/\alpha^2 L^2 \csc^2\theta\}. \tag{3}$$

The z' direction is that of the incident beam and thus makes an angle of $\theta/2$ with the z-axis shown in Figure 1. α is the ratio of a characteristic length of the scattering volume in the z' direction to L, a measure of its width. An explicit result for the time correlation function $F_2(\mathbf{q},t)$ can be obtained by substituting equation (3) into (1). The result, after transforming flow coordinates to primed coordinates and integrating over $\mathbf{x}'$-space, is

$$F_2(\mathbf{q},t) = \frac{1}{(2\pi)^3} \exp\left\{ -\frac{q^2\gamma^2L^2t^2}{2} \cdot \left[\left(\frac{1+\lambda}{2}\right)^2 \sin^2 2\phi \left(\cos^2\tfrac{1}{2}\theta + \alpha^2 \frac{\sin^2\frac{1}{2}\theta}{\sin^2\theta} \right) + (\cos^2\phi - \lambda\sin^2\phi)^2 \right] \right\}. \tag{4}$$

In further use of equation (4) the preexponential factor will be dropped for convenience.

Two special cases of equation (4) are obtained when **q** is aligned with either the x or y-axis, *i.e.*, ϕ=0 or 90°, respectively. In particular, when ϕ=0 the time-correlation function becomes

$$F_2 = \exp\{-\tfrac{1}{2}\, q^2\gamma^2 L^2 t^2\}, \tag{5}$$

and is dependent on the velocity gradient, γ, but is independent of the flow type, λ. If, on the other hand, $\phi = 90°$, one obtains

$$F_2 = \exp\{-\tfrac{1}{2}\, q^2\gamma^2\lambda^2 L^2 t^2\} \tag{6}$$

for any arbitrary value of λ, $-1 \leq \lambda \leq 1$. It is evident from equations (5) and (6) that independent measurements of the correlation function for ϕ=0 and ϕ=90° provide a way of determining both λ and γ in the four- and two-roll mills. The data of Figure 3 demonstrates this. The line with steepest slope passes through measurements of γ (with ϕ=0) versus ω and for various values of λ. The slope, which represents the proportionality between the decay rate of the correlation function and γ, is independent of λ as predicted by equation (5). The other data points in Figure 3 provide measurements of $\gamma\lambda$ (with ϕ=90°). Data for a given value of λ fall on a line with slope proportional to λ just as predicted by equation (6).

There are two sources of uncertainty which limit the usefulness of this light-scattering technique for determination of absolute velocity gradients. One is the intensity profile of the incident beam. This is known to fluctuate on time periods of the order of a day. This leads to uncertainty in the true functional form of the correlation function as discussed by Fuller *et al.*[17] Therefore, instead of using a least squares fit to a Gaussian or some other shape-dependent fitting procedure, we simply determine the half-height time of the correlation function, t_h. Then equation (5) gives $\gamma = \sqrt{2\ln 2}\,/qLt_h$. The correct L to use for the characteristic scattering volume dimension is hard to determine *a priori*. The best solution is to use t_h^{-1} as a

relative velocity gradient and calibrate the measurements from day-to-day by using a known flow field to determine an effective L. This effective L eliminates the need to know either the intensity distribution or the scattering volume dimensions. We have found the results to be quite reproducible, and L is typically about half the beam width, or about 70 μm.

In the velocity gradient data presented throughout this paper, each point represents an average of several correlations, whether plotted as a relative gradient (t_h^{-1}) or an actual shear rate γ. When no error bars appear, the error (standard deviation of the averaged values) is less than or equal to the symbol size.

Another limitation of the light-scattering experiment is that the theory has been worked out in detail only for two-dimensional flows, yet any additional components of $\mathbf{\Gamma}$ which might occur in a real flow device will contribute to the correlation. The main causes of such effects in our flow devices are end effects due to the bottom and top covers and misalignment of the scattering vector. Since such effects could obscure the effects of dilute polymer on the flow field, we have done extensive studies to characterize the flow fields with Newtonian fluids. These results will be reported next with special emphasis on the effects of deviations from the idealized, linear flow, equation (2) with $\mathbf{v} = \mathbf{\Gamma} \cdot \mathbf{x}$, that can occur in Newtonian fluids.

2.3 The Four-Roll Mill

The four-roll mill has been described in previous papers.[27] For measuring the flow birefringence, Δn, in order to determine polymer conformation changes in flow, the essential feature of the device is that it simulates the general linear two-dimensional flow[28] which has a velocity field $\mathbf{v} = \gamma(y, \lambda x)$. This flow field is the one that is usually considered in theoretical work. The stream function, ψ, for these flows is given by $\psi = \gamma(y^2 - \lambda x^2)/2$, and the streamlines are sketched for some selected values of λ in Figure 2. The flows with $0 < \lambda \leq 1$ are called strong flows and have a stagnation point and hyperbolic streamlines. Strong flows with

$0 < \lambda < 1$ are generated in the four-roll mill by slowing down the pair of rollers on the x-axis with respect to the pair on the y-axis. The limit of simple shear flow, λ=0, is approached, in principle, when one pair of rollers is stopped altogether. In practice, however, the flows with $|\lambda| < .2$ are not reliable because of constraints on the flow geometry due to the presence of the stationary (or nearly stationary) pair of rollers. We have therefore constructed three new pairs of rollers of different size which approximate the flows λ=.094, .049, and .019 when the flow device is operated as a corotating two-roll mill (*i.e.*, with the second set of rollers removed altogether). Flow types near the simple shear flow limit are important for testing some proposed features of dumbbell models, as will be shown later.

The main requirement for flow modification studies is that the flow field in the absence of polymer be very well characterized. As discussed in the introduction, dilute solutions can be expected to produce very localized flow changes which can be resolved only by measuring velocity gradients. We therefore carried out extensive "calibration" measurements in Newtonian fluids (glycerol and LV) using the HLS technique. The purpose of these measurements is to provide a baseline for Newtonian fluids in order to be able to recognize the distinct non-Newtonian contributions for dilute polymer solutions. In particular, deviations from the *idealized* linear, two-dimensional flows will occur even in Newtonian fluids due to "end effects" and other factors, and it is essential to be able to distinguish these changes from changes that are caused by the addition of polymer.

The initial (HLS) studies of the four-roll mill by Fuller *et al.*[17] showed the characteristic shape of the velocity gradient profile along the "limiting" incoming and outgoing streamlines which emanate from the stagnation point for the purely extensional flow, λ=1. As long as the measurements are taken on the center plane between the top and bottom of the flow device, the profile is symmetric. Furthermore, as long as the angular velocity of the rollers, ω, is low enough, velocity

gradients at any point are directly proportional to ω. The flow visualization study of Lagnado[29] showed that end effects in the form of vortices generated at the top and bottom of the flow device become important at a Reynolds number, Re ≈ 5, where Re $= 2\omega Rh/\nu$ with R being the roller radius, $2h$ the gap width between adjacent rollers, and ν the kinematic viscosity. These end vortices are undesirable for our experiments, because all of the analysis of birefringence data assumes that the flow is uniform from the top to the bottom of the flow device. At Re ≈ 38 the flow became fully three-dimensional and totally unsuitable for our studies. HLS measurements also showed these effects. Figures 4 and 5 show typical HLS measurements at the center stagnation point when end effects are present. The end effects begin in Figure 4 as an upward curvature in the otherwise linear γ versus ω relationship at ω=20, approximately Re=5 for this glycerol/water mixture with $\eta \approx 10$ p. At about Re=36, (ω=20 in Figure 5 for glycerol/water with $\eta \approx 1.4$ p.) the measured velocity gradient increases dramatically or goes through a maximum depending on the orientation of the scattering vector, $\mathbf{q}$. Figure 6 shows how end effects appear in the velocity gradient profiles along incoming and outgoing streamlines. Two values of Re are considered, .37 and 3.7, the latter being the upper limit reached in the solutions of PS8 in LV that we have studied. Both are in the range where γ varies linearly with ω at the center. It is seen that small changes in the profile shape occur away from the center as ω increases, and the incoming profile differs slightly from the outgoing profile for the higher roller speed. We have included these data in order to show that the polymer effects to be presented shortly are easily distinguished from the "non-ideal" flow effects seen in Newtonian fluids with non-negligible inertia. Finally, Figure 7 shows the variation of velocity gradient with position as we move normal to the outgoing streamline in a Newtonian fluid. The x values indicated in Figure 7 are distances from the center stagnation point measured along the outgoing streamline and thus correspond to the abscissa

in Figure 6. These cross-flow profiles are all smoothly varying with either upward or downward curvature, depending on location with respect to the positions of the maxima in Figure 6. As we will see, dilute polymers cause dramatic deviations from these velocity gradient profiles.

2.4 The Two-Roll Mill

The flows in the two-roll mills were characterized using both flow visualization and HLS to determine the angle of crossing of the asymptotic streamlines at the center (*i.e.*, the flow-type parameter λ), and HLS to measure the velocity gradient fields. An advantage of two-roll mills over the four-roll mill is the existence of an analytical solution of the unbounded creeping flow problem in this geometry. This allowed us to predict the complete flow pattern for the dimensions of our two-roll mills, assuming, of course, that the real flow is two-dimensional. These predictions were used in designing the two-roll mills and also in testing the reliability of the HLS measurement. The general form of the creeping flow solution for two cylinders of arbitrary radius and arbitrary center-to-center separation distance was given by Jeffery in 1922.[30] The particular case of a counter-rotating two-roll mill was evaluated by Jeffery and has also been presented several other times in the literature. We are interested here in the solution for corotating rollers, which, to our knowledge, has not been given elsewhere.

Jeffery's general solution is expressed in bipolar cylindrical coordinates, (α, β), which are related to (x, y) coordinates by

$$x = \frac{a \sin \beta}{\cosh \alpha - \cos \beta} \quad \text{and} \quad y = \frac{a \sinh \alpha}{\cosh \alpha - \cos \beta}. \tag{7}$$

Figure 8 shows the coordinate curves of constant α and β. The rollers are curves of constant $\alpha = \pm\alpha_1$ positioned with their centers on the y-axis as shown in Figure 2. The constant a is essentially a scale factor. The two constants a and α_1 are related

to the roller radius R and the gap width $2h$ via the relations

$$1 + \frac{h}{R} = \cosh \alpha_1 \quad \text{and} \quad a = R \sinh \alpha_1. \tag{8}$$

The stream function for corotating rollers is found to be

$$\psi = \frac{a^2 \omega}{\cosh \alpha - \cos \beta}(A \cosh \alpha + D\alpha \sinh \alpha)$$
$$\text{with} \quad A = \frac{\alpha_1}{\alpha_1 + \sinh \alpha_1 \cosh \alpha_1} \quad \text{and} \quad D = \frac{-\coth \alpha_1}{\alpha_1 + \sinh \alpha_1 \cosh \alpha_1}, \tag{9}$$

where ω is the angular velocity of the rollers. In the region very near the stagnation point, the flow field is asymptotically a linear flow with the flow-type parameter λ independent of roller speed.

$$\lambda = \left(\frac{4 \coth \alpha_1}{\alpha_1} - 1 \right)^{-1} \tag{10}$$

The acute angle of crossing, 2φ, of the center streamlines is related to λ by the equation $\lambda = \tan^2 \varphi$. The magnitude of the velocity gradient in this region is proportional to ω.

$$\gamma = \frac{A\omega}{\lambda} \tag{11}$$

We found that values of λ calculated from the measured angle of crossing of the center streamlines agree very well with the theory. Figure 9 shows a photograph of streamlines for a particular pair of rollers (which give λ=0.135 according to equation 10), compared with the exact streamlines calculated from equation (9) and with the linear flow approximation of equation (2) with λ=.135. It is apparent that streamlines are inadequate for resolving quantitative differences between the two analytic representations of the flow. Figure 10, on the other hand, shows a quantitative comparison between velocity gradient profiles measured along the centerline of the gap by HLS and calculated from the exact creeping flow solution. There is good agreement over a reasonable distance. But the region of linear flow

where γ is constant is relatively small, on the order of the gap width. Another important characteristic of the experimental system is the relationship between roller speed and velocity gradient, γ which should be linear according to equation (11). Figure 11 shows typical results for the measured velocity gradient at the stagnation point of the flow versus roller speed. Our experimental studies verified that γ varied linearly with roller speed for Newtonian fluids over the range of speeds used in our experiments for all realizations of the two-roll mill.

We have noted earlier that the critical condition for onset of end effects and three dimensionality in the two-dimensional extensional flow, λ=1 (as realized approximately in the four-roll mill) is Re=5 and Re=38, respectively. The recent theoretical stability analysis of Lagnado *et al.*[31] for a general, *unbounded* linear flow suggests that these critical conditions should vary with flow type, λ as $\gamma\sqrt{\lambda}$ irrespective of whether the flow is produced in a two- or four-roll mill. In practice, however, the flows produced in the two-roll mill are stable and two-dimensional to significantly higher values of $\gamma\sqrt{\lambda}$ than in the four-roll mill. We believe that this is because the gap width in the two-roll mill for the smallest values of λ is much smaller than in the four-roll mill. If we use $\mathrm{Re}\sqrt{\lambda}$ (with the same definition of Re as before) instead of $\gamma\sqrt{\lambda}$, it does seem from limited flow visualization experiments[32] that the critical conditions in both the two- and the four-roll mill vary as $\mathrm{Re}\sqrt{\lambda}\approx$5, and 38. Regardless of the reason, however, the capability of achieving larger values of $\gamma\sqrt{\lambda}$ while maintaining a two-dimensional, stable flow is a definite advantage of the two-roll mill. The actual dimensions and the measured and predicted shear rate proportionality constants of the flow devices are given in Table III. (The two-roll mill with λ=.135 which was photographed for Figure 9 is not included. It is actually two adjacent rollers in the four-roll mill and was not used in the present HLS and flow birefringence studies.)

TABLE III. Characteristics of the Flow Devices

Device	R^a	Measured		From Theory	
	(cm)	λ	γ/ω	λ	γ/ω
2-Rolls #1	2.906	0.09	4.7	0.094	4.66
#2	3.170	0.05	9.5	0.049	9.64
#3	3.361	0.02	25.	0.019	26.12
4-Rolls	1.905	.2–1	0.64	–	.678

[a] $h + R = 3.488$ cm in each case (diagonally in 4-roll mill)

2.5 Flow Birefringence

The most direct and widely used experimental probe of the polymer behavior in strong flow seems to be the flow birefringence (FB) experiment.[14] It has been used to study various aspects of the coil-stretch transition in well-defined flows.[6–11,18–20] It can be used to test predictions of molecular theories of polymer behavior. A schematic of our experimental setup is shown in Figure 12. The flow device can be moved independently of the optics so that almost any position in the flow field can be studied. The same optics are easily realigned to do the HLS experiment described above. The relative orientations of the polarizer, analyzer, solution optic axes (indicative of the orientation of the elongated polymer molecules), and flow field are also shown in Figure 12. The intensity I measured by a laser power meter is related to the incident intensity I_0, wavelength λ_0, the solution thickness d, the birefringence Δn, and the angle ϑ between the polarizer and the optic axis of the solution.

$$I = I_0 \sin^2 2\vartheta \sin^2 \frac{\pi d \Delta n}{\lambda_0} \tag{12}$$

By finding the position of maximum intensity, $\vartheta = 45°$, the polymer orientation angle, χ, can be determined. This angle χ is defined to be consistent with the classical extinction angle from simple shear flow experiments.[14] For all flow types, χ is 45° at low shear rates and approaches the flow direction, φ, at high shear rates.

The birefringence of the solvent LV had to be measured and accounted for when calculating the polymer contribution to the birefringence. The relations recommended by Philippoff[33] were used to subtract off the solvent contribution.

$$\Delta n_p^2 = \Delta n^2 + \Delta n_s^2 - 2\Delta n_s \Delta n \sin 2\chi$$
$$\cos 2\chi_p = \frac{\Delta n}{\Delta n_p} \cos 2\chi \tag{13}$$

Here the subscript p refers to the polymer, s to the solvent, and no subscript for the measured solution property. The Philippoff relation assumes that the solvent orientation angle is always 45°. This was found to be true for LV. The Δn of LV in the four- and two-roll mills is plotted in Figure 13 versus the Newtonian rate of strain $\gamma(1+\lambda)/2$, which is proportional to the stress. Since the data fall on a single straight line, the stress-optical law is valid for these Newtonian liquids and can be generalized for the class of two-dimensional linear flows. The Maxwell constant or "dynamo-optic" constant,[14] M_c, has been customarily defined for simple shear flow. It can be defined more generally by the equation

$$\Delta n_s = M_c \gamma(1+\lambda). \tag{14}$$

In Reference 11, the Δn of PCB was plotted versus $\gamma\sqrt{\lambda}$, the eigenvalue of $\mathbf{\Gamma}$ or the persistent strain rate,[19] rather than the actual rate of strain. Since $\sqrt{\lambda} \approx (1+\lambda)/2$ for $\lambda \sim 1$, the data seemed to correlate only because the two possible correlating parameters differed by at most 20% for the lowest λ value of 0.25 that these authors could acheive. For the range of λ considered here, there is no such ambiguity in the data, since the two possible correlating parameters differ by a factor of almost 4 for our lowest value of λ=0.019. The Maxwell constants for the three solvents are given in Table I. These turn out to be $\sim 10^3$ times larger than values reported for typical organic solvents.[14] This is as one would expect because $M_c \propto \eta_s$ for solvents of similar molecular structure, and the solvents we use have viscosities $\sim 10^3$ times larger than the viscosities for typical organic solvents.

3. RESULTS

We now turn to the results of our flow birefringence and velocity gradient measurements in dilute solutions of polystyrene. Before presenting detailed comparisons between FB and HLS, we present extensive FB data showing the general behavior of the polymer in different solvents. Previous published data from our laboratory[11] had considered only a single, viscous solvent. The present birefringence data also extend previous work[11] to lower values of the flow type parameter, λ. Following the birefringence data, we show extensive velocity gradient measurements for polystyrene in Chlorowax LV.

3.1 Flow Birefringence

The primary purpose of the FB measurements in this study is to connect the coil-stretch transition with the flow modification results that are reported below. However, we have also extended previous FB studies[11] of polymer extension to include several solvents and much smaller values of the flow-type parameter λ. The importance of lower λ values was stressed by Fuller and Leal[11] in connection with the evaluation of internal viscosity contributions for dilute solutions. In this region of flow types, the behavior must change qualitatively from the small deformations produced in simple shear flow to the nearly complete extensions obtained in flows with only slightly more extension than rotation. A fully successful model should be able to describe not only simple shear flow and pure extension, but also the "transition" for flow types in between.

We measured the FB of PS8 at a weight concentration of 100 ppm in TCP and in LV at the center stagnation point of the three two-roll mills and of the four-roll mill for different values of λ. Similar measurements using PS2 at the same 100 ppm concentration in LV were also done. The data are plotted as Δn versus $\gamma\sqrt{\lambda}$ and presented in Figures 14–16. (Here we initially use the values of λ and γ calculated from measured roller speeds, ω, using the *Newtonian* relationships from

Table III.) In these plots, the solvent contribution to the flow birefringence has been removed using equations (13). It is typically an insignificant fraction of the total birefringence except at the highest shear rates which occur in the two-roll mills of smallest gap.

The main result of varying the flow type was previously found to be the existence of a correlation between FB and $\gamma\sqrt{\lambda}$, the eigenvalue of $\mathbf{\Gamma}$, for all λ in the range $.2 < \lambda \leq 1$. The effect of including smaller λ values is obviously to show that this correlation of Δn with the eigenvalue $\gamma\sqrt{\lambda}$ is still excellent down to very much smaller values of λ. Though $\lambda = .019$ implies a ratio of extension to vorticity of only 1.039, the flow still acts qualitatively similar to pure extension insofar as its effect on the polymer is concerned (*i.e.*, it is still a strong flow). Based upon these new data, a target for any theoretical model would seem to be an ability to predict a correlation of the onset of the coil-stretch transition process with $\gamma\sqrt{\lambda}$ down to at least $\lambda = .019$.

All of the PS8 data in the two-roll mills as well as that for $\lambda = 1$ in the four-roll mill are replotted in Figure 17, this time versus the *dimensionless* eigenvalue, $\tau\gamma\sqrt{\lambda}$, based upon the characteristic solution relaxation time scale, τ, that is determined from intrinsic viscosity measurements. Also included are the data of Fuller and Leal in PCB.[11] The characteristic times, τ, are given in Table II. It is not surprising that the data for the three solvents correlate when plotted in this way, but this fact has not previously been demonstrated in the literature for strong flows so far as we know. The characteristic relaxation time, τ, should account for differences in temperature, solvent viscosity, and solvent quality among the three solvents. The fact that the birefringence correlates with $\tau\gamma\sqrt{\lambda}$ suggests that the onset point for the coil-stretch transition scales as τ does, *i.e.*, with $[\eta]M_w$. The data in Figure 17 can (after correcting for velocity gradient effects as described in the next section) be considered to be a master birefringence curve for this particular polymer in any

strong two-dimensional flow. It is probably *only* representative of this particular polystyrene sample, however, because the molecular weight *distribution* affects the *shape* of the data significantly.[10] Though τ accurately correlates the onset point for birefringence, the degree of apparent smoothing of the coil-stretch transition is determined directly by the spread in the molecular weight distribution. Therefore, τ alone cannot be expected to correlate the shapes of the birefringence curves of polymer samples with different polydispersities. In fact, we found that the PS2 and PS8 data in the same solvent and same flow do not correlate with each other as well as the PS8 data for different solvents.

The saturation behavior of the birefringence is surprisingly complicated. Examining Figure 17, we see, first of all, that different *apparent* saturation values of the birefringence are obtained in the three solvents and in the two kinds of flow devices. This was not expected because if the maximum, Δn_∞, represents fully extended polymer chains, it should only depend on the total amount of polymer in solution and the total intrinsic optical anisotropy of the polymer, $(N\Delta\alpha)$, both of which are constant in these experiments,

$$\Delta n_\infty = \frac{2\pi}{9}\frac{(n^2+2)^2}{n}\frac{N_A c}{M}N\Delta\alpha \tag{15}$$

where N_A is Avagadro's number and N is the number of statistical (Kuhn) segments in the polymer chain. The highest measured value for Δn_∞, $\sim 5\times 10^{-6}$, was obtained in the two-roll mills for both PS8 and PS2 in LV. This asymptotic value is about twice what Fuller and Leal obtained in the four-roll mill with the PCB solvent.[11] If we assume that the present measurement represents 100% extension of the polymer and that $\Delta\alpha = -145 \times 10^{-25}$cc,[34] equation (15) gives a value of $N \approx 5000$ for PS8 and 1200 for PS2. This corresponds to ~16 monomers per statistical segment and stretch ratios of ~70 and 35, respectively, at full extension. The same Δn_∞ was reached in TCP in the two-roll mill with the smallest gap (#3). Since it is independent of M_w, η_s and flow type for the two-roll mills, it seems certain that

this saturation value represents the complete (or very nearly complete) extension of the polymers.

The saturation values in the four-roll mill do not reach the same high value and they are strongly dependent on solvent viscosity. Δn_∞ is lowest for TCP which has the lowest viscosity and almost reaches the two-roll mill value for LV which has the highest viscosity of the three solvents. The dependence of the "apparent" asymptotic birefringence level on solvent viscosity (in the flows with $\lambda = 1$) seems to be $\Delta n_\infty \sim \eta_s^{2/3}$. The corresponding Reynold's numbers are 22 for TCP and 3.8 for LV at saturation. Thus, according to the results of Lagnado's recent flow visualization study of the four-roll mill,[29] the effects of the secondary flows, induced at the top and bottom of the flow device, may be a major contributor to the appearance of an "apparent" asymptotic level for Δn in the four-roll mill, which is dependent on solvent viscosity and is lower than the actual asymptotic value that is attained in the two-roll mill. We may recall from Lagnado's work that end effects in Newtonian fluids become increasingly important above Re$\approx$5 in the four-roll mill.

There is something more happening in the polymer solutions, however. Even in the more stable two-roll mills the last data points reported represent the highest shear rates for which a stable birefringence value could be measured. For higher shear rates the birefringence intensity fluctuated wildly, indicating a very unstable flow. This always occurred, even when the Reynold's number at Δn_∞ was only 0.2 (for LV in two-roll mill #3). Also, flow visualization revealed no changes in flow structure similar to the large vortices observed in "unstable" Newtonian fluids. Figure 18 shows a series of vertical sections of the flow for a 118 ppm solution of PS8. End effects appear to be minimal in these photos, even at shear rates more than twice the shear rate at which the FB becomes unstable (*i.e.*, up to Re $\approx$ 10). Thus the unstable flow evidenced in the FB data must result from a different type of localized, or smaller scale flow instability than occurs in Newtonian fluids for

which larger values of Re are required for instability.

It may be noted that recent experimental studies of concentrated polymer solutions flowing through a contraction have identified a localized, distinctly viscoelastic instability which also occurs at low Reynold's numbers in the extensional region of flow.[35] Furthermore, a recent analysis of the stability of extensional flow, based upon a constitutive equation of the "Oldroyd-type," has predicted a "viscoelastic" instability to short wave-length disturbances at a finite, $O(1)$ value of the dimensionless strain rate (*i.e.*, of the Weissenberg number).[36] It is not known, at the present time, whether either of these observations is related to the (apparently) short wave-length instability that our FB data exposes in *dilute* solutions.

3.2 Velocity Gradient Measurements

Using the light-scattering technique previously described, we have examined the velocity gradient fields in the four- and two-roll mills for 80 and 100 ppm solutions of PS8 in LV and for a 118 ppm solution of PS8 in an LV/TCP mixture with η_s=8.3 p. In this section, we report the variation of velocity gradient with roller speed and with position in the flow, and compare these data with measurements of flow birefringence at the same positions and shear rates.

Figure 19 shows typical velocity gradient data for a number of different flow types measured at the stagnation point of the four-roll mill. The data are plotted as measured versus theoretical (Newtonian) values of $\gamma\sqrt{\lambda}$ for the same 100 ppm PS8 in LV solution that was used in obtaining the FB data in Figure 14. In the case of pure solvent, measurements described earlier show a direct proportionality of shear rate to roller speed except when "end effects" set in from the top and bottom of the flow device. This linearity holds true at each position in the flow for a Newtonian fluid and is represented by the straight line in Figure 19, as well as in Figures 20 and 21 which we shall discuss shortly. At low roller speeds, it can be seen from Figure 19 that the same linear relationship between γ and ω is followed

in the polymer solution as for a Newtonian fluid. However, at a certain value of ω, a rather sharp transition is observed. From that point on, the velocity gradient in the polymer solution is significantly (up to 20%) less than in pure solvent at a given roller speed.

Several points should be noted with regard to this measured effect of the polymer on the flow. First, we shall see shortly that the magnitude of the effect, for a given roller speed and flow type, increases significantly with position as we move along the outflow axis away from the stagnation point. Thus, the magnitude measured at the stagnation point provides a conservative indication of the decrease in the velocity gradient. Second, the *onset* of a measurable effect of the polymer on the velocity gradient appears to correlate with the eigenvalue of $\mathbf{\Gamma}$ (*i.e.*, with $\gamma\sqrt{\lambda}$). Since the FB data also correlates with $\gamma\sqrt{\lambda}$, and is indicative of the degree of polymer extension, we infer that the onset point for flow modification occurs, for any flow with $\lambda > 0$, at a critical level of polymer extension which depends on the concentration and M_w for a given polymer. Finally, we note that the weaker flows in the four-roll mill (*i.e.*, those with lower values of λ) show larger decreases in velocity gradient at higher shear rates than pure extensional flow ($\lambda=1$) at equal values of $\gamma\sqrt{\lambda}$.

The magnitude of the velocity gradient decrease shown in Figure 19 is larger than found by Fuller and Leal[11] for a 100 ppm solution of PS8 in PCB. We believe that their measurements show smaller effects than ours because their solutions were filtered several times (to eliminate the adverse effects of dust on the HLS experiments), thereby reducing the polymer concentration and possibly degrading the molecular weight. To test this hypothesis, we filtered a 100 ppm solution of PS8 in LV once (using a 5 μm Millipore filter) and compared HLS and FB data with the data for the original solution. Figure 20 shows HLS and FB data (at the stagnation point in pure extension) for both the unfiltered and the filtered solutions. The FB

data shows a significant difference between the original and the unfiltered solutions. The shift in the onset point of the FB is indicative of about a 15% decrease in M_w during filtering. The decrease in the apparent value of Δn_∞ indicates that the actual concentration of polymer is only about 80 ppm after filtering. The velocity gradient data also show the effects of filtering on the molecular weight and/or the concentration. The onset of the velocity gradient effect occurs at a higher shear rate in the filtered (80 ppm) solution than in the unfiltered solution. The magnitude of the effect is also less after filtering.

In Figure 20, it can also be seen that the onset of the velocity gradient decrease results in a change in slope in the birefringence data, and that this change in slope occurs approximately midway through the coil-stretch transition process for these particular solutions. Thus the FB data alone can be useful in showing flow effects for very dilute polymer solutions. For example, the smoother appearance of the FB data for PS2 in Figure 16 agrees with the absence of any measurable flow effects in this solution. Knowing now what to look for, we can detect these same FB and HLS effects (though less dramatic) in the data of Fuller and Leal (Reference 11, Figures 10 and 21). Since the actual shear rates have now been measured, the FB data can be replotted versus true shear rates. This has been done, and the resulting data will be used to test various forms of the dumbbell model.

The 118 ppm solution shows the largest changes in the flow field due to the polymer. Figure 21 shows the flow birefringence for this solution at the center of two-roll mill #2 and at three positions (0, 0.3, and 0.6 inches from the stagnation point) on the outgoing streamline of the four-roll mill (with λ=1). The nip of the rollers is about 1 inch downstream, and the .6-inch position coincides with the location of the maximum velocity gradient in the Newtonian profiles of Figure 6. The corresponding velocity gradients measured by HLS are shown in Figure 21 as $\gamma\sqrt{\lambda}$ versus ω. The straight lines (representing Newtonian behavior) have

different slopes for different positions in the four-roll mill, the steepest being at 0.6 inches from the center. Figure 21 shows that the reduction in shear rate by the polymers can be significantly more 0.6 inches from the center than at the center. The flow effect is also seen to commence at lower roller speeds at X=.6" than it does at the center. The birefringence indicates that the polymers are slightly more extended downstream of the stagnation point, but not nearly as much as would be expected, since the peak velocity gradient is about 45% higher than that at the center for a Newtonian fluid. In other words, the reduction in γ coincides with reduced macromolecular extension, with the greatest effects occuring where the shear rate is the greatest.

We have also measured velocity gradient profiles along the outgoing streamline of pure extensional flow in the four-roll mill for the 80 ppm solution of PS8 in LV. The data are plotted in Figure 22 as a ratio of the measured t_h^{-1} to that of a Newtonian fluid at the center position. This allows a direct comparison of the shape of the profile at different roller speeds. The profile for the polymer solution coincides with that of the pure solvent (Figure 6) at roller speeds below the critical value for onset of a measurable effect of the polymer on the velocity gradients. Typical profiles for roller speeds above the critical value are also shown in Figure 22. The shear rates are found to decrease all along the outgoing streamline. As in the 118 ppm data of Figure 21, the effects are seen to begin at lower ω in the regions of the peaks than at the center of the flow device. Thus, the locations of the flow with the greatest strain rates are influenced the most by the polymer. It will be seen, however, that velocity gradients on the incoming streamlines are not reduced nearly as much as on the outgoing streamline, even though in this symmetric flow the shear rates are equally large (in a Newtonian fluid). This is because the residence time in the region of high shear rate must be long enough to allow sufficient extension of the macromolecules before the flow will be measurably

affected. The incoming streamline does not usually meet this requirement.

We have also measured the spatial variation of velocity gradient away from the center streamline of the four-roll mill flow with λ=1 at fixed roller speed in order to determine the spatial extent and magnitude of the polymer-induced flow modification. The cross-flow velocity gradient profiles in the pure solvent have already been discussed, and this data will now be compared with the results for dilute polymer solutions. One well-known characteristic of the birefringence is its localization in a very narrow region near the outgoing streamline of the flow. We find that the velocity gradient field can be modified over a significantly larger area.

The variation of the velocity gradient perpendicular to the outgoing axis and at various positions along it is plotted in Figures 23 and 24. The two graphs of Figure 23 are for the 118 ppm solution at two roller speeds. The top one is for ω=3.5 s^{-1}, which is below onset of the flow modification effect. The bottom graph is for 10.5 s^{-1}, and the modification of the flow by the polymer is quite dramatic in this case. Figure 24 shows data for the 80 ppm solution at many positions along the outgoing axis (solid lines). The dashed lines are the measured profiles perpendicular to the *incoming* streamline, which show little or no difference from the Newtonian profiles of Figure 7. The most important "new" observation from this data is that the influence of the polymer on the velocity gradient field extends well beyond the region of large polymer extension and high FB. The width of the measurable birefringent region is typically $<$ 0.05 cm while the velocity gradient field is altered over ~0.5–0.8 cm. We believe that this is completely reasonable. If the birefringent region is considered to act as a line of much higher viscosity than the bulk of the fluid (or even as a solid wall), then the extent of influence of this line will be the length scale, l, for vorticity diffusion on time scale of order $1/\gamma$. Thus, $l \sim \sqrt{\nu/\gamma}$, which is about 1 cm for LV at $\gamma = 15\,s^{-1}$.

In Figure 25, we attempt to provide a better picture of the overall appearance

of the velocity gradient field in the four-roll mill. The cross-axis profiles from Figure 24 are plotted with their center points positioned at the location of the measurement in the flow. The incoming and outgoing cross-profiles are combined for comparison. Also shown are the profiles *along* the incoming and outgoing axes (rotated 90°). The same velocity gradient scales apply to all points so the relative size of the dips is not exaggerated. The cross-profiles located beyond the nip of the rollers are negative shear rates.

3.3 Degradation

One more set of observations should be mentioned here. Mechanical degradation of the polymer was observed in the PS8 solutions. It was evidenced by irreversible decreases in birefringence after running the rollers for a few minutes at a high enough speed to produce nearly complete extension of the polymers. Figure 26 shows the changes in FB typically observed for a 100 ppm PS8 in LV solution. After about 23 hours of extensive HLS and flow visualization studies at values of $\gamma\sqrt{\lambda}$ up to about 40 s^{-1}, the birefringence versus shear rate curve strongly resembles what we would expect for a sample with $M_w = 4 \times 10^6$. Thus the polymer chains break at or near the center bond after being completely stretched out by the flow. The same conclusion was reached by Odell *et al.* on the basis of FB measurements in a cross-slot flow device.[37] Mechanical degradation probably contributes to the scatter in plots such as Figures 14–17 and 19 in which many data points taken over a period of hours or even days are included. We always attempted to minimize the possible influence of degradation by using the shortest correlation duration times practical in the HLS experiments and only running the rollers long enough to get a steady intensity measurement in the FB experiments, but degradation cannot be totally avoided: if the polymers are extended, then they are likely to be broken eventually!

4. DISCUSSION

4.1 Flow Modification Onset

As shown above, the onset of flow modification occurs at a higher shear rate than the onset of the coil-stretch transition and at a lower shear rate than the onset of instability in the birefringence, which in turn occurs well before significantly three-dimensional flow would be seen in a Newtonian fluid. The effect of polymer on the flow can be thought of as correlating with an increased effective volume concentration as the polymers become greatly extended. A dilute solution of hydrodynamically isolated polymer molecules would not be expected to affect the flow macroscopically. A flow effect is not expected at least until neighboring polymer molecules begin to influence each other hydrodynamically. From the birefringence measured at the critical roller speed for onset of a flow effect in the 100 ppm solution of PS8 in LV, we estimate that the polymers are extended to about half their total contour length when an effect on the flow first occurs. Calculating the effective volume concentration, $\phi_{eff} = \frac{4}{3}\pi r_{eq}^3 N_A c/M$, of spheres with a radius equal to one-half the total contour length, L, using $r_{eq} = \frac{L}{2}\sqrt{\Delta n/\Delta n_\infty}$, gives a critical effective volume concentration $\phi_{crit} \approx 3900$. This very large value suggests strongly that very extensive interactions are necessary before the polymer solution exhibits measurable flow modification due to the presence of the polymer. The same type of behavior was seen in the 80 ppm solution, except that the critical roller speed (*i.e.*, the critical velocity gradient) is somewhat higher, because greater extension is required to give the same effect when c is lower. In this case, the polymers are estimated to be at ~60% of full extension at the onset of a measurable change in the velocity gradient, giving $\phi_{crit} \approx 5600$. For the 118 ppm solution, ϕ_{crit} is estimated to be $\sim 10^4$ at the stagnation point, but only ~5500 at the location of the maximum in γ (.6 inches from the center). In 100 ppm PS2 in LV no flow effect was observed. The calculated effective volume concentration at *full* extension for this solution was

only ~1800, or less than half the critical value estimated from the PS8 data for onset of measurable flow field effects. Thus from these limited measurements the critical effective concentration seems to be on the order of 4000–6000 for the appearance of a flow effect in the four-roll mill.

An alternative though related interpretation is that the presence of a measurable flow effect correlates with an increased elongational viscosity in the narrow region of high birefringence. An equation proposed by Batchelor[38] may be used to estimate the ratio of the polymer contribution to the stress, σ_p, to that of the solvent, σ_s, when the polymers are nearly completely stretched and aligned in the flow. Here,

$$\frac{\sigma_p}{\sigma_s} = \frac{\frac{4\pi}{9}\frac{N_A c}{M}L^3}{\log\frac{2L}{r}\log\frac{h+2L}{h} - \frac{3}{2}} \quad \text{and} \quad h = \left(\frac{2N_A cL}{M}\right)^{-\frac{1}{2}}, \tag{16}$$

where L/r is the polymer axis ratio, and h is the lateral distance between polymers. Using the measured birefringence to estimate the length of the polymer, one obtains a critical stress ratio of 421 for the 100 ppm PS8 solution and 577 for the 80 ppm solution. The 100 ppm PS2 solution gives a stress ratio of 171 at full extension. Thus the critical stress ratio appears to be 400–600, an order of magnitude less than the effective volume fractions estimated. This reflects the fact that when the elongated polymer molecules are all oriented in the same direction the effective volume concentration should be based on the volume of circumscribed *cylinders* rather than spheres.[38] At this point it is not clear why either the large volume fraction or the high stress ratio is an appropriate criterion for an order one flow effect to occur. One possible explanation is that the direct influence of polymer on the flow is so localized that it does not show up, when the data is effectively averaged over the finite width or the scattering volume, until there is a very strong effect on the outflow axis (presumably, well beyond the point of actual onset) which can be propagated via vorticity diffusion. However, a satisfactory quantitative explanation

may require an analysis of the flow field using an appropriate constitutive equation for dilute polymer solutions, and efforts in this direction are now under way.

The value of ϕ_{crit} for flow modification, estimated above, may be used to estimate the minimum weight concentration of polymer that is required to affect the flow for a given molecular weight, assuming that the polymer becomes fully extended. The results are ~12–18 ppm for PS8 and 200–300 ppm for PS2. Conversely, we can also estimate the minimum molecular weight which will affect the flow when the polymer is fully extended, and for a 1000 ppm solution the result obtained is $M_{min} \approx 1 \times 10^6$. These estimates both seem reasonable in light of general trends in drag reduction and other dilute polymer solution flow phenomena.

4.2 Dumbbell Models

The final question that we would like to address is whether anything new can be learned about molecular models for dilute solutions with this new flow birefringence versus velocity gradient (or eigenvalue) data. From the point of view of fluid mechanics, the object of modeling is to describe the rheology of the dilute polymer solution and ultimately to derive a constitutive equation that is useful for a complete fluid mechanical description of flows of these liquids. In a dilute polymer solution, substantial differences from Newtonian behavior occur only when the flow conditions produce a transition in the polymer conformation from the equilibrium coil to a highly unraveled or elongated state. The initial goal of our modeling is, therefore, a proper description of the dynamics of this coil-stretch transition.

The essential features of any polymer model *for strong flows* are deformability and orientability. In other words, the model must properly describe the finite, but very high degree of extensibility of a high molecular weight polymer and its hydrodynamic response to the flowing solvent over the whole range of accessible conformations, from the equilibrium coil to the fully extended state. The elastic dumbbell model, which has been widely adopted for dilute solutions, is basically a

vector model in which the polymer conformation is represented by a vector, $\mathbf{r}$. The magnitude of $\mathbf{r}$ represents the end-to-end distance of the polymer (or some measure of its largest dimension when in a given conformation). The restriction to a single relaxation time should not be bad for the large deformation, low-frequency type of dynamics that occurs in extensional flow. Though the dumbbell model is typically pictured as two spherical beads connected by a spring,[22] with a proper mathematical description of the spring-force law and the hydrodynamic behavior, the motion of $\mathbf{r}$ can, in principle, be dynamically similar in behavior to any deformable or rigid hydrodynamic object, including flexible polymers.[24]

The form for the spring force, F_s, can be derived from statistical mechanics for a given theory of the equilibrium statistics of the polymer. It is obtained from the distribution function for the end-to-end distance of the polymer.[39] Thus the equilibrium end-to-end distance, the dependence of the entropic "spring" force on end-to-end distance, and the finite extensibility of the polymer can be derived for the dumbbell model using the "best" statistical theories available. However, the essential correct qualitative behavior in strong flows will result as long as the spring force increases linearly with $\mathbf{r}$ at small deformations (this corresponds to Gaussian chain statistics) and increases very rapidly as the full contour length of the polymer, L, is approached (*e.g.*, Langevin statistics).Of the various spring laws proposed in the past,[22] the simplest one that also has some statistical mechanical justification[41] is the Warner spring,[40]

$$\mathbf{F}_s = -\xi_0 H(r)\,\mathbf{r} = -\frac{3NkT}{L^2}\frac{1}{1-\frac{r^2}{L^2}}\mathbf{r}. \tag{17}$$

We have used the Warner spring exclusively in the calculations to be presented. It is not surprising that a nonlinear spring law of this type is an essential feature for modeling polymer behavior in any flow which produces significant polymer deformation, since a linear spring law allows the unrealistic prediction of infinite extension.

The hydrodynamics of the dumbbell is not so simple an issue. In general, the friction force, $\mathbf{F}_f$, is proportional to the difference between the bead and solvent velocity,

$$\mathbf{F}_f = \zeta(\boldsymbol{\Gamma}\cdot\mathbf{r} - \dot{\mathbf{r}}). \tag{18}$$

The problem of deriving the correct friction coefficient, ζ, for a polymer has not been completely solved. The simplest approach is to use a Stokes' law frictional force for each bead, with $\zeta=\zeta_0$, a constant. The dumbbell model with the Warner spring law and constant bead friction coefficient will be referred to as the CF model. We will present the predictions of the CF model (also called the FENE dumbbell) since it has been used widely in the literature and has been shown to give reasonable large-deformation behavior.[22]

However, during a coil-stretch transition a polymer goes from a nearly spherical configuration to a very long, slender configuration. It seems clear that completely different frictional behavior must result at these two extremes because of the dramatic increase in length scale and the change in polymer shape. Two approaches have been taken to handle this change in hydrodynamic interaction with the solvent. The oldest and most common imagines the frictional centers of resistance of the polymer to be literal spherical beads. The exact fluid mechanical description of the flow about neighboring, hydrodynamically interacting beads is then attempted. This approach might be expected to provide reasonable results for the limiting case of many beads fairly close together (*i.e.*, a physically realistic model). However, the only rigorous attempts with many-bead models have used far-field (Oseen) interactions (and linear springs), resulting in only a very weak dependence of hydrodynamic interaction on conformation. The next logical step in this approach would be near-field interactions and nonlinear springs, but such a model would be hopelessly complicated and unsuitable for subsequent analysis.

Thus, we advocate a completely different approach to describing the hydrody-

namic friction between solvent and polymer. The convenient dumbbell (or bead–spring) imagery may be retained, but the hydrodynamics is modified from the usual Stokes' law so that the dumbbell (or **r**) moves in the solvent in a manner qualitatively similar to other deformable bodies of finite cross section.

The most obvious change needed in the dumbbell hydrodynamics is that the frictional resistance must become dependent on conformation instead of being constant. Since the frictional resistance between any particle and the solvent in a low Reynold's number flow is approximately proportional to the largest dimension of the particle, a bead friction coefficient, $\zeta = \zeta_0 Q(r)$, which increases linearly with r has been extensively studied.[15,16,23,42] This simple variable friction (VF) model is the second version of the dumbbell for which detailed predictions will be given.

Another general feature of the motion of particles with any rigidity in Stokes flow is an inefficiency of rotation in straining flow, (or, more accurately, in the strain portion of any linear flow). This effect was introduced into the dumbbell model in simple shear flow by Abernathy *et al.*[43] who used the usual dumbbell equation of motion for changes in dumbbell length, $\dot{r}$, but prescribed the rotation to be that of an ellipsoid of revolution with an axis ratio determined by r. It is also apparent that the friction law should become anisotropic as the polymer elongates. A nonlinear dumbbell model with full conformation-dependent, anisotropic friction and strain-inefficient rotation was studied in strong flows by Phan-Thien, *et al.*[24] They adopted the hydrodynamics of *rigid* ellipsoids, for lack of any better choice, but this choice probably overestimates the anisotropy and strain-inefficiency for a macromolecule. This SI model is the third version for which detailed comparisons with FB data will be made in the present work. To date the SI model is the most complete attempt at dumbbell modeling of dilute solutions. This approach results in a model for the deformation and orientation of the end-to-end vector of a polymer with equilibrium statistics and relaxation behavior derived from polymer statistical

mechanics, and hydrodynamic interaction with the solvent adapted from particle dynamics in Stokes' flow.

A fourth version of the dumbbell model will be discussed later, since it incorporates a different feature, internal viscosity.

The theoretical studies referred to above have shown that, qualitatively at least, the dumbbell gives reasonable rheological predictions for polymer solutions. More relevant to our work are its predictions concerning the coil-stretch transition and particularly its dependence on flow type. These are the predictions which need to be quantitatively tested and our data allow us to do just that. We will first describe the relevant predictions of the model and the consequences of each of the features and then show the quantitative comparisons with our data.

The dumbbell model always predicts a coil-stretch transition in strong flows at an onset shear rate, $\gamma_c \sim O(1/\tau_{db})$ where τ_{db} is the model relaxation time at equilibrium. This onset scales with $\sqrt{\lambda}$ for two-dimensional flows with some rotation. In the linear dumbbell model, the transition is a singularity in the model since the resulting growth in r is unbounded. The nonlinear spring in the CF model solves this problem by limiting the maximum amount of extension and smoothing out the transition over a range of shear rates. A major result of adding the conformation-dependent friction to the nonlinear dumbbell model (the VF model) is a discontinuous jump in r at γ_c to a nearly fully extended state. The increased frictional grip of the solvent on the dumbbell allows it to remain in such a state when γ is reduced below γ_c. Thus, in the preaveraged form usually studied, the isotropic variable friction (VF) model predicts a hysteresis in the steady-state end-to-end distance in extensional flows. The hysteresis also appears in any other steady-state property dependent on $\mathbf{r}$, such as the birefringence or the stress. Since experimental realizations of extensional flow are always limited to a finite portion of the flow domain, polymer molecules enter from regions of weak flow and spend only a finite

time period in the extensional flow region. Thus polymer deformation is always transient, and it is very difficult to verify or disprove the existence of such an effect. More realistic "*quasi*-steady-state" predictions based on transient calculations with a finite residence time[11] predict that the coil-stretch transition would be smoothed over a range of shear rates much as in the constant-friction (CF) nonlinear dumbbell model. For this reason, steady extensional flow experiments can be modeled almost as well by the CF model as by the VF model. However, the increased frictional grip in the VF model also causes relaxation from an extended state to occur on a much longer time scale than the near equilibrium relaxation of r, and there is clear experimental evidence that polymer relaxation from an extended state is much slower, as predicted by the VF model.[10] This experimental result is also suggestive of the existence of at least an effective hysteresis effect. Another experimental test of the VF model is provided via FB measurements in steady two- and four-roll milling flows of polyelectolyte solutions.[44] The change in hydrodynamics and the resulting shift in the critical shear rate for onset of birefringence due to the electrostatic expansion of the equilibrium dimensions can be predicted by the charged dumbbell model[45] with VF (and nonlinear, or FENE, spring), but not by a charged FENE model with only CF.[44]

Another effect of VF in the nonlinear dumbbell is that the model approaches full extension even in simple shear flow at not so very high shear rates, $\gamma \sim O(10/\tau_{db})$. This directly conflicts with all available data, including FB data for our PS solutions in a Couette device, which show no more than 20% of Δn_∞ ever attained even at shear rates where $\gamma\tau \sim 200$. This model prediction also shows up as an *increase* in the shear viscosity with increasing shear rate, which also lacks any experimental justification. Including the effect of strain-inefficiency in rotation is expected to remedy this shortcoming.[24] The theoretical study of the anisotropic, variable friction, strain-inefficient dumbbell (the SI model) does show improved simple shear

behavior, including, at least qualitatively, the expected rheological predictions for polymer solutions, such as shear thinning and non-zero first and second normal stress differences. We will present some quantitative tests of the SI model as well as the simpler CF and VF forms of the model. Our data are particularly suitable because they cover the range of flow types very near simple shear flow where the VF model begins to break down and where it is hoped that the SI features will improve the model predictions.

The detailed development of the CF, VF, and SI versions of the dumbbell model has been given in other references.[22-24] Our nomenclature follows as closely as possible that of References 23 and 24. However, the dimensionless shear rates defined in these two papers differ by a factor of two. Here, we choose to define the relaxation time to be $\zeta_0/4\xi_0$ which gives a model consistent with those of most other authors.[22,23,40,42,47-49] With this choice of relaxation time, the model predicts the dimensionless shear rate at the onset of the coil-stretch transition to be $\gamma_c \sim \frac{1}{2}$. The other choice sometimes used[24,45] gives $\gamma_c \sim 1$.

The calculations we present are based on the "preaveraged" equation for the evolution of the second moments of $\mathbf{r}$. We cast it in the dimensionless form

$$\frac{\mathrm{d}\langle \mathbf{rr} \rangle}{\mathrm{d}t} = \mathbf{L} \cdot \langle \mathbf{rr} \rangle + \langle \mathbf{rr} \rangle \cdot \mathbf{L}^{\mathrm{T}} - f(r) \langle \mathbf{rr} \rangle + \frac{\mathbf{I}}{3NQ(r)} \tag{19}$$

in which r and $\mathbf{r}$ are now dimensionless variables, having been divided by the contour length, L. In equation (19), $\mathbf{I}$ is the unit tensor, and $\mathbf{L}$ is the effective velocity gradient tensor, $\mathbf{L}=\tau_{db}(\mathbf{\Gamma} - \frac{\epsilon_0}{Nr^2+3}\mathbf{D})$, with $\mathbf{D}$ the rate of strain tensor and ϵ_0 a parameter specifying the amount of strain-inefficiency present. The function $Q(r)=1$ for the CF model, and $Q(r)=\sqrt{N}r$ for the VF and SI models. The function $f(r)$ also depends on the particular choice of model features. For the CF model, $f(r) = H(r) = 1/(1-r^2)$. For the VF model, $f(r) = (H(r) + 1/3Nr^2)/Q(r)$. For

the full anisotropic, variable friction, dumbbell with strain-inefficient rotation (SI),

$$f(r) = \frac{1}{\sqrt{N}r}\left\{\frac{H(r)}{1-\sigma} + \frac{1}{3Nr^2}\left[1 - \frac{1}{r\sqrt{N}+1}\left(\frac{2r\sqrt{N}}{r\sqrt{N}+1} + 2(r\sqrt{N}-1)\right)\right]\right\}. \tag{20}$$

The function $2Q(r)f(r) \equiv$ X in the notation of Reference 24, and $\sigma = \frac{1}{2}(1-1/r\sqrt{N})$. The flow birefringence is obtained from the moments using the relation[46]

$$\frac{\Delta n}{\Delta n_\infty} = [\langle x^2 - y^2\rangle^2 + 4\langle xy\rangle^2]^{\frac{1}{2}}. \tag{21}$$

Two experimental "facts of life" must be included for quantitative comparisons of the model predictions with our data. As mentioned above, extensional flow is always transient in nature from the Lagrangian point of view of the macromolecules, because they follow streamlines which always connect regions of relatively weak extension with the stronger extensional flow regions. Only at a stagnation point will there be true steady-state extensional flow, and no finite size particle (or polymer molecule) will remain there indefinitely. We therefore integrate the moment equations from an initial equilibrium configuration for a finite transit time increment which was estimated following the approach of Reference 11 with l/D=.003. In addition we perform an average of all predictions over the molecular weight distribution using a log-normal distribution. These two steps have been shown to be necessary to predict the shape of the data quantitatively, even for the fairly narrow molecular weight distributions of our polystyrene samples.[11,47]

Besides the general shape of the flow birefringence data, the feature of interest for model comparison is the dependence of the FB on flow type, especially for flows that are only slightly more extensional than simple shear flow. The main feature of the FB data is its degree of correlation with $\gamma\sqrt{\lambda}$ for $.019 \leq \lambda \leq 1$. Since our FB data show essentially perfect correlation at onset, and the scatter in saturation behavior at high shear rates for different flow types is probably within experimental uncertainty, we will use a single master curve taken from the PS8 in LV data of

Figure 14 (correctly plotted versus measured velocity gradients) and a master curve from the PS2 in LV data of Figure 16 for our comparisons with model predictions.

An attempt was made to make physically reasonable choices for the two parameters appearing in the dumbbell model, N and τ_{db}, which are the number of statistical segments and the dumbbell model relaxation time, respectively. The value for N was obtained from the measured value of Δn_∞ using equation (15) (with $\Delta\alpha = -145 \times 10^{-25}$cc [34]), and was found to be ~5000 for PS8 and ~1200 for PS2. The relaxation time appropriate to the polymer can be estimated from Table II using the Zimm formula $\tau_1 = .422\tau$.[48] The work of Peterlin[49] showed that the linear dumbbell model overestimates the relaxation time by a factor of 2.214 when compared to the Zimm model.[48] He did this by comparing the predicted amounts of extension of the dumbbell, $\frac{r^2}{r_0^2} - 1$, in simple shear flow at small shear rates as a function of dimensionless shear rate, $\beta = \gamma\tau$, where τ is the experimental relaxation time from $[\eta]$ measurements. The same calculation shows that the variable friction models also overestimate the relaxation time, but by a factor of 4.067 with respect to the Zimm model. Table IV shows the the predicted values of τ_{db} to be used in the CF and VF models for PS8 and PS2 in LV. These compare quite well with the values which give the best fit to the data which are also given in the table. The small differences observed are to be expected since these solutions are not exactly at theta conditions as the Zimm formula implies.

TABLE IV. Dumbbell Model Parameters

	PS2		PS8		Predicted τ_{db}	
	N	τ_{db}	N	τ_{db}	PS2	PS8
Constant Friction	1200	.041	5000	.42	.040	.35
Variable Friction	1200	.025	5000	.19	.022	.19

First of all, we compare the model predictions for the CF (or FENE) dumbbell with the FB data. Figures 27 and 28 show predicted FB curves for $\lambda = 1$ and 0.019 and representative data for PS8 and PS2, respectively, in LV. The correlation of the model predictions for different flow types agrees with the data and the quantitative prediction of the shape of the FB curves is very good, too. This model also gives reasonable simple shear flow predictions. Considering our arguments for using variable friction, one may well wonder how the CF model can do so well in extensional flow. These results suggest that the importance of increased frictional grip in an unraveling polymer is secondary to that of the finite residence time for stretching in the strong flows that we have studied. Since both models would be allowed the same time increment, and therefore the same total possible deformation at a given shear rate, they can be expected to give about the same FB predictions in "steady" strong flows.

The solid curves in Figure 29 and Figure 30 show predictions for the variable friction (VF) model with $\lambda = 1$ and 0.019. It is apparent that the FB data for small λ correlates much better with the data for λ=1 than this version of the dumbbell model predicts. The model fits for λ=1 but not for λ=.019. This reveals a tendency for the VF model to overestimate the polymer extension in flows that are slightly more extensional in character than simple shear flow, as well as in simple shear flow which was pointed out earlier. Fuller and Leal presented similar VF model predictions[11] for values of λ down to 0.1 showing that this tendency begins to appear at about λ=0.2.

It seems that there are two possible explanations for the failure of the VF model to properly describe flows with small values of λ. In light of the success of the CF model, it might be suggested that VF is simply wrong, or at best, that the friction force is drastically overestimated. Though the linear form for the variable friction coefficient which has been studied to date may be greatly simplified with

respect to reality, the experimental evidence mentioned above (relaxation[10] and polyelectrolyte expansion[44]) and the sound physical reasoning behind conformation-dependent friction, leads us to conclude that the model is neither invalid nor that it greatly overestimates the friction. Rather, we feel that the failure of the model reflects its lack of proper rotational behavior in simple shear and near simple shear flows. This is exactly what the SI model seeks to remedy by giving the dumbbell the same rotational motion as an axisymmetric particle with finite axis ratio, in low Reynolds number flow.[24] Unfortunately, however, the absence of a better alternative led to the use of an equation of motion based on that of a fully *rigid* ellipsoidal particle. As a consequence, we may anticipate that the "strain-inefficient" rotation effect for a polymer will be overestimated by the SI model, but the importance of this needs to be established by comparison of model predictions with data, as presented below.

The amount of strain-inefficiency introduced is governed by the parameter ϵ_0.[24] Phan-Thien *et al.* suggested as an initial estimate a value of ϵ_0=1 based on the resulting predictions of no shear-thickening and a reasonable second normal stress ratio. We have found that this value inhibits the stretching of the dumbbell in extensional flows with flow type parameter $\lambda \leq .2$. Since our FB data for smaller λ values do not show a similar inhibition, a smaller value of ϵ_0 is suggested. Figure 31 illustrates predictions of the SI model for birefringence as a function of the eigenvalue of the velocity gradient tensor for $\lambda = 0.019$ and various values of ϵ_0. Finite transit time has been included (thus no hysteresis appears) but not polydispersity which would broaden the coil-stretch transition. It is apparent from Figure 31 that in order for the model to give full extension of the dumbbell for $\lambda = 0.019$, ϵ_0 must be 0.3–0.4 at the most. Figure 32 compares the strain-inefficient (SI) model (with ϵ_0=0.4 and with variable anisotropic friction) with the FB data for PS8 in LV. Two values of λ, 1 and 0.019 are included, and polydispersity has also been

included in the calculation. At this value of ε_0, the correlation near the onset shear rate is much improved over the VF (ε_0=0) model because the low λ curves are closer to the $\lambda = 1$ behavior. In this respect the model is an improvement over the VF model. However, the predicted saturation behavior seems to be different than our FB results. For example, in Figure 14, the λ=1 data fall below the λ=.019 data at high shear rates, just the opposite of the predicted behavior. It should be pointed out, however, that the previously mentioned instability in the FB measurement at high shear rates, and the presence of "end effects", combined with the naturally more stable flow characteristics of the two-roll mill, may be responsible for the apparent reversal of saturation values in the experimental data. The main rheological ramifications of $\varepsilon_0 \approx 0.4$ are that the predicted normal stress *ratio* is reduced to ~4% instead of 12%,[24] and that there is a slight shear thickening in the shear viscosity. The degree of shear thickening for various values of ε_0 is shown in Figure 33. At this point there are probably too little dilute solution data to judge these rheological predictions further. It is likely, however, that the description of a polymer's hydrodynamic behavior could be improved over this first attempt, which is based upon the predicted hydrodynamic behavior of a *rigid* axisymmetric particle with a finite axis (or effective axis) ratio. It seems obvious that a polymer molecule may act more like a viscous drop or some other particle with only partial "rigidity" in its rotational motion than a solid particle. The development of a more realistic hydrodynamic theory for macromolecular motion is likely to be a good topic for further research on dumbbell modeling. Better relaxation data would be very useful for further testing of these models, as well as steady-state data in flows even closer to simple shear flow, or with "semi-rigid" polymer-solvent systems which might be more likely to show inhibited stretching due to strain-inefficiency at the values of λ currently available.

One final proposed feature of polymer behavior which has been widely studied

in dumbbell models is internal viscosity (IV).[23] This is a force proportional to the rate of stretching of the dumbbell and is intended to model the finite response time which a real polymer probably exhibits in response to a deforming force. Large values of the internal viscosity actually produce a reduced stretching effect in the dumbbell model similar to that produced by the inclusion of strain-inefficiency. Since the resistance to large stretch rates makes the response of the dumbbell much slower, it can not be as greatly extended in extensional flows with considerable rotation as in pure extension. It will tend to rotate away from the strain axis before it can be stretched. However, a significant difference between internal viscosity and strain-inefficiency is that IV has its largest effects in flows with values of λ between 0.2 and 0.5, while SI affects simple shear the most with the effects decreasing as λ approaches ~0.2. The IV model thus seems to be less likely to produce the same degree of correlation of extension in various flow types with $\gamma\sqrt{\lambda}$ as the data show.

Predictions for $0.1 \leq \lambda \leq 1$ were given by Fuller and Leal[11] for the dumbbell model with conformation-dependent friction and several values of the internal viscosity parameter, ϵ. Their results showed good correlation only for $\lambda > 0.2$ and values of $\epsilon < 0.3$. They also showed that the internal viscosity in the model had a strong effect on the predicted correlation of FB with $\gamma\sqrt{\lambda}$. It seemed that the degree of correlation with the λ=1 curve was made worse for values of λ between 0.2 and 0.5, but for λ=0.1 it improved, as ϵ was increased. Extending the calculation to lower values of λ shows that internal viscosity in general only *improves* the correlation for a small range of λ near .1, but *worsens* the correlation for the values of λ closer to 1 which are obtained in the four-roll mill. For the range of λ very near simple shear as obtained in the two-roll mills, the correlation is left unchanged. The dashed lines in Figure 29 show that with conformation-dependent friction there is a similar spread with or without internal viscosity between the λ=1 and 0.019 predictions. Thus it appears that internal viscosity combined with variable friction

cannot make the model show the same correlation as the data, and is therefore not a necessary or even a desirable feature in the dumbbell model for flexible polymers such as polystyrene.

5. CONCLUSIONS

We have measured the flow birefringence of PS in viscous solvents in the four-roll and two-roll mills. The data obtained correlate with the dimensionless eigenvalue of the velocity gradient tensor $\tau\gamma\sqrt{\lambda}$. The time constant τ is based on intrinsic viscosity measurements, 0.422τ being the longest Zimm time. Data taken over a wide range of extensional flow types (λ values) and the entire range of polymer extensions collapse to a single curve for a given polymer sample. This master curve is very sensitive to the molecular weight distribution of the sample and also to the transient nature of the extensional flow field.

Various forms of the dumbbell model were evaluated for their ability to match the shape of the FB data and the high degree of correlation over the wide range of flow types, $.019 \leq \lambda \leq 1$. The dumbbell model with nonlinear spring (FENE dumbbell) gives very good modeling of this approximately steady-state data in spite of the fact that it does not include conformation-dependent friction which is believed necessary to properly model the drastic changes in hydrodynamic interaction between solvent and polymer as it undergoes the transition from coiled to stretched state. The need for the correct form of conformation-dependent friction is most evident in modeling the relaxation of a polymer from the extended state, and, in a more subtle way, by birefringence studies of the effect of variable degrees of rest-state expansion in polyelectrolyte solutions with various levels of salt.

All of the forms of the variable friction model predict the shape of the data for λ=1 (pure extension) very well, but the high degree of correlation with $\gamma\sqrt{\lambda}$ for flow types close to simple shear flow (λ=0.019) is not well predicted by the VF model. This is not improved by adding internal viscosity. Changing the hydrodynamic behavior of the dumbbell to that of a rigid particle with finite axis ratio in Stokes flow by adding a limited amount of strain-inefficiency[24] (SI) does improve the model comparisons with the FB data, though not as much as could be desired.

This is not too surprising, in view of the fact that the polymer "particle" is not rigid as effectively assumed by the SI model, and it is likely that more realistic behavior for a polymer can be found, possibly by using results from the dynamics of viscous drops or other (partially) deformable particles. Nevertheless, the strain-inefficient dumbbell model is a reasonable first attempt at including all the proper fluid mechanics for the entire range of conformations involved in a coil-stretch transition. Its predictions give very reasonable quantitative agreement with our FB data and also qualitative agreement with currently available dilute solution rheological data.

The main accomplishment we report is having demonstrated that dilute solutions produce significant, measurable changes in the flow fields in these flow devices. The onset point for these changes corresponds in these PS solutions to an increase in the stress of ~500 times that of the Newtonian solvent, but only in a very localized region along the outgoing streamline. The local nature of the viscosity increase is indicated by the flow birefringence, which also directly connects the coil-stretch transition with the flow-modification effects. This was accomplished by measuring velocity gradients directly instead of velocities or streamlines. The results support the view derived from more concentrated solution studies and physical reasoning that polymers in dilute solution can significantly alter flow fields by inhibiting the development of high strain rates in extensional regions of the flow. Though the solution is nominally very dilute, the flow modification seems to have its onset when the polymers are stretched to an effective volume concentration of ~5000.

Further work is being directed at correlating this onset of flow field changes with concentration, molecular weight, and method of solution preparation. Full scale numerical calculations using dumbbell type constitutive equations are also being carried out to try to understand and predict the flow changes observed. This work may also allow us to determine whether the observed instabilities in the FB measurements are related somehow to the well-known numerical problems at $O(1)$

Deborah numbers.

References

1. F. Durst, R. Haas, and W. Interthal, *Rheol. Acta*, **21,** 572 (1982).
2. G. Chauveteau, M. Moan, and A. Magueur, *J. Non-Newtonian Fluid Mech.*, **16,** 315 (1984).
3. E. W. Merrill and A. F. Horn, *Polym. Comm.*, **25,** 144 (1984).
4. D. F. James and J. H. Saringer, *J. Rheol.*, **26,** 321 (1982).
5. A. V. Shenoy, *Coll. Polym. Sci.*, **262,** 319 (1984).
6. O. Scrivener, C. Berner, R. Cressely, R. Hocquart, R. Sellin, and N. S. Vlachos, *J. Non-Newtonian Fluid Mech.*, **5,** 475 (1979).
7. R. Cressely and R. Hocquart, *Optica Acta*, **27,** 699 (1980).
8. D. P. Pope and A. Keller, *Colloid Polym. Sci.*, **256,** 751 (1978).
9. C. J. Farrell, A. Keller, M. J. Miles, and D. P. Pope, *Polymer*, **21,** 1292 (1980).
10. M. J. Miles and A. Keller, *Polymer*, **21,** 1295 (1980).
11. G. G. Fuller and L. G. Leal, *Rheol. Acta*, **19,** 580 (1980).
12. A. Ambari, C. Deslouis, and B. Tribollet, *Chem. Eng. Comm.*, **29,** 63 (1984).
13. J. N. Hoyt, J. J. Taylor, and R. L. Altman, *J. Rheol.*, **24,** 685 (1980).
14. V. N. Tsvetkov, V. E. Eskin, and S. Y. Frenkel, *Structure of Macromolecules in Solution, Vol. 3, trans. by* C. Crane-Robinson, National Lending Library for Science and Technology, Boston, 1971.
15. P. G. DeGennes, *J. Chem. Phys.*, **60,** 5030 (1974).
16. E. J. Hinch, *Phys. Fluids*, **20,** S22 (1977).

17. G. G. Fuller, J. M. Rallison, R. L. Schmidt, and L. G. Leal, *J. Fluid Mech.*, **100,** 555 (1980).

18. F. C. Frank and M. R. Mackley, *J. Polym. Sci. Polym. Phys. Ed.*, **14,** 1121 (1976).

19. M. V. Berry and M. R. Mackley, *Phil. Trans. Roy. Soc. Lond.*, **A287,** 1 (1977).

20. M. R. Mackley, *J. Non-Newtonian Fluid Mech.*, **4,** 111 (1978).

21. K. Gardner, E. R. Pike , M. J. Miles, A. Keller, and K. Tanaka, *Polymer*, **23,** 1435 (1982).

22. R. B. Bird, O. Hassager, R. C. Armstrong, and C. F. Curtiss, *Dynamics of Polymeric Liquids: Vol. 2, Kinetic Theory*, John Wiley & Sons, New York, 1977.

23. G. G. Fuller and L. G. Leal, *J. Non-Newtonian Fluid Mech.*, **8,** 271 (1981).

24. N. Phan-Thien, O. Manero, and L. G. Leal, *Rheol. Acta*, **23,** 151 (1984).

25. B. K. Varma, Y. Fujita, M. Takahashi, and T. Nose, *J. Polym. Sci. Polym. Phys. Ed.*, **22,** 1781 (1984).

26. B. J. Berne and R. Pecora, *Dynamic Light Scattering*, John Wiley & Sons, New York, 1976.

27. G. G. Fuller and L. G. Leal, *J. Polym. Sci. Polym. Phys. Ed.*, **19,** 557 (1981).

28. G. Marrucci and G. Astarita, *AIChE J.*, **13,** 931 (1967).

29. R. L. Lagnado, *Ph. D. Thesis*, California Institute of Technology, Pasadena, 1985.

30. G. B. Jeffery, *Proc. Roy. Soc. Lond.*, **A101,** 169 (1922).

31. R. L. Lagnado, N. Phan-Thien, and L. G. Leal, *Phys. Fluids*, **27,** (1984).

32. R. Ng, *private communication*, 1985.

33. W. Philippoff, *Proc. IV Int. Cong. on Rheol., Part 2, ed.* E. H. Lee, Interscience, New York, p. 343 (1980).

34. V. N. Tsvetkov, in *Polymer Handbook, eds.* J. Bandrup and E. H. Immergut, Interscience, New York, p. V-75, 1966.

35. S. I. Muller, R. C. Armstrong, and R. A. Brown, Paper presented at the International Conference on Viscoelasticity of Polymeric Liquids, Grenoble, France (Jan. 1986).

36. R. L. Lagnado, N. Phan-Thien, and L. G. Leal, *J. Non-Newtonian Fluid Mech.*, **18,** 25 (1985).

37. J. A. Odell, A. Keller, and M. J. Miles, *Polym. Comm.*, **24,** 7 (1983).

38. G. K. Batchelor, *J. Fluid Mech.*, **46,** 813 (1971).

39. H. Yamakawa, *Modern Theory of Polymer Solutions*, Harper & Row, New York, 1971.

40. H. R. Warner, *Ind. Eng. Chem. Fundam.*, **11,** 379 (1972).

41. G. Ronca and D. Y. Yoon, *J. Chem. Phys.*, **80,** 930 (1984).

42. R. I. Tanner, *Trans. Soc. Rheol.*, **19,** 557 (1975).

43. F. H. Abernathy, J. R. Bertschy, R. W. Chin, and D. E. Keyes, *J. Rheol.*, **24,** 647 (1980).

44. P. N. Dunlap, C.-H. Wang, and L. G. Leal, "An Experimental Study of Dilute Polyelectrolyte Solutions in Strong Flows," *submitted to J. Polym. Sci. Polym. Phys. Ed.*, 1986.

45. P. N. Dunlap and L. G. Leal, *Rheol. Acta*, **23,** 238 (1984).

46. A. Peterlin, *Polymer*, **2,** 257 (1961).

47. L. G. Leal, G. G. Fuller, and W. L. Olbricht, in *Viscous Flow Drag Reduction, ed.* G. R. Hough, *Prog. Astro. Aero.*, **72,** 351 (1980).

48. B. H. Zimm, *J. Chem. Phys.*, **24,** 269 (1956).

49. A. Peterlin, *J. Chem. Phys.*, **39,** 224 (1963).

Figure Captions

Figure 1. Schematic of the homodyne light-scattering setup showing angle definitions, vector orientations, *etc.* The flow is in the xy-plane.

Figure 2. Streamlines of the various idealized, linear two-dimensional flows and how they are obtained in four- and two-roll mills.

Figure 3. Relative values of γ or $\gamma\lambda$ measured at the center of the four-roll mill with ϕ=0 or 90°, respectively, and plotted versus the angular velocity of the faster pair of rollers.

Figure 4. Relative velocity gradient versus roller speed at the center of the four-roll mill for a glycerol/water mixture with $\eta \approx 10$ p. For this solution, $\mathrm{Re} \approx 0.25\omega$.

Figure 5. Relative velocity gradient versus roller speed at the center of the four-roll mill for a glycerol/water mixture with $\eta \approx 1.4$ p. For this solution, $\mathrm{Re} \approx 1.8\omega$.

Figure 6. Velocity gradient profiles along the incoming and outgoing streamlines in the four-roll mill in glycerol at two values of ω corresponding to Re=.37 and 3.7.

Figure 7. Velocity gradient profiles across the outgoing axis in glycerol. X is the distance from the stagnation point (measured along the outgoing axis), and Y is the distance from the center streamline.

Figure 8. Bipolar cylindrical coordinates used in the analytical solution for creeping flow in the two-roll mill.

Figure 9. Comparison of *top:* plot of the exact streamlines calculated from equation (9); *center:* photo of actual streamlines in a two-roll mill with λ=0.135 according to equation (10); *bottom:* plot of the corresponding theoretical linear flow field.

Figure 10. Comparison of velocity profiles measured along the gap centerline in two-roll mills for glycerol with exact theoretical predictions. Inset shows orientation of scattering vector and approximate location of the measurements.

Figure 11. Measured velocity gradients for Newtonian fluid at two-roll mill stagnation points versus the angular velocity of the rollers.

Figure 12. Relative orientations of the polarizer, analyzer, flow field, and polymer in the flow birefringence experiment.

Figure 13. Flow birefringence of the solvent LV plotted versus the rate of strain. Data cover the range of flow types $1 \geq \lambda \geq 0.019$.

Figure 14. Flow birefringence of 100 ppm solution of PS8 in LV versus velocity gradient tensor eigenvalue.

Figure 15. Flow birefringence of 100 ppm solution of PS8 in TCP.

Figure 16. Flow birefringence of 100 ppm solution of PS2 in LV.

Figure 17. Plot of flow birefringence versus dimensionless eigenvalue of the velocity gradient tensor. The solutions are 100 ppm PS8 in three solvents and in the two- and four-roll mills as labeled. The characteristic times, τ, are given in Table II.

Figure 18. Flow visualization of a vertical plane of the flow at the center of the four-roll mill for a 118 ppm PS8 solution. The Reynold's numbers range from about 1.2 to 10.

Figure 19. Measured values of $\gamma\sqrt{\lambda}$ in the 100 ppm PS8 in LV solution of Figure 14 versus the Newtonian values for many values of λ.

Figure 20. Flow birefringence and velocity gradients at the center of the four-roll mill for a 100 ppm solution of PS8 in LV before and after filtering (which appears to reduce the concentration to 80 ppm).

Figure 21. Flow birefringence and velocity gradients measured at the stagnation point in two-roll mill #2 and at three positions in the four-roll mill versus roller speed for 118 ppm PS8 in LV/TCP mixture. X is the distance of the measurement downstream from the stagnation point.

Figure 22. measured velocity gradient versus position on the outgoing streamline in pure extension in the four-roll mill for 80 ppm PS8 in LV and for pure LV.

Figure 23. Variation of measured velocity gradients with position along lines perpendicular to the outgoing streamline (*i.e.*, the y direction) at several positions along it for 118 ppm PS8 in LV/TCP. *Top:* ω=3.5 s^{-1} and *Bottom:* 10.5 s^{-1}.

Figure 24. Variation of measured velocity gradients with position along lines perpendicular to the outgoing streamline (solid lines) and also along lines perpendicular to the incoming streamline (dashed lines). These cross-profiles are measured at several positions along the axes in pure extension in the four-roll mill at ω=17.5 s^{-1} for 80 ppm PS8 in LV.

Figure 25. To scale plot of velocity gradient field in the four-roll mill. The cross-profiles of Figure 24 are positioned so that the center point of the incoming profile is at the actual location of the measurement. The profiles measured *along* the incoming and outgoing axes for this roller speed from Figure 22 are also included. All data are scaled properly for direct comparison of shapes.

Figure 26. Flow birefringence at stagnation point of four-roll mill in pure extension for 100 ppm PS8 in LV. Data was taken on a fresh solution, after a complete set of FB measurements (about 3 hours of shearing at $\gamma\sqrt{\lambda}$ up to 20 s^{-1}), and after extensive HLS experiments and flow visualization studies (about 20 hours more at up to 40 s^{-1}).

Figure 27. Predictions of the FENE dumbbell with constant friction (CF) for $\lambda =$ 1.0 and 0.019 along with representative flow birefringence data for PS8 in LV in flow types ranging from $\lambda = 1.0$ to 0.019.

Figure 28. Predictions of the FENE dumbbell with constant friction (CF) for $\lambda =$ 1.0 and 0.019 along with representative flow birefringence data for PS2 in LV in flow types ranging from $\lambda = 1.0$ to 0.019.

Figure 29. Predictions of the FENE dumbbell with variable but isotropic friction (VF model) for λ=1.0 and 0.019 along with representative flow birefringence data for PS8 in LV. Solid curves are with no internal viscosity and dashed curves with the internal viscosity parameter ϵ=0.5.

Figure 30. Predictions of the FENE dumbbell with variable but isotropic friction (VF model) for λ=1.0 and 0.019 along with representative flow birefringence data for PS2 in LV.

Figure 31. Model predictions of birefringence versus eigenvalue of velocity gradient tensor for λ=0.019 with N=5000 and various values of the strain-inefficiency parameter, ϵ_0. Finite transit time has been included but not polydispersity.

Figure 32. Comparison of FB data for PS8 in LV with dumbbell model predictions. Model includes variable anisotropic friction, and strain-inefficiency parameter, ϵ_0=0.4.

Figure 33. Shear viscosity (λ=0) predictions of the SI model with N=5000 and for various values of the strain-inefficiency parameter, ϵ_0.

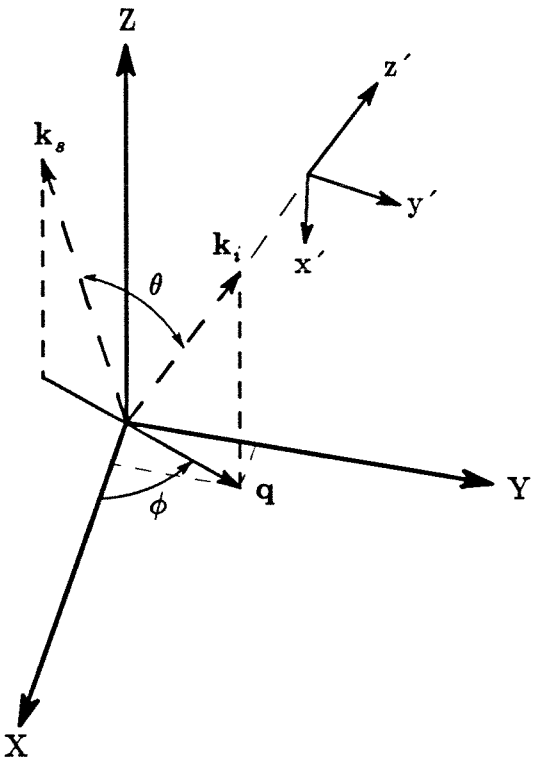

Figure 1.

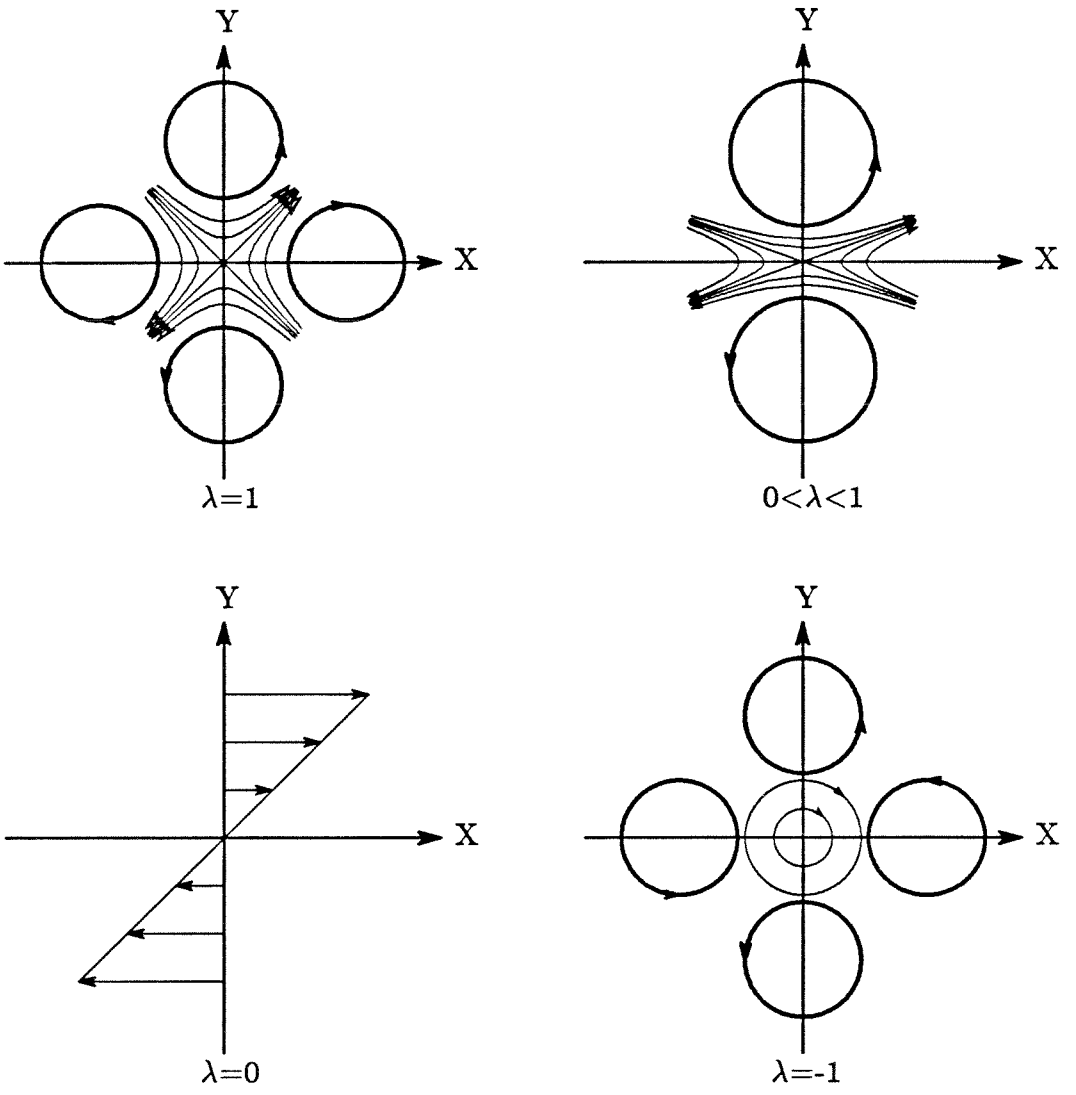

Figure 2.

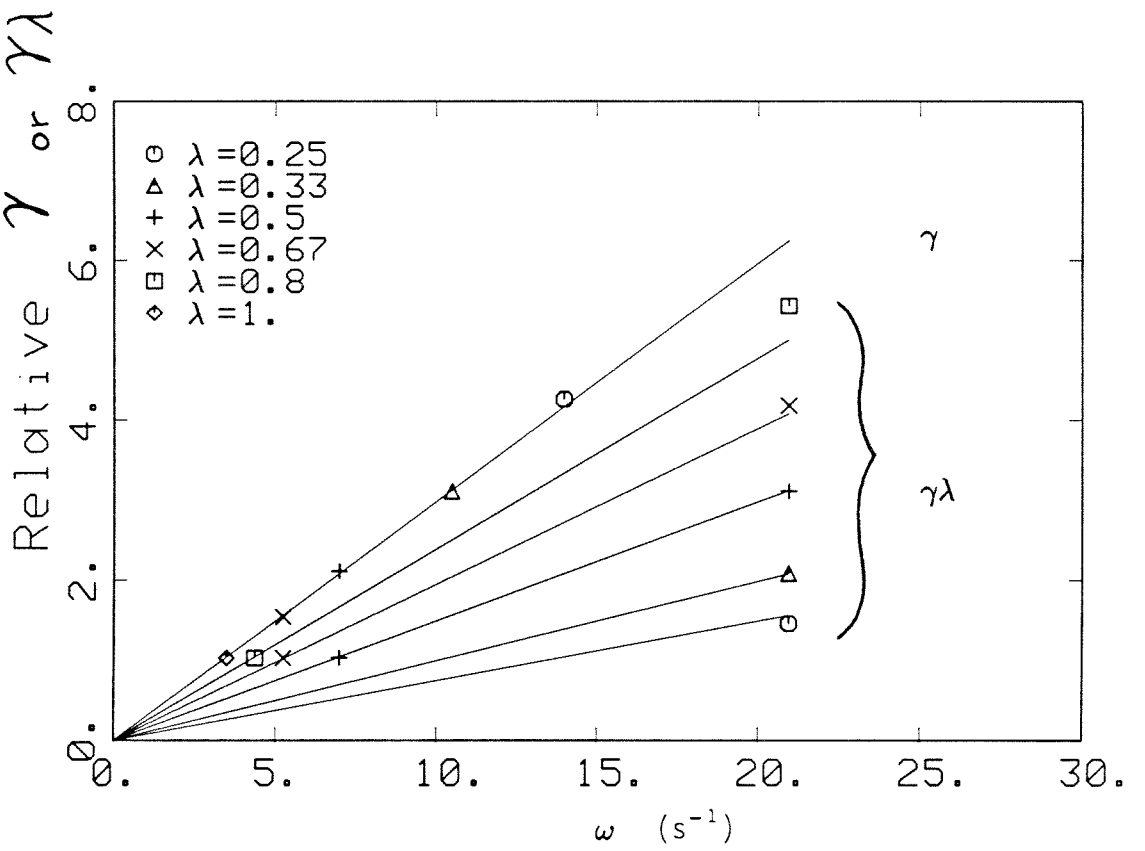
Relative γ or γλ
λ =0.25
λ =0.33
λ =0.5
λ =0.67
λ =0.8
λ =1.
γ
γλ
0.
2.
4.
6.
8.
0.
5.
10.
15.
20.
25.
30.
ω (s⁻¹)

Figure 3.

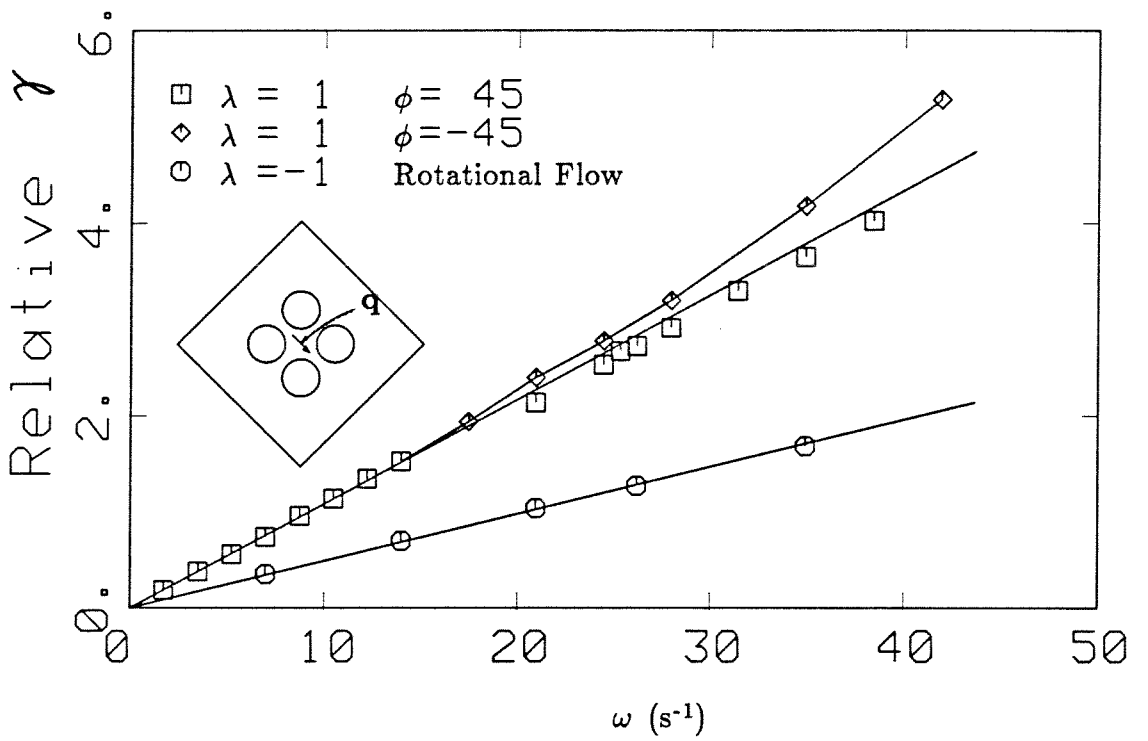
Relative γ
0.
2.
4.
6.
0
10
20
30
40
50
ω (s-1)
λ = 1 φ= 45
λ = 1 φ=-45
λ =-1 Rotational Flow
q

Figure 4.

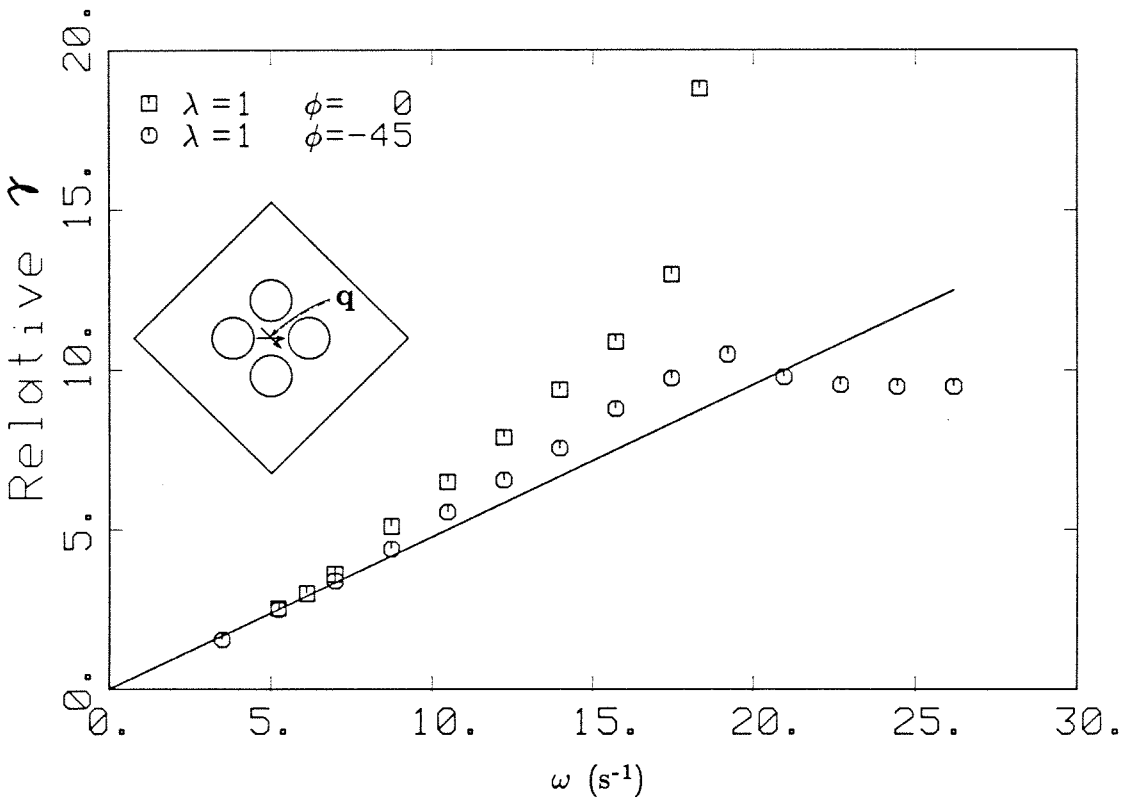

Figure 5.

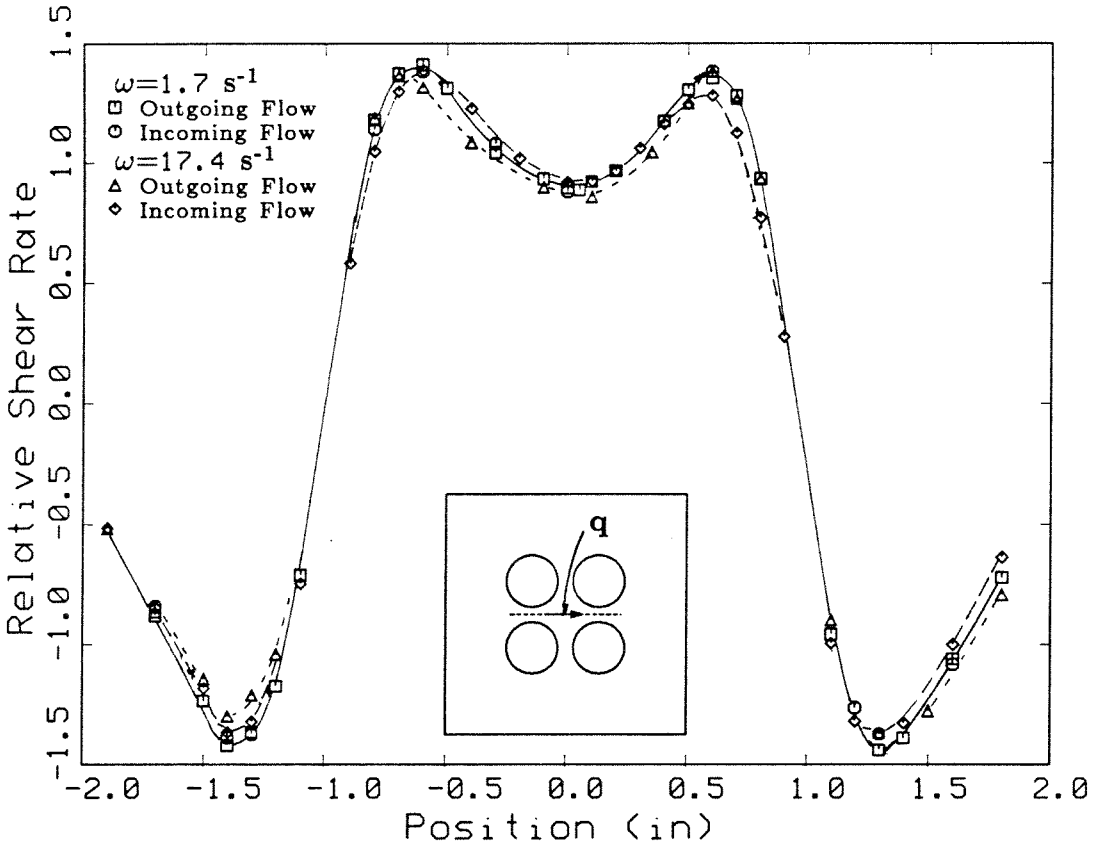
ω=1.7 s-1
Outgoing Flow
Incoming Flow
ω=17.4 s-1
Outgoing Flow
Incoming Flow
q
Relative Shear Rate
Position (in)
-2.0
-1.5
-1.0
-0.5
0.0
0.5
1.0
1.5
2.0

Figure 6.

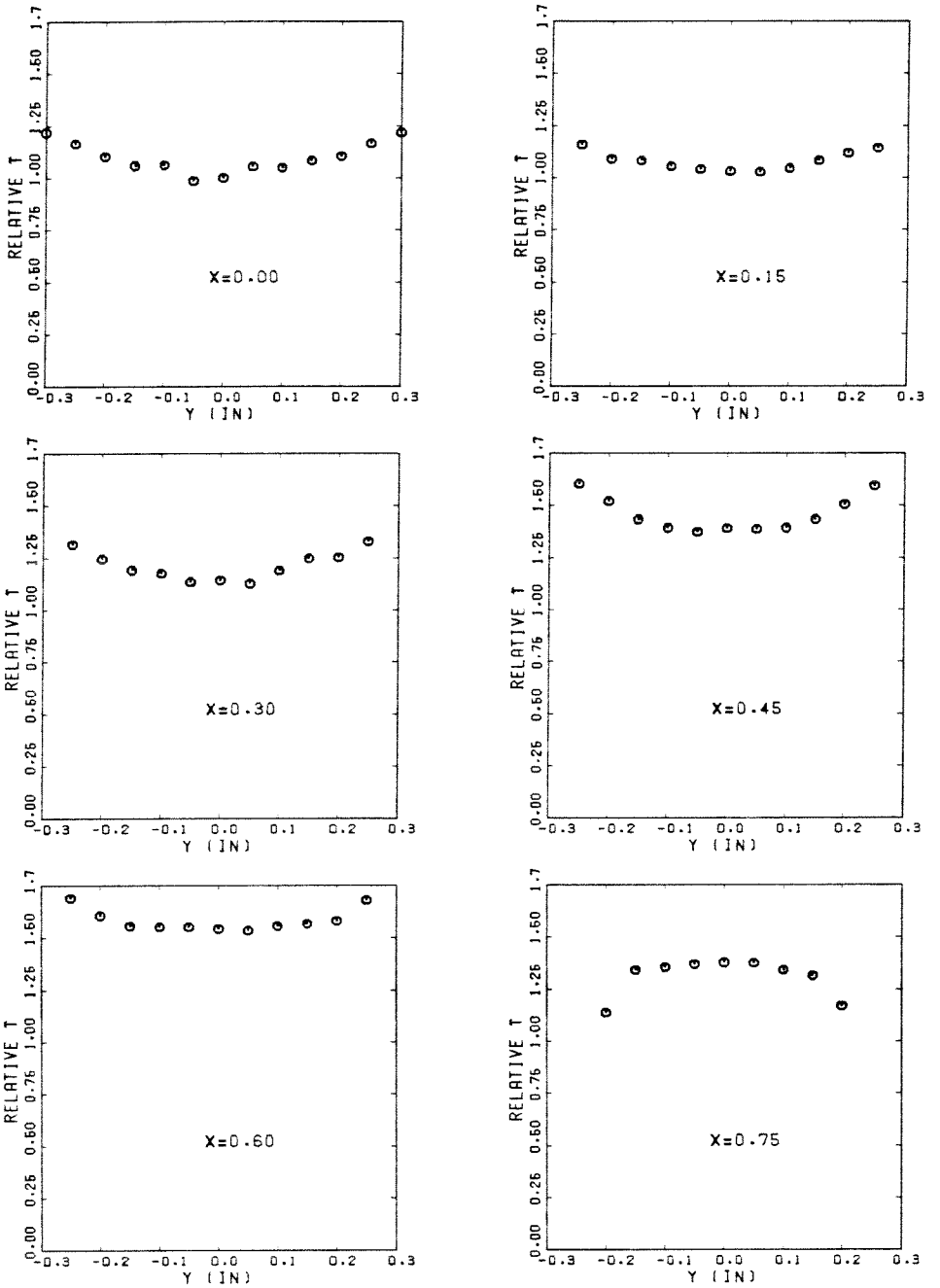
RELATIVE T
X=0.00
X=0.15
X=0.30
X=0.45
X=0.60
X=0.75
Y (IN)
0.00
0.25
0.50
0.75
1.00
1.25
1.50
1.7
-0.3
-0.2
-0.1
0.0
0.1
0.2
0.3

Figure 7.

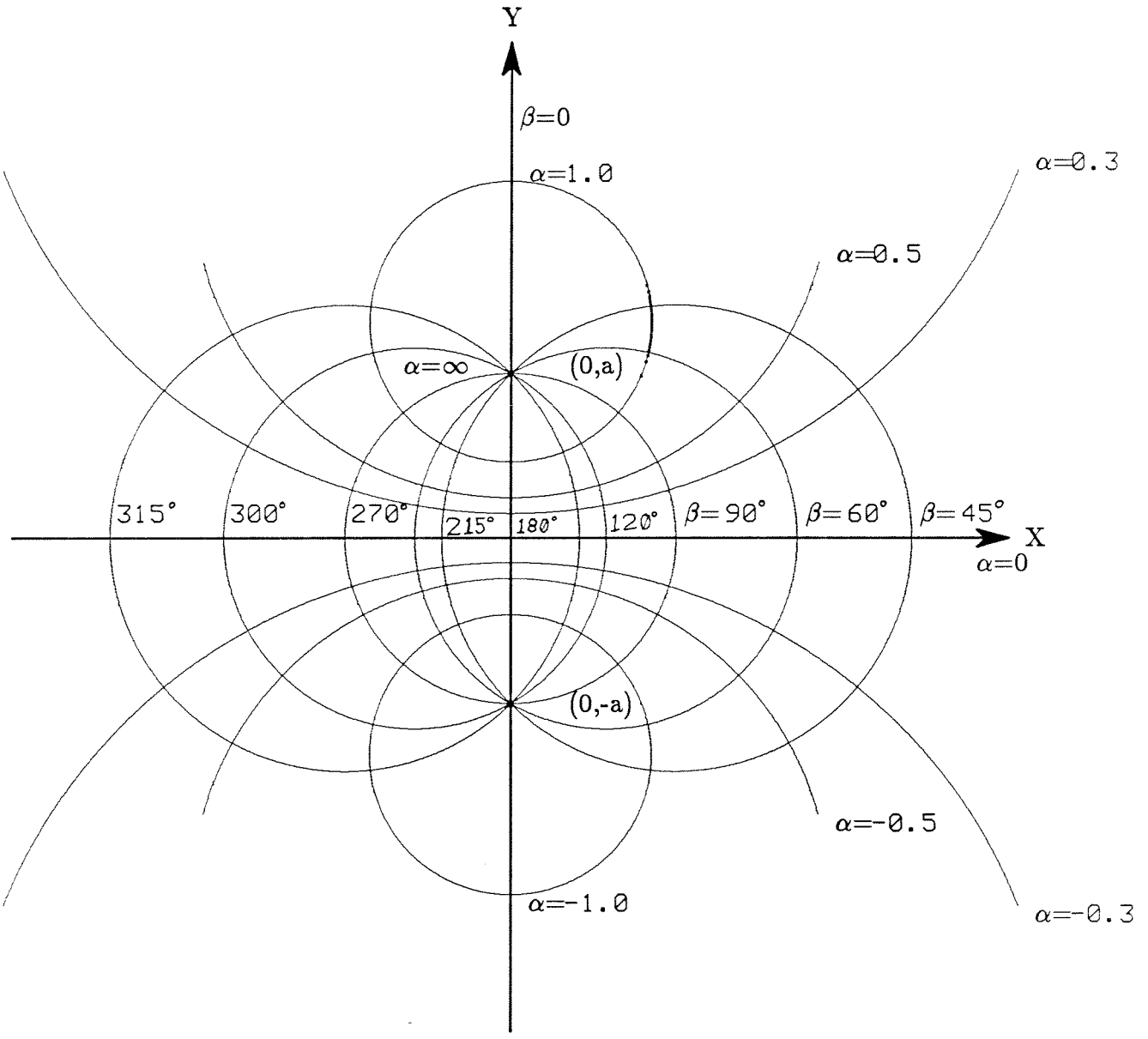
Y
β=0
α=1.0
α=0.3
α=0.5
α=∞
(0,a)
315°
300°
270°
215°
180°
120°
β=90°
β=60°
β=45°
X
α=0
(0,-a)
α=-0.5
α=-1.0
α=-0.3

Figure 8.

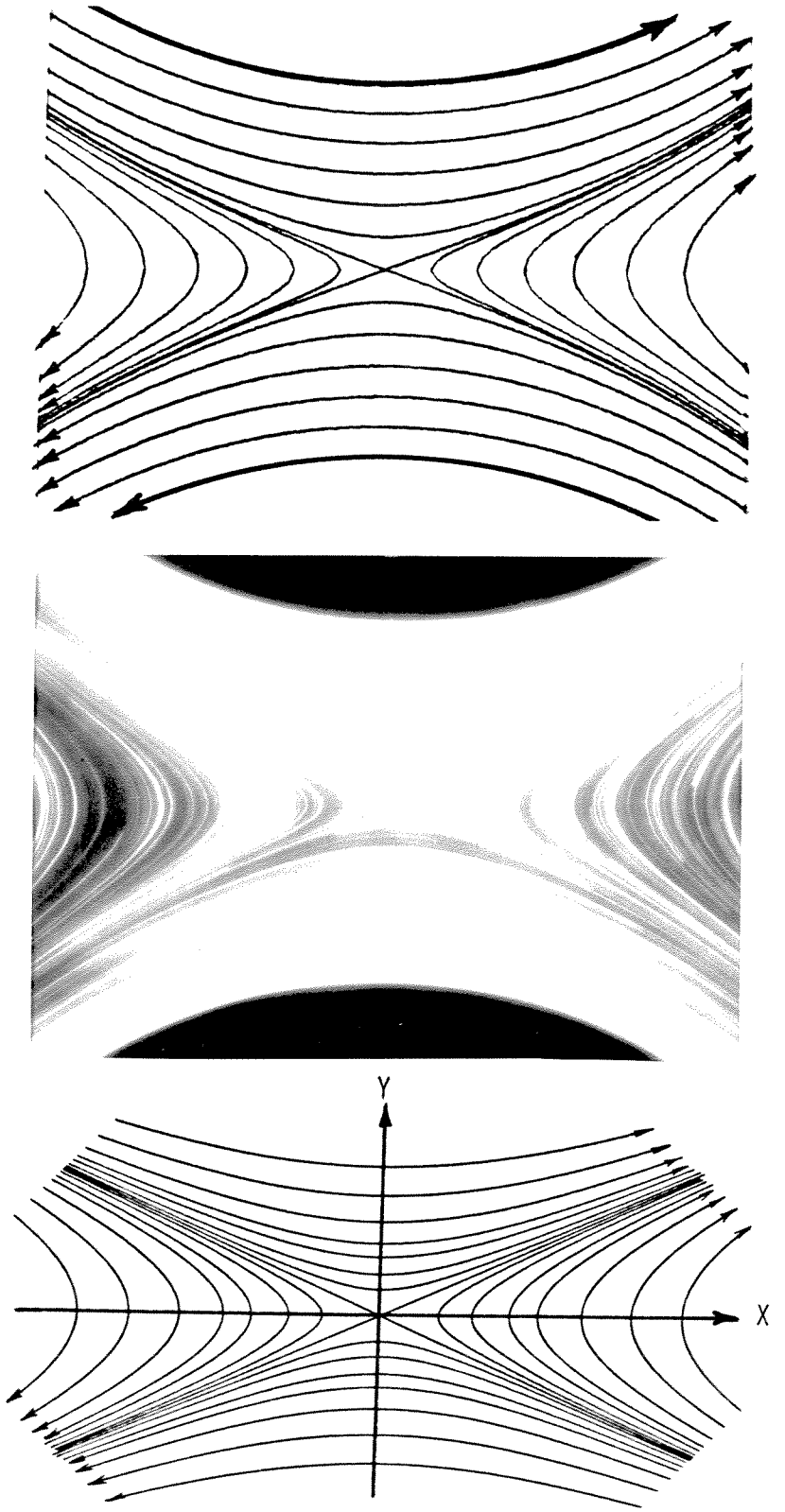

Figure 9.

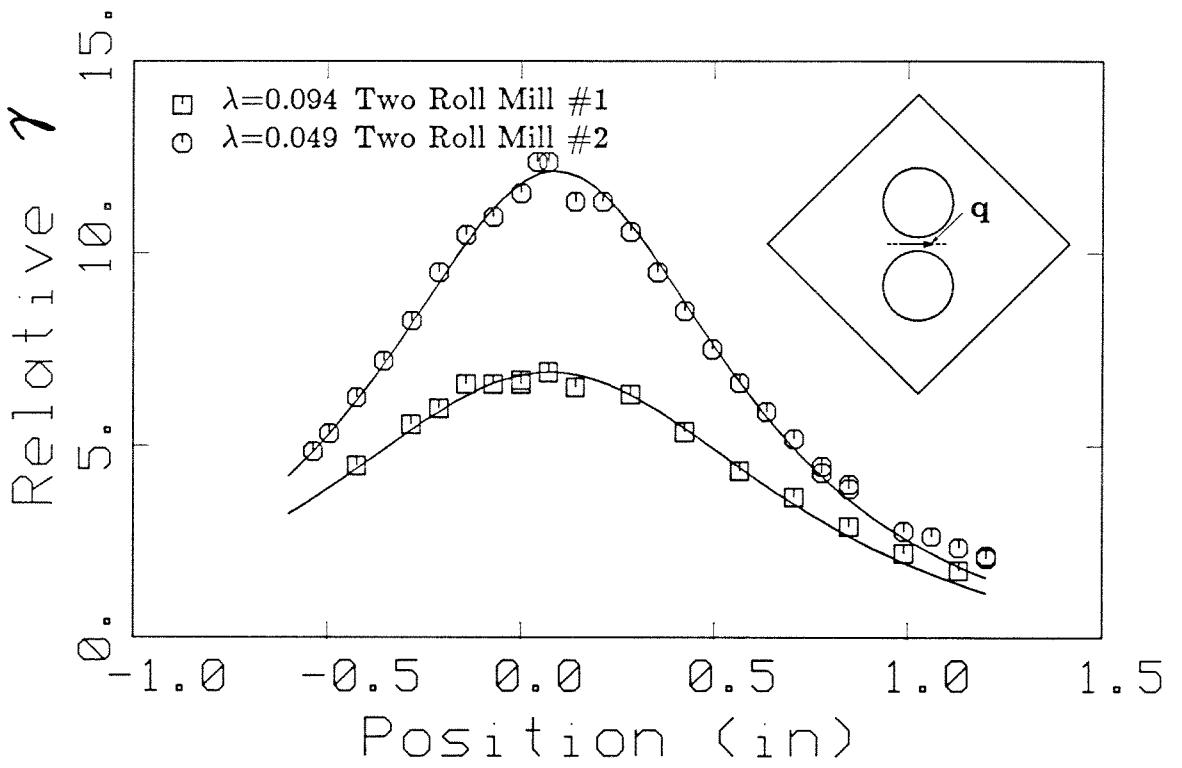
λ=0.094 Two Roll Mill #1
λ=0.049 Two Roll Mill #2
q
Relative γ
0.
5.
10.
15.
-1.0
-0.5
0.0
0.5
1.0
1.5
Position (in)

Figure 10.

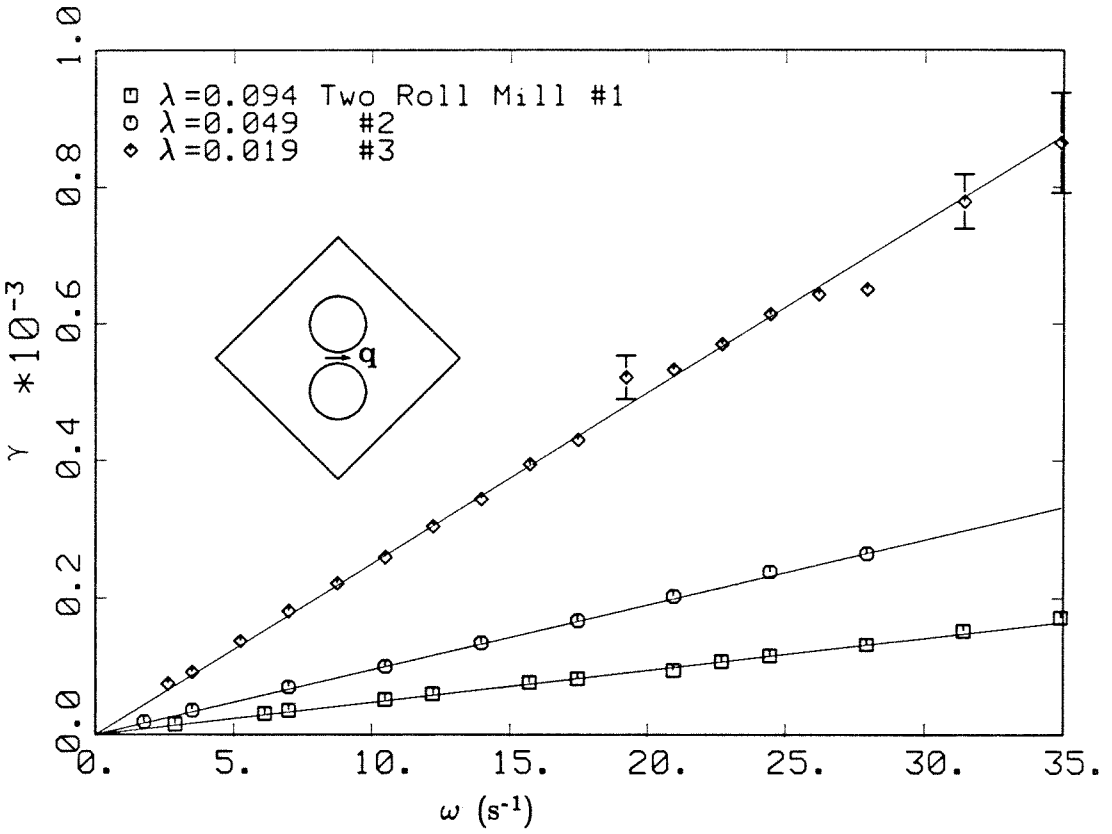
λ=0.094 Two Roll Mill #1
λ=0.049 #2
λ=0.019 #3
q
γ *10-3
0.0
0.2
0.4
0.6
0.8
1.0
0.
5.
10.
15.
20.
25.
30.
35.
ω (s-1)

Figure 11.

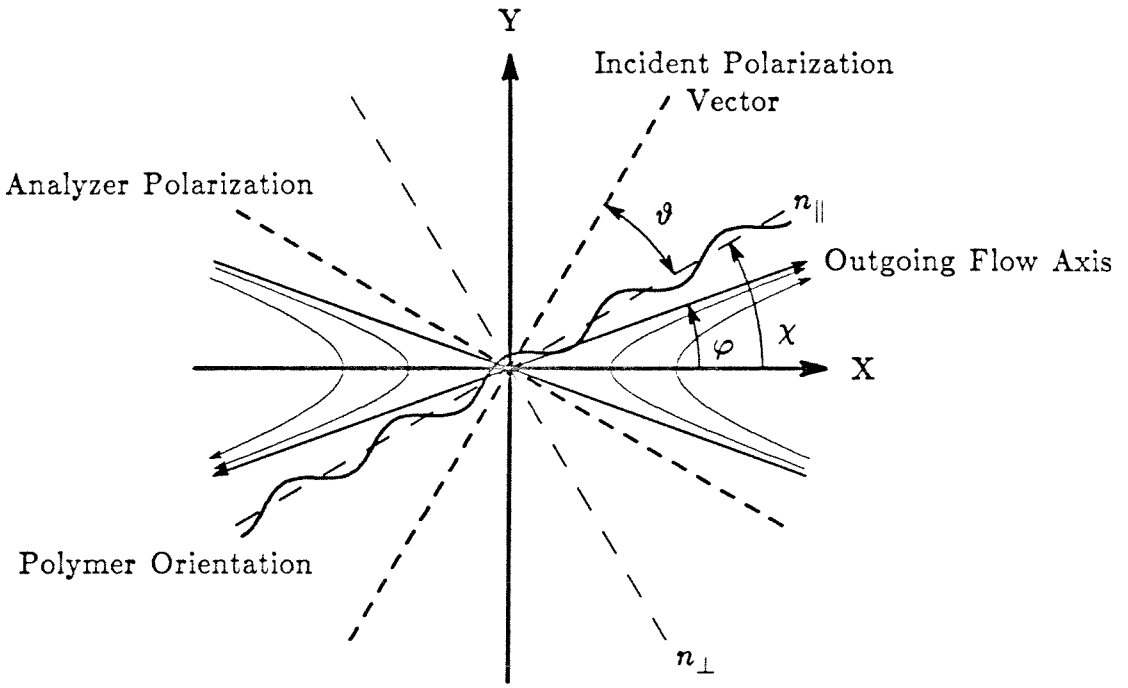
Y
Incident Polarization
Vector
Analyzer Polarization
ϑ
$n_{\parallel}$
Outgoing Flow Axis
φ
χ
X
Polymer Orientation
$n_{\perp}$

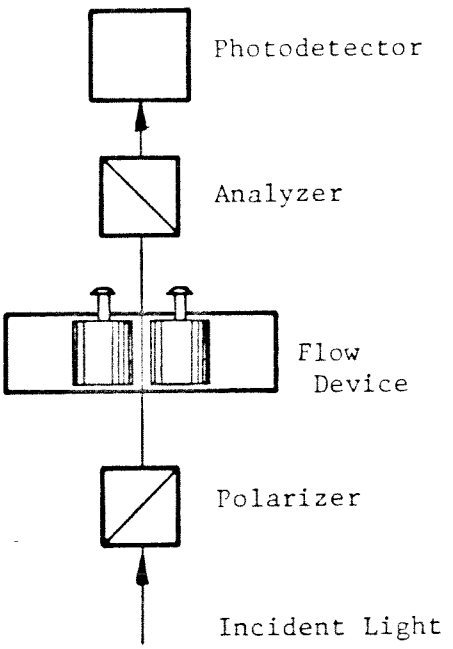
Photodetector
Analyzer
Flow
Device
Polarizer
Incident Light

Figure 12.

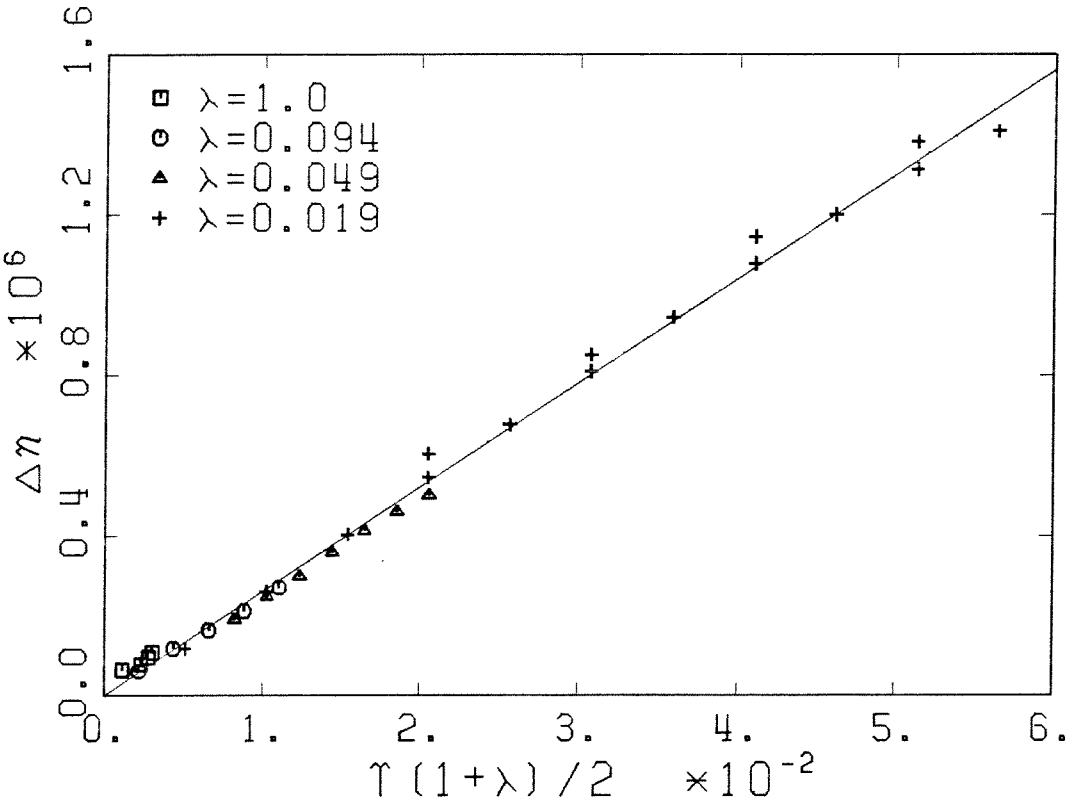

BIREFRINGENCE OF CHLOROWAX LV

Figure 13.

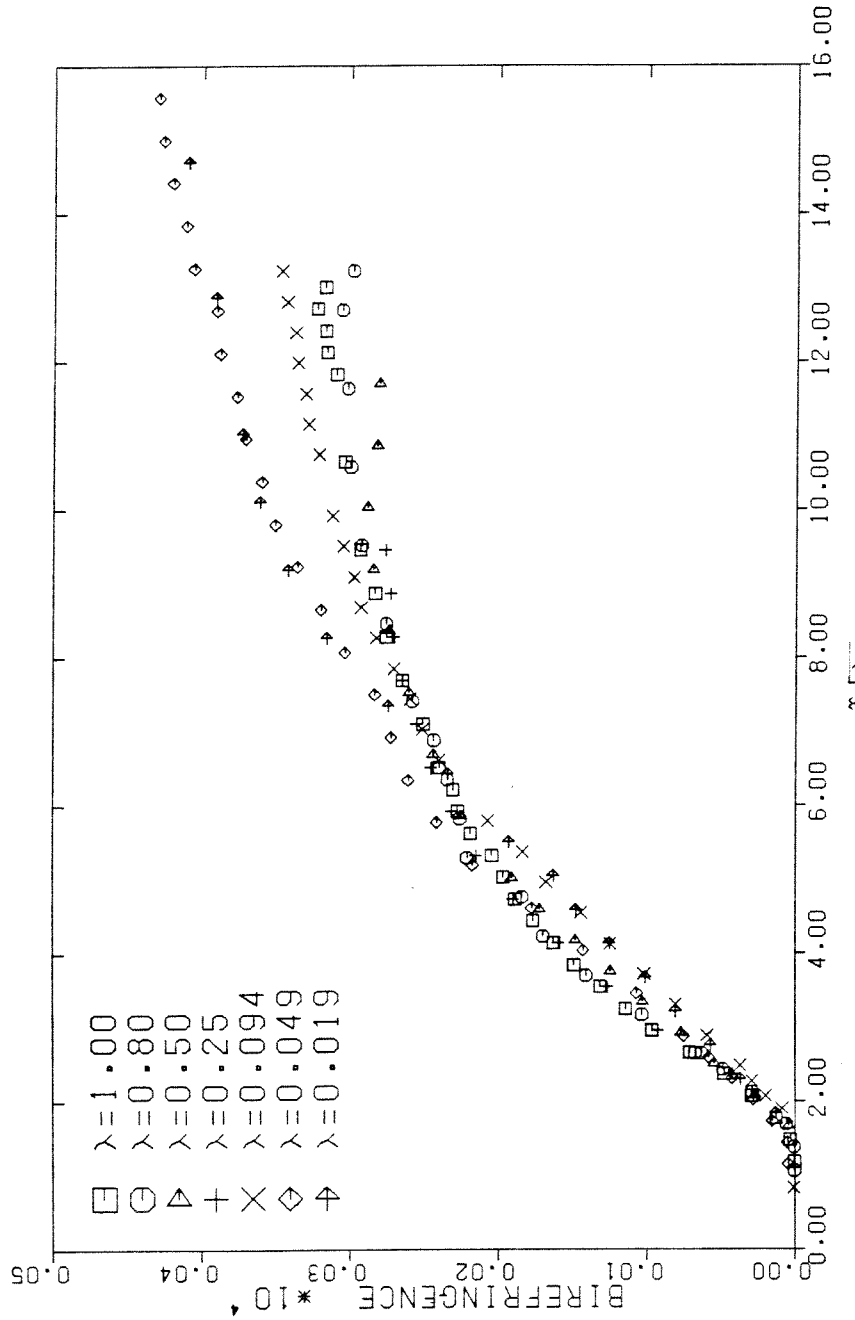

100 ppm PS8 in Chlorowax LV

Figure 14.

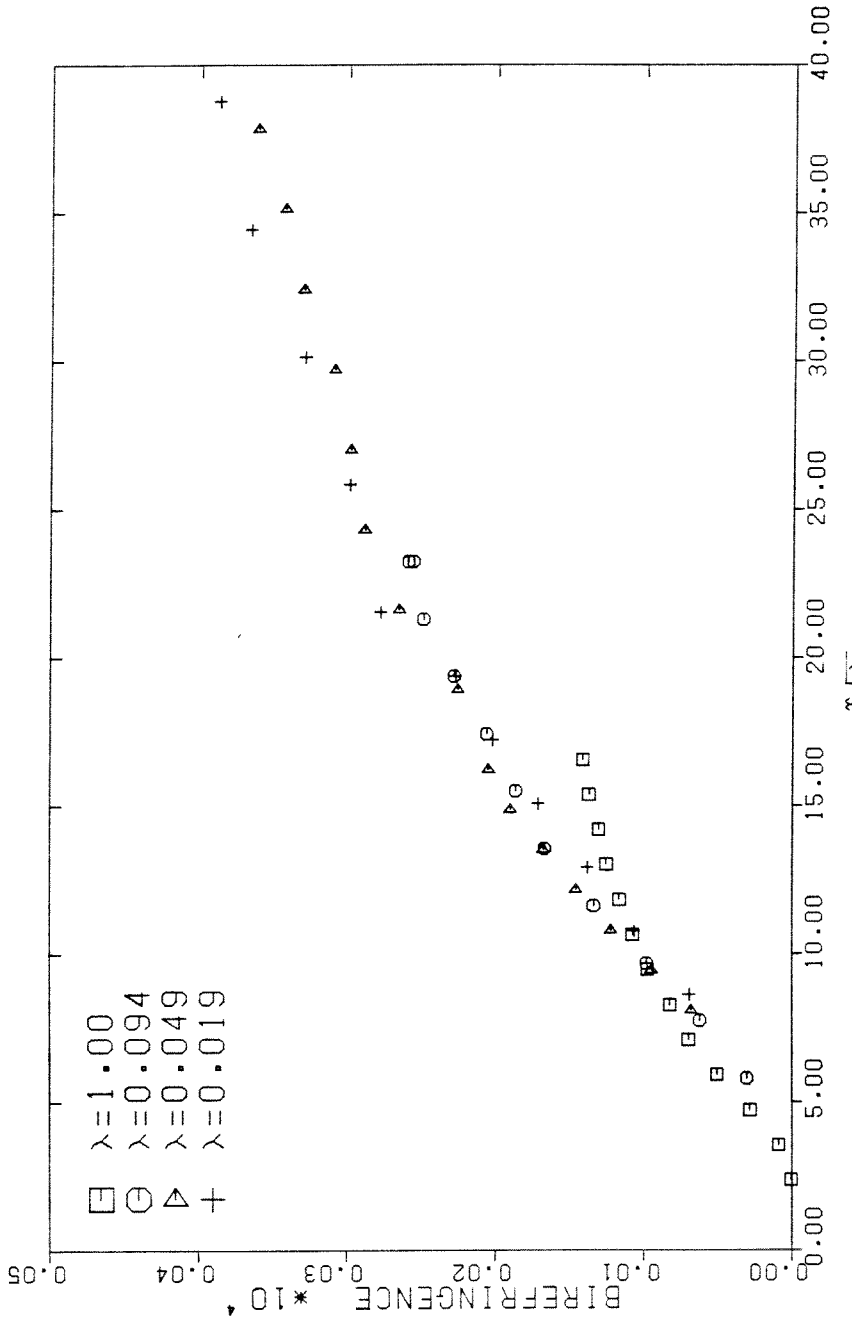

POLYSTYRENE (8.42E6 M) IN TCP

Figure 15.

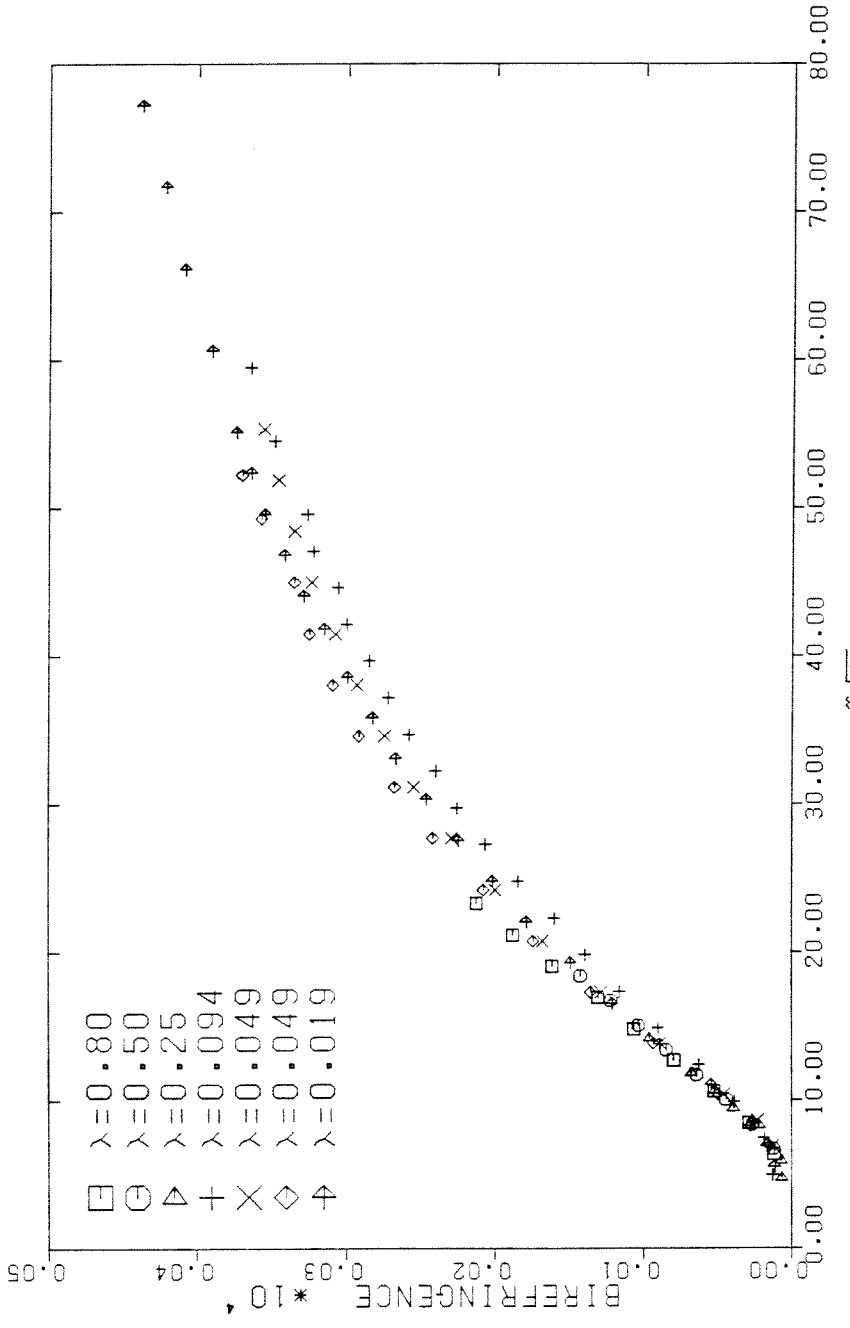

POLYSTYRENE (PS2) IN CHLOROWAX LV

Figure 16.

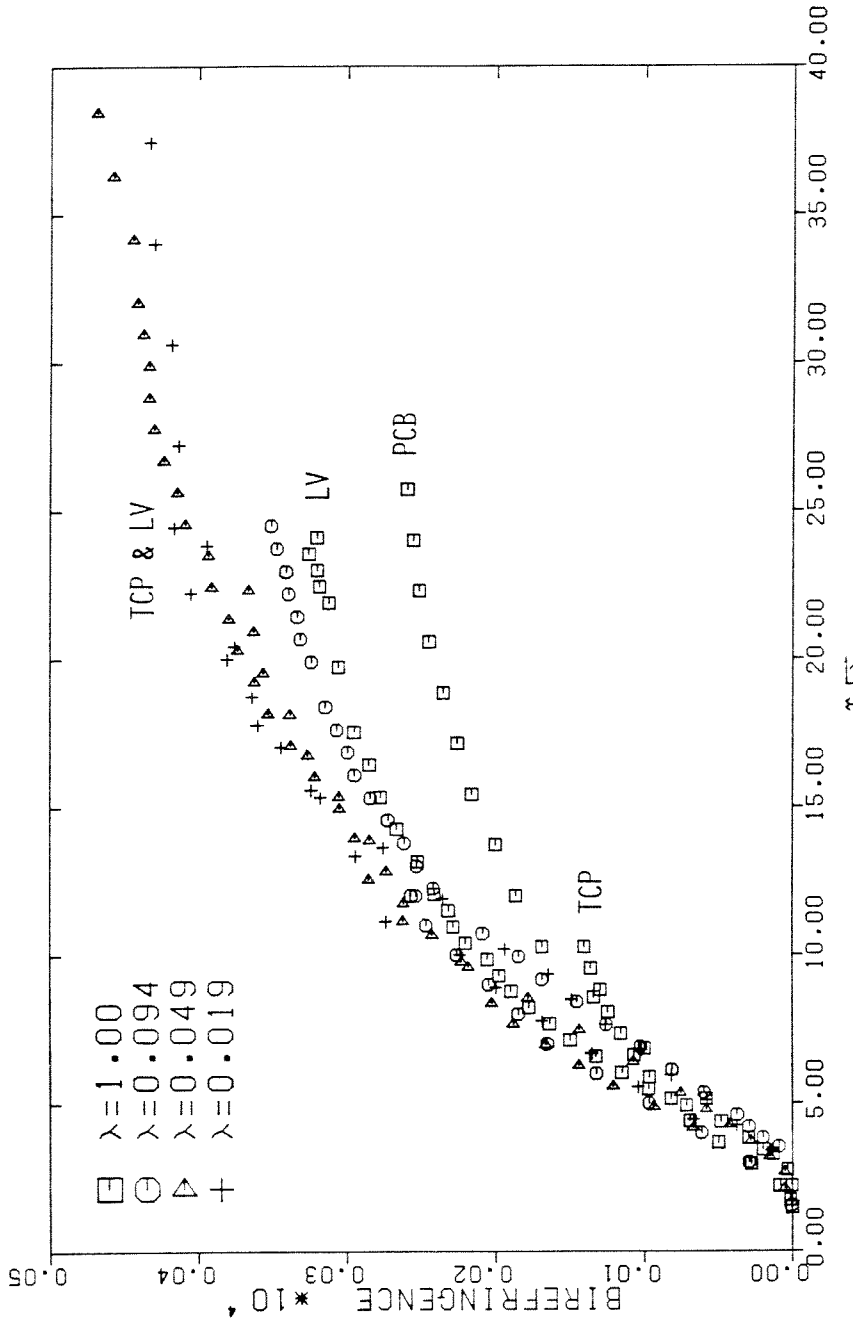
POLYSTYRENE (8.42E6 MJ IN VARIOUS SOLVENTS
BIREFRINGENCE *10⁴
τ √λ
λ=1.00
λ=0.094
λ=0.049
λ=0.019
TCP & LV
LV
PCB
TCP
0.00
0.01
0.02
0.03
0.04
0.05
5.00
10.00
15.00
20.00
25.00
30.00
35.00
40.00

Figure 17.

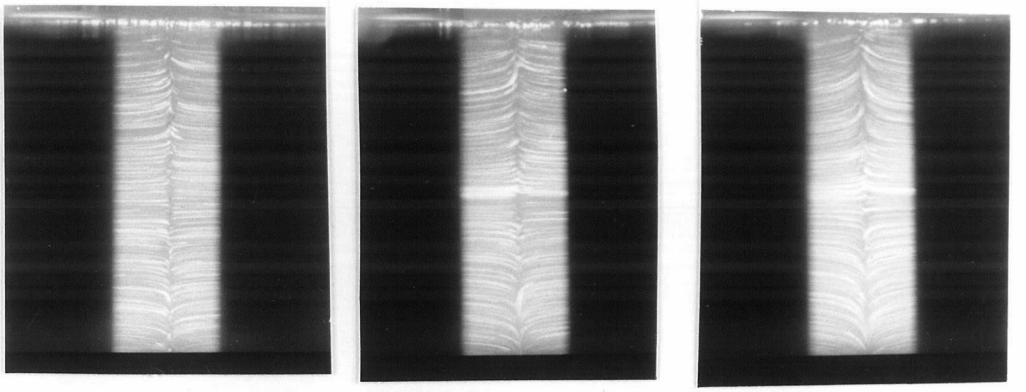

(a) ω=4.4 s^{-1} (b) 7.0 (c) 10.5

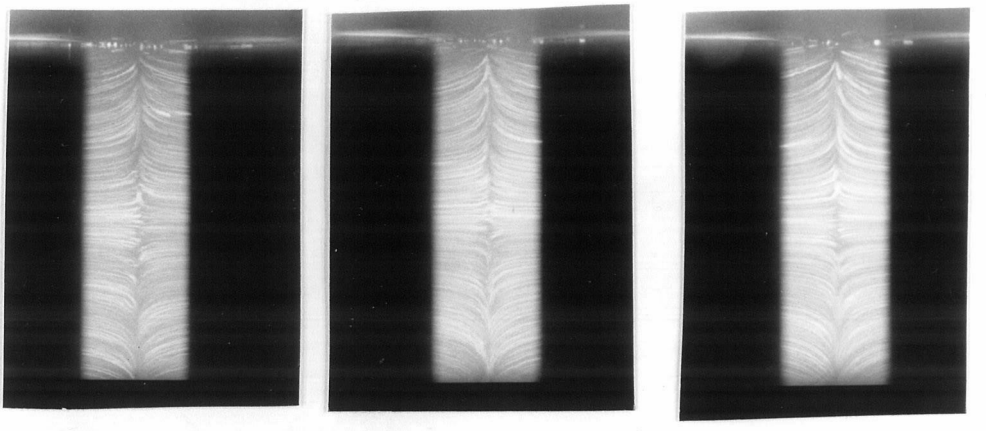

(d) 14.0 (e) 17.5 (f) 20.9

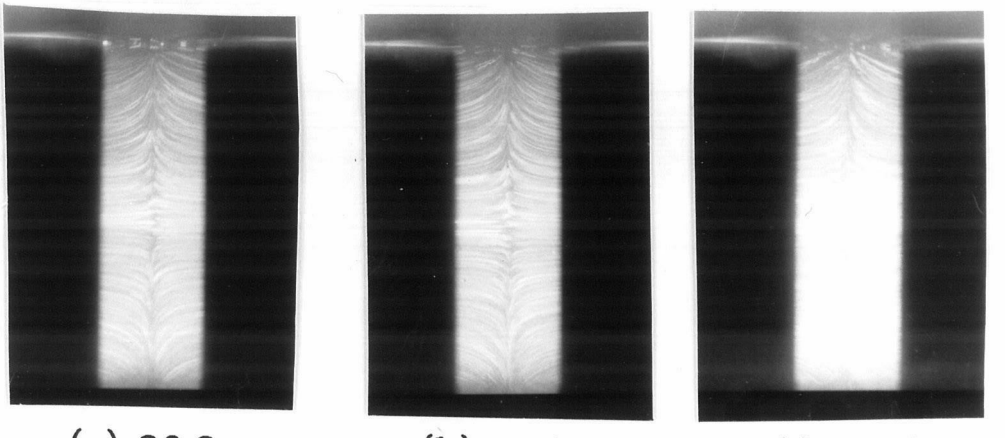

(g) 26.2 (h) 29.7 (i) 34.9

Figure 18.

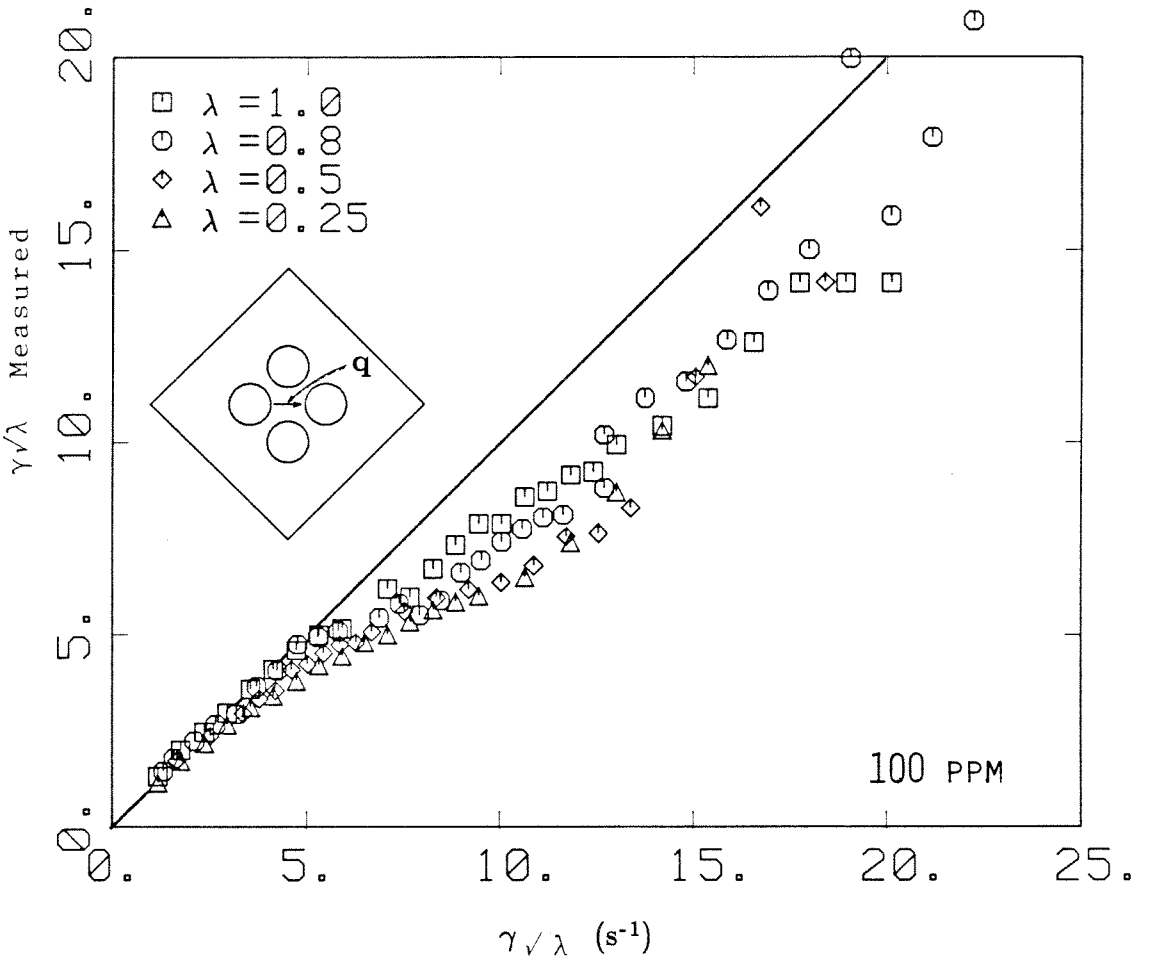

Figure 19.

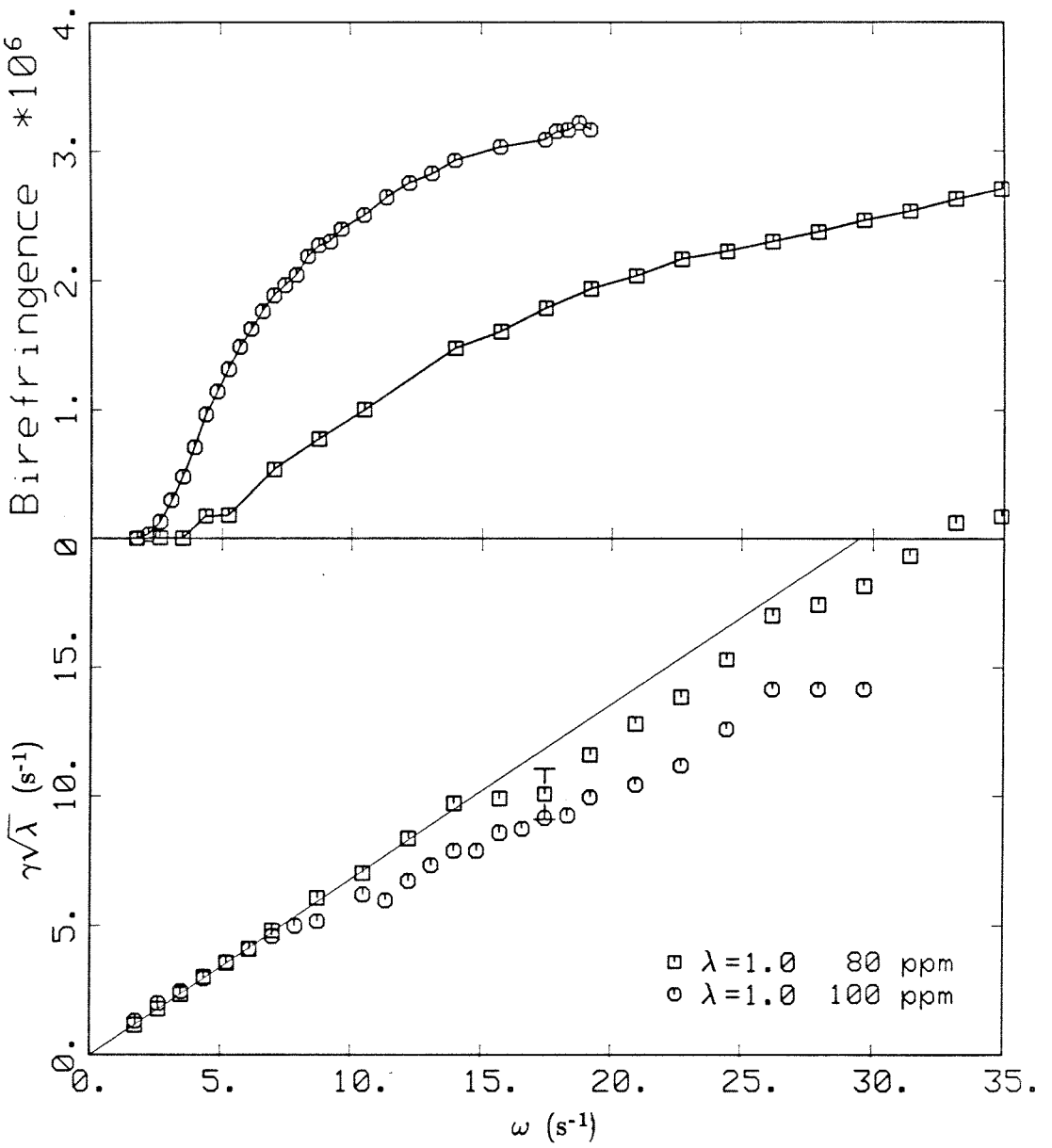
Birefringence *10^6
0.
1.
2.
3.
4.
γ√λ (s^-1)
0.
5.
10.
15.
ω (s^-1)
0.
5.
10.
15.
20.
25.
30.
35.
λ=1.0 80 ppm
λ=1.0 100 ppm

Figure 20.

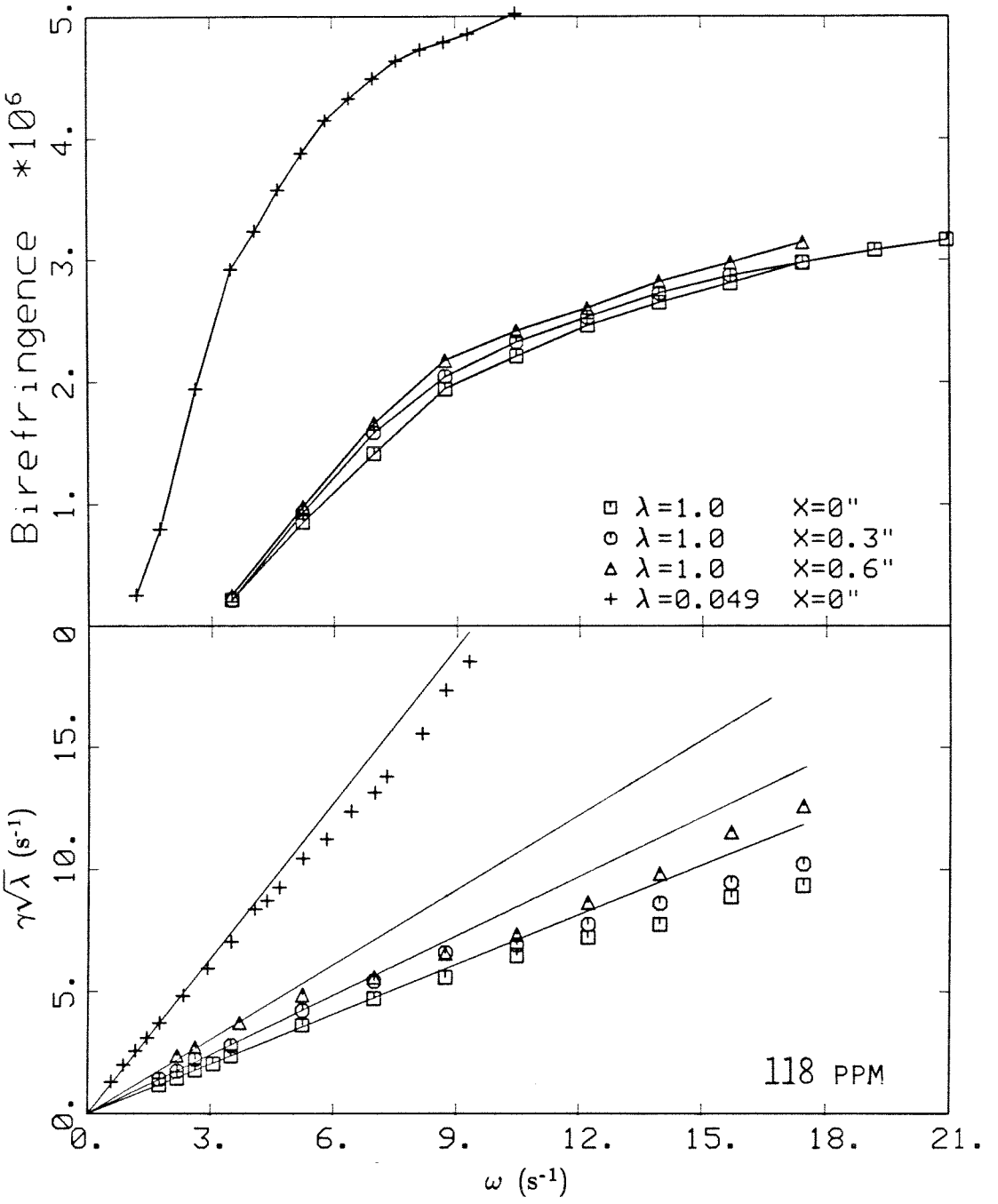
Birefringence *10^6
5.
4.
3.
2.
1.
0
□ λ=1.0 X=0"
○ λ=1.0 X=0.3"
△ λ=1.0 X=0.6"
+ λ=0.049 X=0"
γ√λ (s^-1)
0.
5.
10.
15.
0
118 PPM
0.
3.
6.
9.
12.
15.
18.
21.
ω (s^-1)

Figure 21.

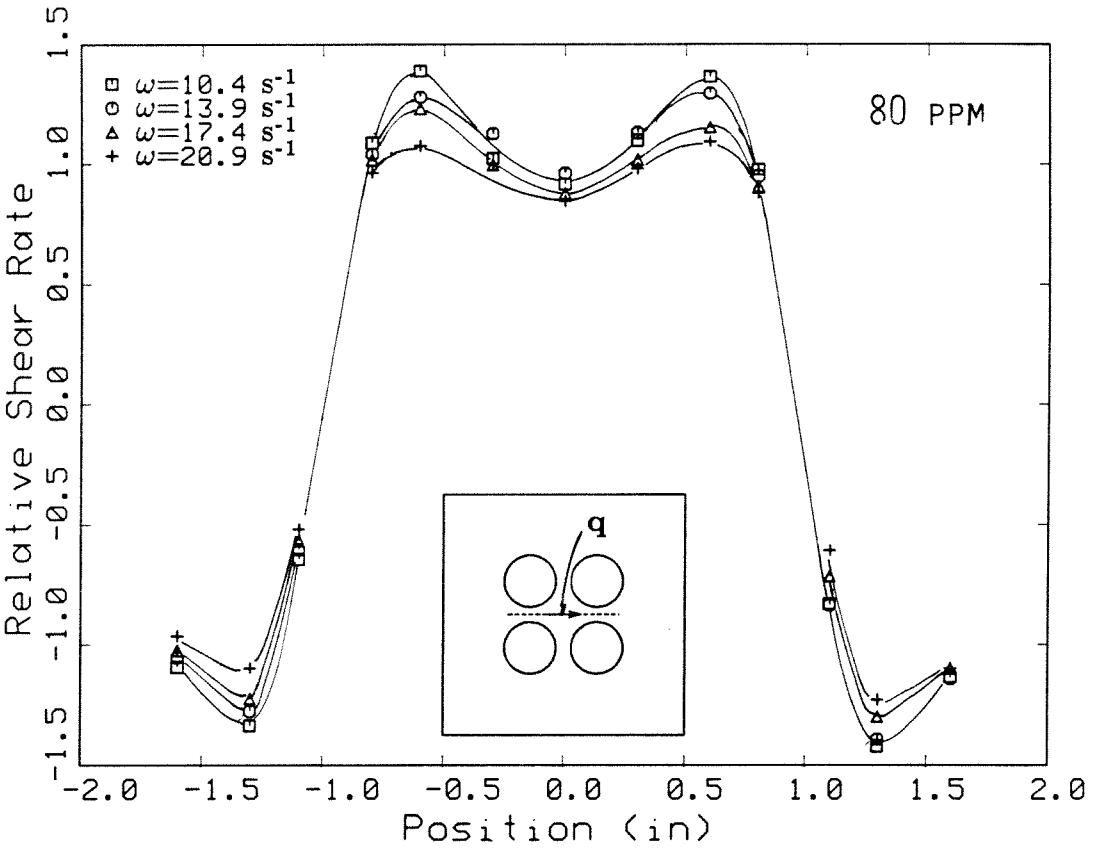
ω=10.4 s-1
ω=13.9 s-1
ω=17.4 s-1
ω=20.9 s-1
80 PPM
Relative Shear Rate
Position (in)
q
-2.0
-1.5
-1.0
-0.5
0.0
0.5
1.0
1.5
2.0

Figure 22.

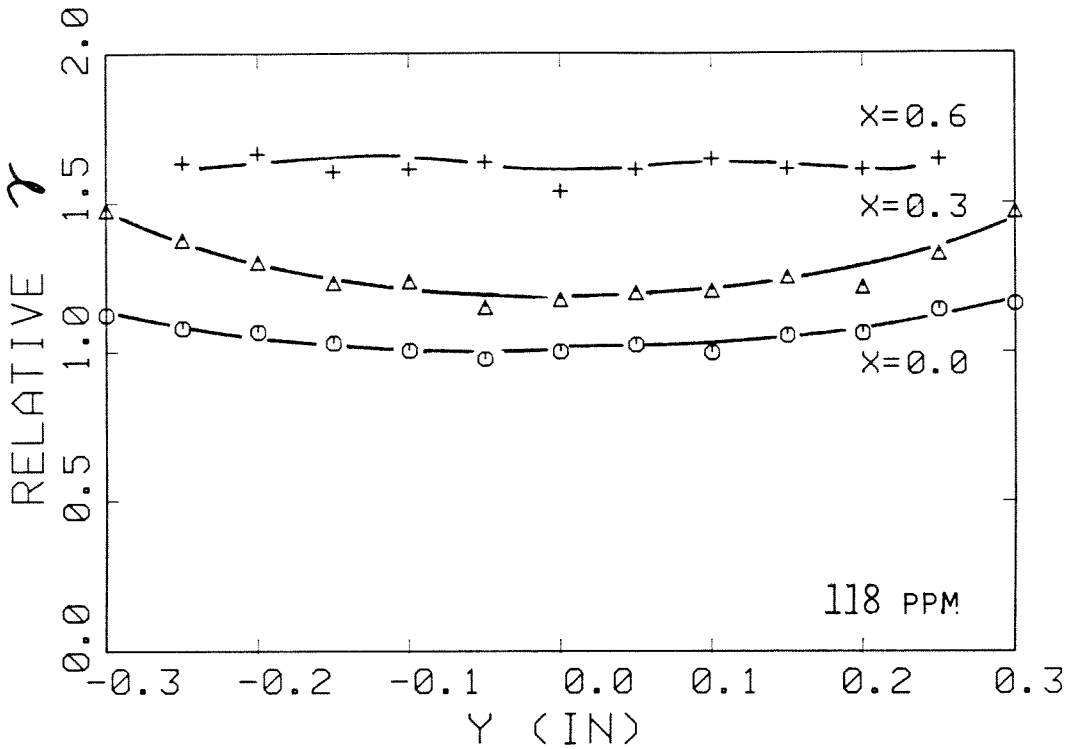
RELATIVE γ
2.0
1.5
1.0
0.5
0.0
X=0.6
X=0.3
X=0.0
118 PPM
-0.3
-0.2
-0.1
0.0
0.1
0.2
0.3
Y (IN)

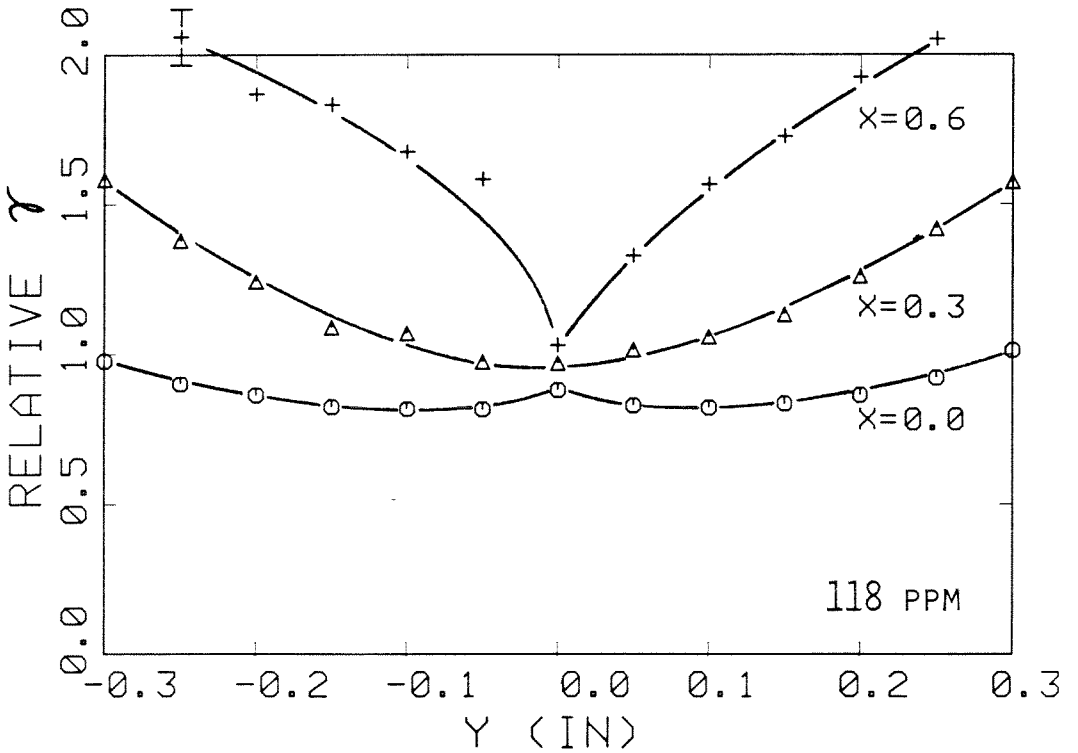
RELATIVE γ
2.0
1.5
1.0
0.5
0.0
X=0.6
X=0.3
X=0.0
118 PPM
-0.3
-0.2
-0.1
0.0
0.1
0.2
0.3
Y (IN)

Figure 23.

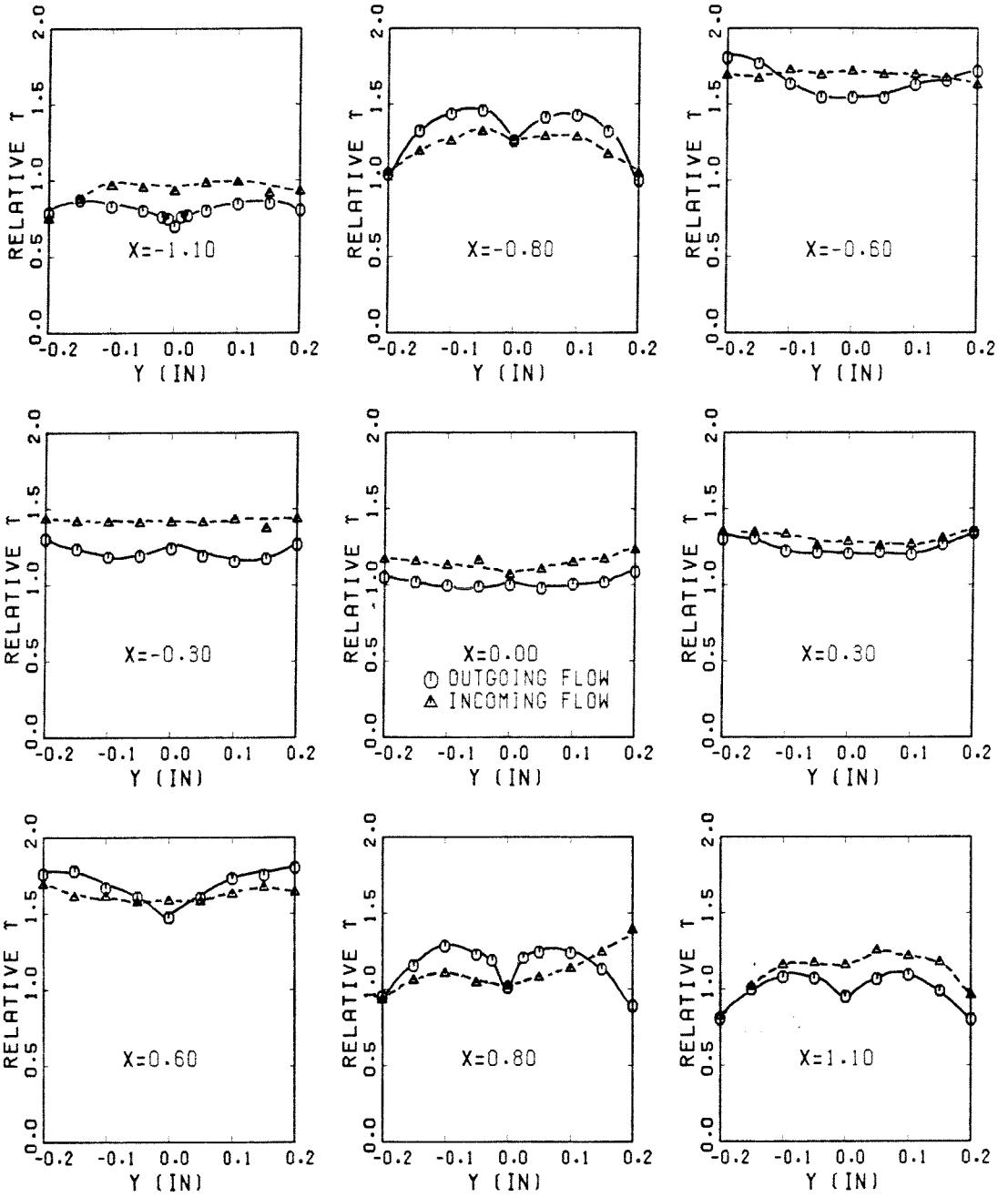
RELATIVE T
Y (IN)
X=-1.10
X=-0.80
X=-0.60
X=-0.30
X=0.00
OUTGOING FLOW
INCOMING FLOW
X=0.30
X=0.60
X=0.80
X=1.10
80 PPM

Figure 24.

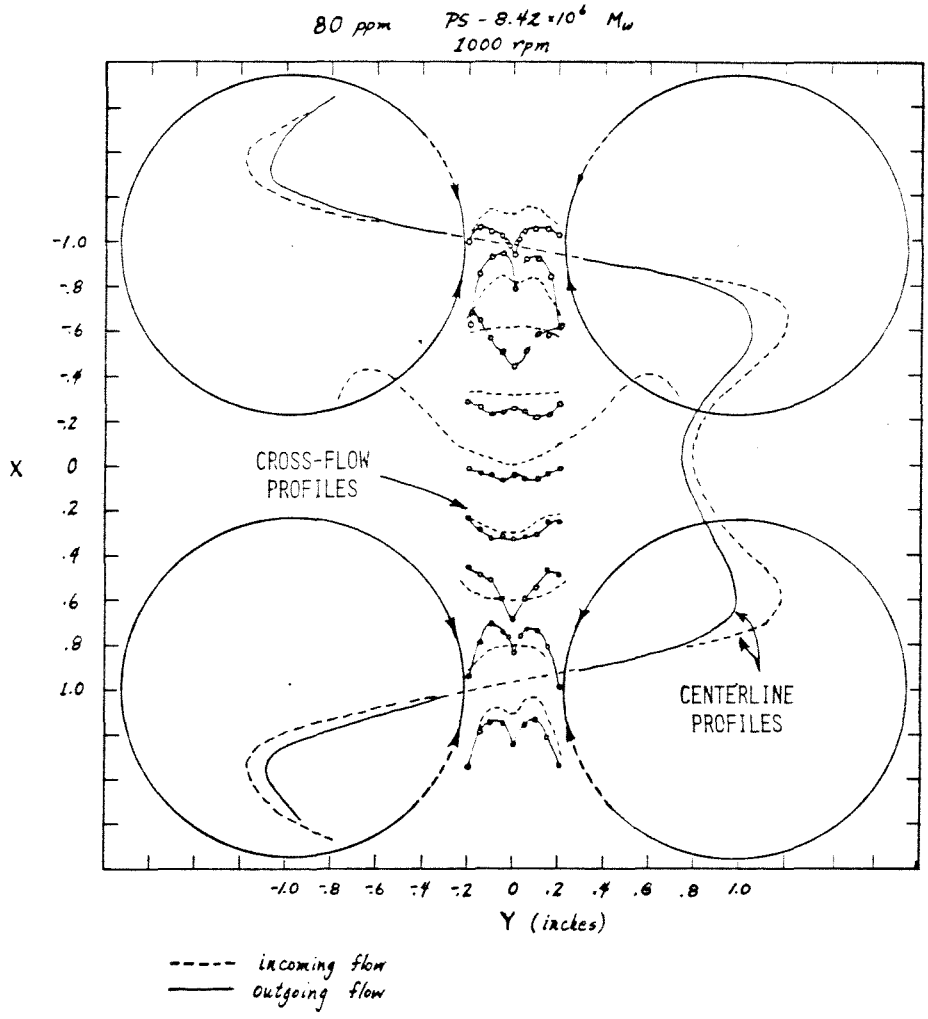
80 ppm PS - 8.42 ×10⁶ Mw
1000 rpm
-1.0
-.8
-.6
-.4
-.2
X 0
.2
.4
.6
.8
1.0
CROSS-FLOW PROFILES
CENTERLINE PROFILES
-1.0 -.8 -.6 -.4 -.2 0 .2 .4 .6 .8 1.0
Y (inches)
incoming flow
outgoing flow

Figure 25.

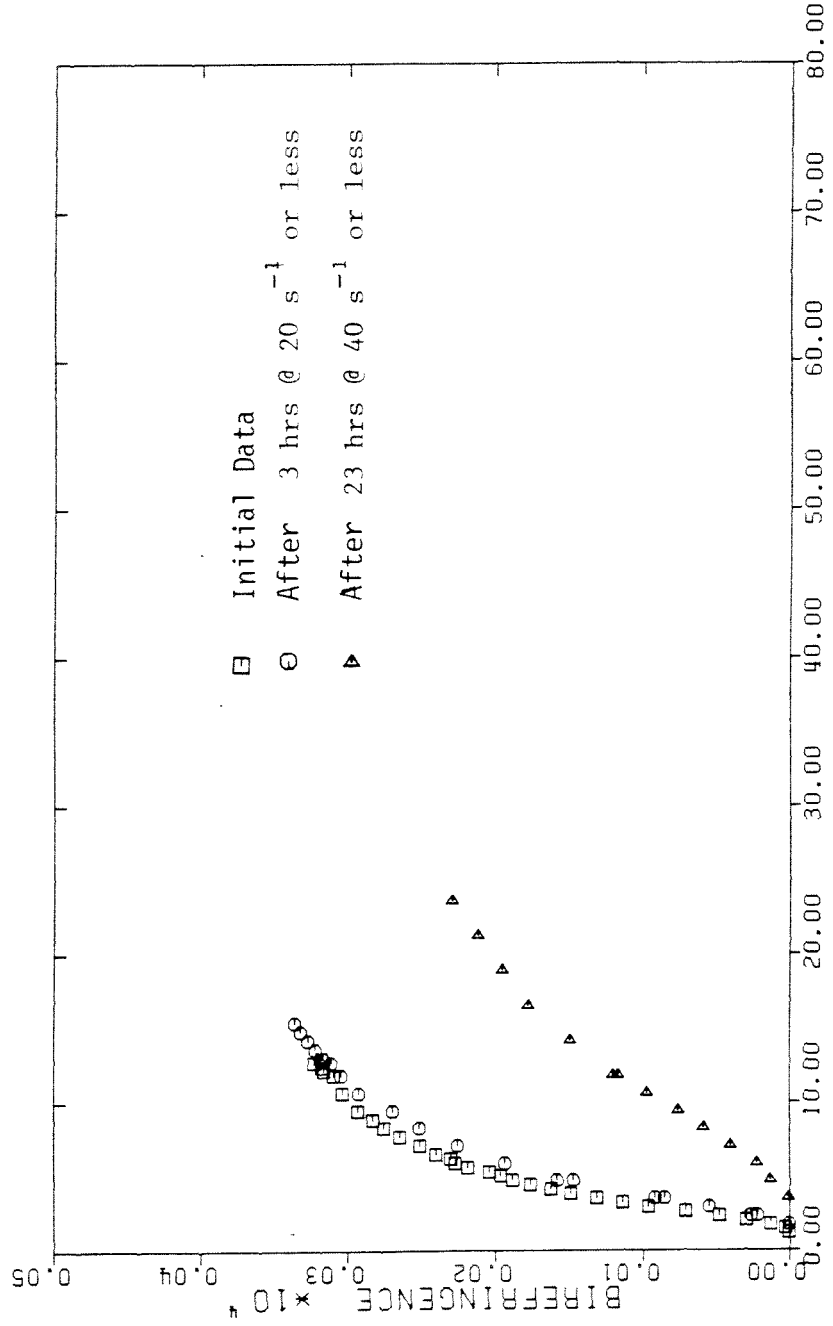

100 PPM PS (8 M) IN CHLOROWAX LV

Figure 26.

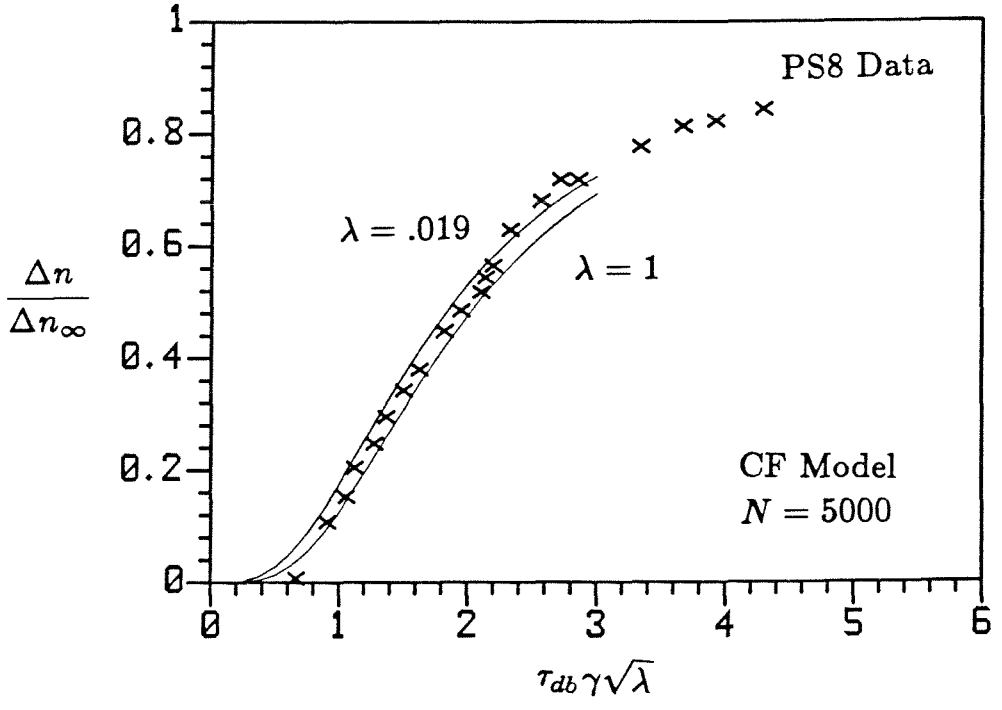
1
0.8
0.6
0.4
0.2
0
0
1
2
3
4
5
6
PS8 Data
$\lambda = .019$
$\lambda = 1$
CF Model
$N = 5000$
$\frac{\Delta n}{\Delta n_\infty}$
$\tau_{db}\gamma\sqrt{\lambda}$

Figure 27.

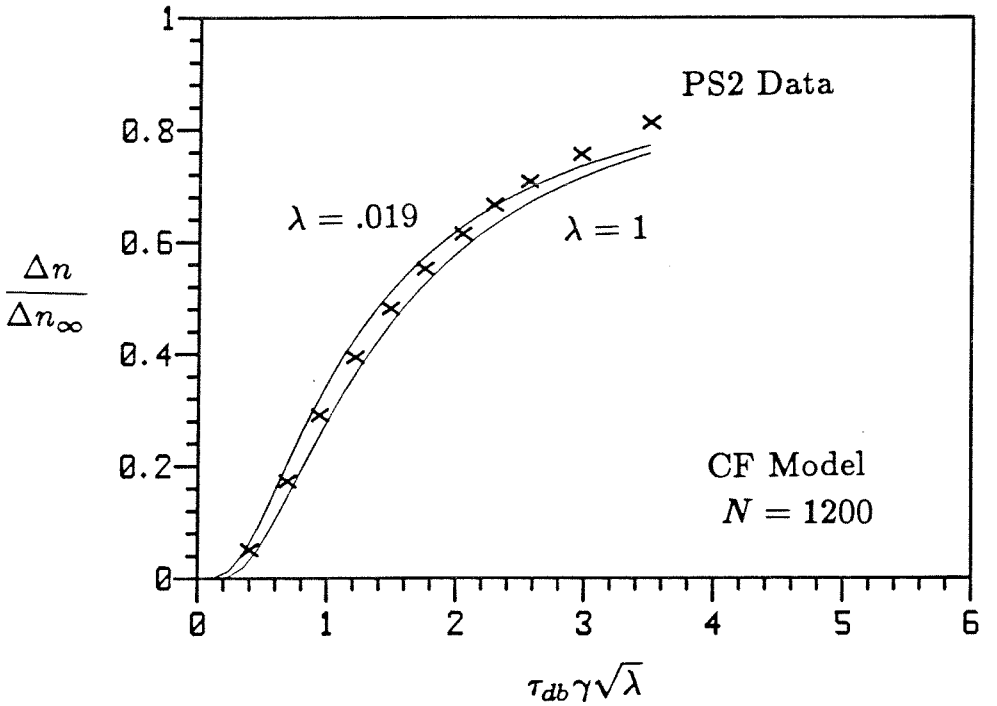
PS2 Data
$\lambda = .019$
$\lambda = 1$
CF Model
$N = 1200$
$\frac{\Delta n}{\Delta n_\infty}$
$\tau_{db}\gamma\sqrt{\lambda}$
0
0.2
0.4
0.6
0.8
1
0
1
2
3
4
5
6

Figure 28.

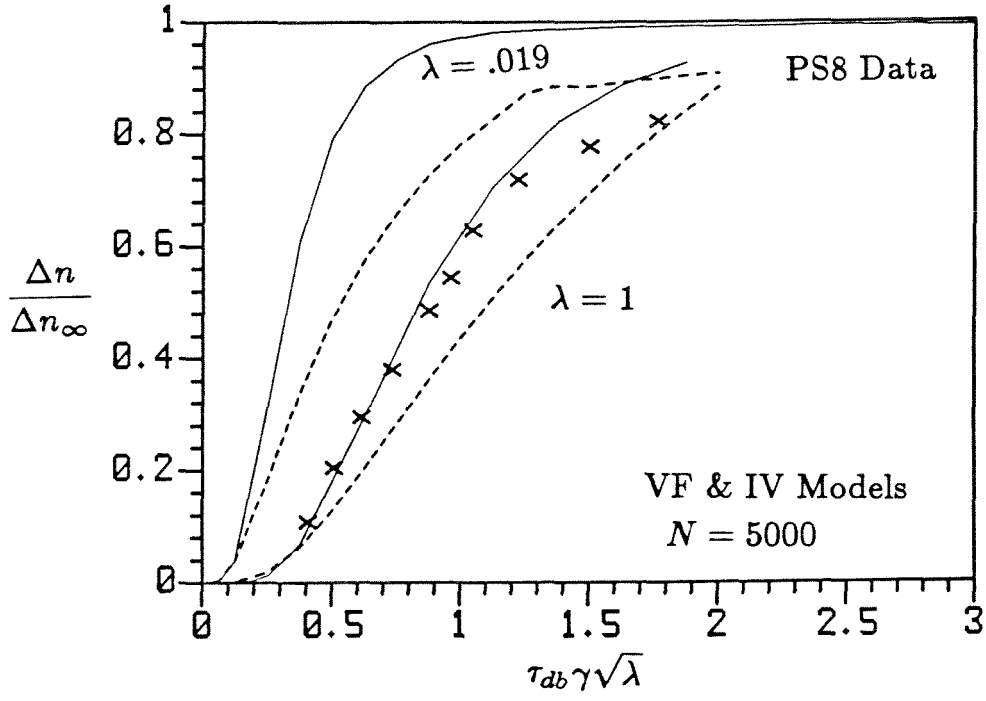
1
0.8
0.6
0.4
0.2
0
0
0.5
1
1.5
2
2.5
3
$\frac{\Delta n}{\Delta n_\infty}$
$\tau_{db}\gamma\sqrt{\lambda}$
$\lambda = .019$
PS8 Data
$\lambda = 1$
VF & IV Models
$N = 5000$

Figure 29.

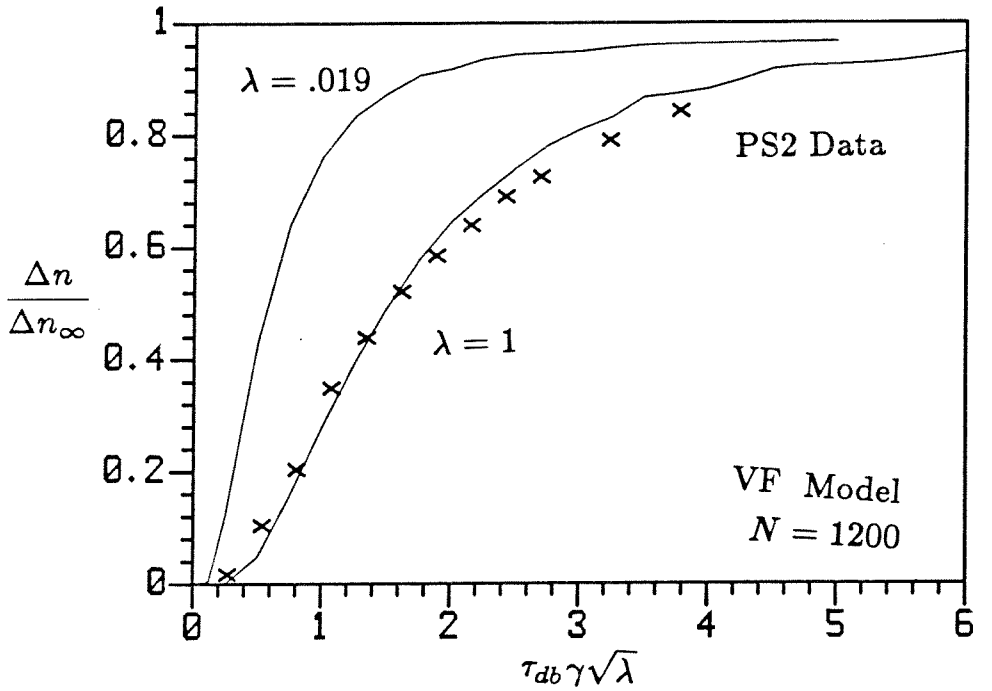
1
0.8
0.6
0.4
0.2
0
0
1
2
3
4
5
6
$\frac{\Delta n}{\Delta n_\infty}$
$\tau_{db}\gamma\sqrt{\lambda}$
$\lambda = .019$
$\lambda = 1$
PS2 Data
VF Model
$N = 1200$

Figure 30.

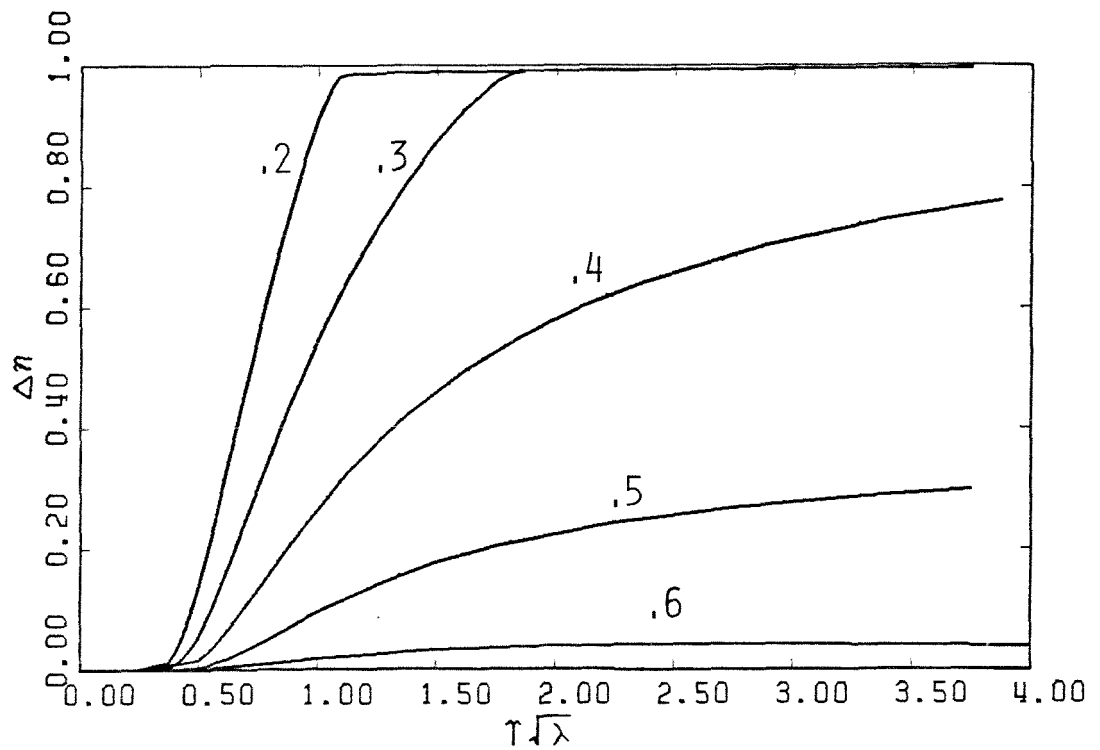
1.00
0.80
0.60
0.40
0.20
0.00
Δn
.2
.3
.4
.5
.6
0.00
0.50
1.00
1.50
2.00
2.50
3.00
3.50
4.00
τ√λ

Figure 31.

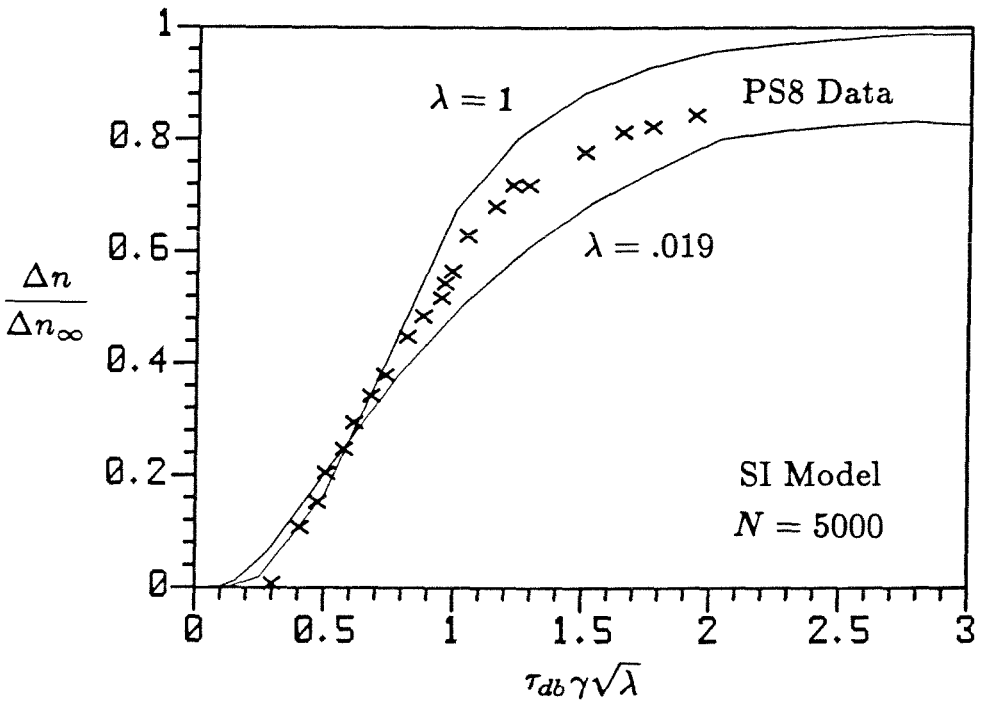
1
0.8
0.6
0.4
0.2
0
0
0.5
1
1.5
2
2.5
3
$\frac{\Delta n}{\Delta n_\infty}$
$\tau_{db}\gamma\sqrt{\lambda}$
$\lambda = 1$
PS8 Data
$\lambda = .019$
SI Model
$N = 5000$

Figure 32.

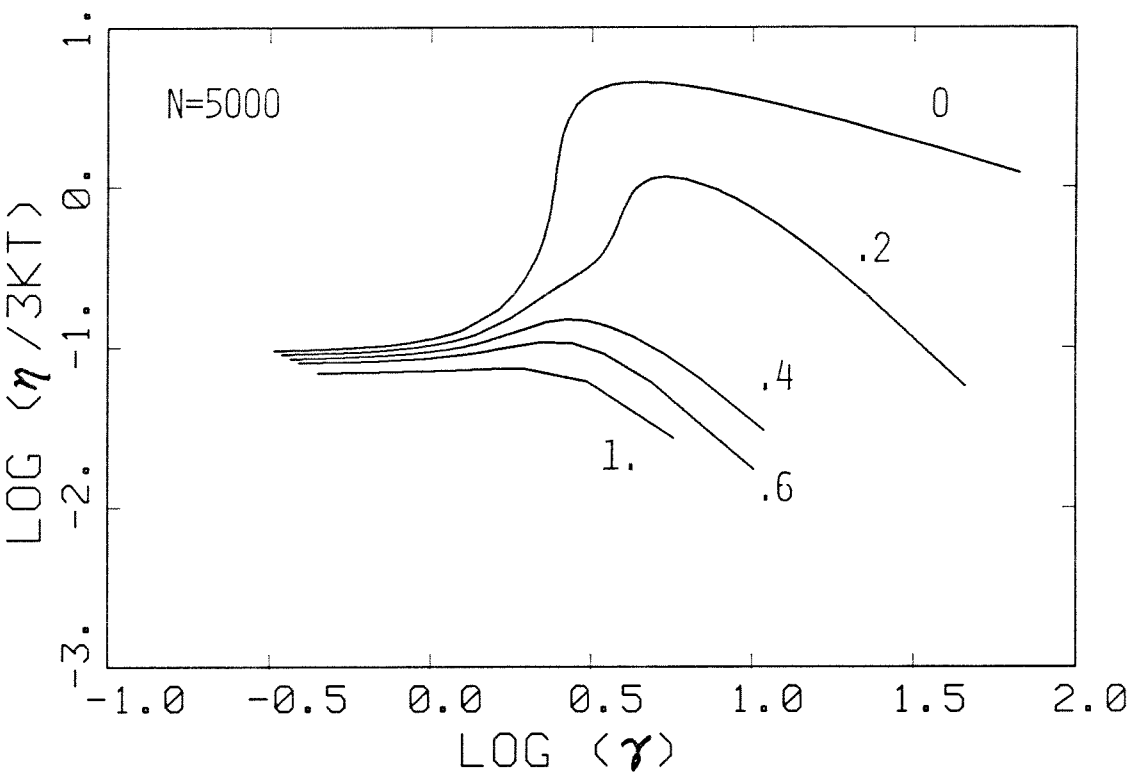

Figure 33.

CHAPTER II.

The Charged Dumbbell Model for Dilute Polyelectrolyte Solutions in Strong Flows

Rheologica Acta

Rheol Acta 23:238–249 (1984)

The charged dumbbell model for dilute polyelectrolyte solutions in strong flows

P. N. Dunlap and L. G. Leal

Department of Chemical Engineering, California Institute of Technology, Pasadena, California (USA)

Abstract: A charged dumbbell model is used to investigate the behavior of dilute polyelectrolyte solutions in a general linear two-dimensional flow. The model studied has a nonlinear spring, conformation dependent friction and a Coulombic repulsive force due to an effective electrostatic charge on the two beads. The relative importance of the electrostatic charge is reflected by an effective charge density parameter, E. Equilibrium properties such as end-to-end distance and intrinsic viscosity are strongly dependent on E. In strong flows, which produce a dramatic increase in the dumbbell dimensions (a coil-stretch transition), the onset behavior is influenced by E. Increasing E causes the onset velocity gradient to shift to much lower values. Large values of E change the qualitative behavior to that of rigid (or slightly extensible) macromolecules or fibers. Results are presented for a charged dumbbell at equilibrium, in steady flows, and in transient flows.

Key words: Dumbbell model, extensional flow, polyelectrolyte, dilute polymer solution

1. Introduction

Dilute polymer solutions exhibit macroscopically observable effects of viscoelasticity only in flows in which a strongly anisotropic conformation of the macromolecules is induced by the motion of the solvent. Recent studies of linear, flexible polymer systems have thus concentrated on both the prediction and measurement of conditions for the transition from the coiled near-equilibrium state to a highly stretched and oriented state [1, 2]. For this purpose, bead-spring type molecular models have proven particularly useful. However, in order to mimic the polymers' behavior in both the near-equilibrium random-coil configuration and in the highly stretched state, such a model must include both a nonlinear entropic spring (i.e. the possibility of non-Gaussian conformational statistics) and a conformation dependent friction coefficient as first suggested by de Gennes [3] and Hinch [4]. As a practical matter, this makes the use of many-bead "necklace" type models extremely difficult, and the majority of recent theoretical work on the coil-stretch transition has been focused on the simpler elastic dumbbell models. Although dumbbell models cannot reproduce the small-scale, higher-frequency modes of deformation that occur, for example, in oscillatory shear flows, the onset of strong non-Newtonian effects associated with the coil-stretch transition involves *overall* changes in macromolecular conformation, and existing work suggests that these "large-scale", lower frequency modes can be reproduced adequately by the dumbbell model. Indeed, comparison between the dumbbell model (with nonlinear spring and conformation dependent friction), and experimental birefringence data for narrow molecular weight distribution samples of polystyrene in Arochlor showed nearly quantitative agreement for a variety of two-dimensional strong flows when the model parameters were determined from independent light scattering data [2].

In the present study, our goal is to understand and model the behavior of dilute solutions of *polyelectrolytes* in strong flows. In this work, the polyelectrolyte is represented by a generalization of the nonlinear dumbbell model. In addition to the nonlinear spring and conformation dependent friction, we include Coulombic repulsion between the beads in an attempt to incorporate the effects of charge repulsion between ionizable groups on the polyelectrolyte chain. In this model, each bead is assigned an *effective* charge, q, that is chosen for the particular polyelectrolyte/solvent/counter-ion system so that the correct degree of rest-state expansion is obtained (relative to the linear dimensions of the same polymer and solvent at very large counter-ion concentrations). For the equilibrium (or rest) state, the

qualitative influence of the degree of polyelectrolyte ionization or of the levels of counter-ions in the solvent is well documented. When the degree of ionization is low, or the charge sites are shielded from one another by high concentrations of counter-ions in the solvent, the coil dimensions are only slightly increased and the polymer behaves essentially as a typical nonionic polymer. Indeed, there is often a concentration of salt which produces theta conditions for a given polyelectrolyte [5]. These cases correspond to low values of the effective charge, q, in the model. However, at low salt concentrations and high degrees of ionization, the polyelectrolyte is greatly expanded, and its rest state conformation is modified from an essentially spherical, random coil to a more anisotropic, elongated structure. As a result, there is typically a large increase in the intrinsic shear viscosity. These cases correspond to larger values of the effective charge in the model. In flows involving some degree of extensional motion such as porous media flow [6], or orifice flow [7], or even turbulent pipe flow [8], the changes in equilibrium conformation due to the addition of salts can lead to qualitative changes in the behavior of dilute solutions. In particular, if charge repulsion is weak (i.e. salt concentration is high) the extensional flow property being measured typically shows a sharp increase or onset at a critical magnitude of the velocity gradient, and this is similar to flexible nonionic polymers [1]. If charge repulsion is strong, the critical onset point typically disappears and departures from near-equilibrium values of the flow property are evident at all shear rates [6]. This latter behavior is also typical of fiber suspensions or solutions of rigid macromolecules [8].

The attempt to simulate the behavior of dilute polyelectrolyte solutions by the use of an effective charge on the beads of a dumbbell is not unique to this study, but has been used in a number of earlier works. However, in all cases, these preceding studies were confined to simple, linear shear flow. In the first, King and Eisenberg [9] showed that the increase in intrinsic viscosity with increasing charge repulsion could be predicted via the dumbbell model, as well as a corresponding increase in the relaxation time. In addition, using a three-bead, two-spring model, King and Eisenberg found that the ratio between the two relaxation times increased with charge. Further computer calculations by Nakajima and Wada [10] and Fujimori et al. [11] with up to nine beads revealed that all the relaxation times increased with charge, but that the longest time increased proportionately more. Fujimori et al. [11] attributed this to a transition from relaxation via conformational diffusion to an end-to-end Brownian rotation of the dumbbell as the molecule becomes increasingly elongated (and rigid) due to increased electrostatic repulsion. These predictions were supported by linear viscoelastic measurements for polyacrylic acid in water [12] and for polystyrene sulfonate in glycerol and water [13]. The fact that the dominant effect of Coulombic repulsion in shear flow is to increase the largest relaxation time lends support to our use of the two-bead dumbbell model in the present work.

The following sections describe the model, the results of our calculations and qualitative comparison with data from the literature. An experimental study of dilute polyelectrolyte solutions using birefringence in strong flows, similar to the earlier study of nonionic polystyrene solutions by Fuller and Leal [2], will be reported in a later publication. A related experimental investigation has been published recently by Miles, Tanaka and Keller [14].

2. The model

We begin with a description of the elastic dumbbell model, modified (following Fuller and Leal [1] and earlier workers) so that it yields proper behavior for nonionic polymers in the highly stretched state, but also including an electrostatic repulsion between beads with an *effective* charge assigned as outlined in the preceding section. Indeed, apart from the Coulombic repulsion between beads, the model used here differs little from that applied very successfully for polystyrene/Arochlor and other nonionic polymers by Fuller and Leal [2]. This model includes the nonlinear Warner spring [15], and an isotropic but conformation dependent bead friction coefficient with a magnitude which is linearly proportional to the end-to-end dimension of the dumbbell. The Coulombic repulsion effect is modeled as point charges of magnitude q (at the beads) separated by a distance r' (the end-to-end distance for the dumbbell) and acting through a fluid with dielectric constant, ε. The charge q assigned to the beads is an effective value intended to mimic for the dumbbell, the charge repulsion between ionized sites that are distributed all along the backbone of the real polyelectrolyte. The magnitude of q is chosen so that the dumbbell model gives the correct degree of "coil" expansion in the rest state. With the rest state expansion given correctly, it is hoped that the model will give at least qualitatively accurate results for the same solvent/polyelectrolyte system in flow. A simple Coulombic force law is assumed to be applicable, independent of the concentration of counterions in the solvent. Thus, any influence of counterions, due to shielding of the charges along the polymer backbone, can only be accounted for in the charged dumbbell model by decreasing the value of the effective charge q. Although this is not strictly correct and a more appropriate (Debye-Huckel) force law accounting for the inter-

[1] The critical velocity gradient depends upon the molecular weight. Thus, a monodisperse system would show a discontinuous onset, while any spread in the molecular weight distribution tends to smooth or spread the onset velocity gradient over a range of values

action of counterion charge clouds was determined many years ago, the use of the Debye-Huckel expression only complicates the analysis without producing any qualitative differences from the simpler Coulombic force law which we use here [9]. Whether or not the drastic simplifications inherent in this approximate description of charge repulsion effects can yield reasonable results in flow will only finally be decided by comparison with experimental data.

Following the usual procedure of deriving an "equation of motion" for the dumbbell from a simple force balance on each bead (cf. Fuller and Leal, [1]), it can be shown easily for the model described above that

$$\frac{-\zeta_0 \dot{\boldsymbol{r}}'}{\sqrt{N}a}(\dot{\boldsymbol{r}}' - \gamma' \Gamma \cdot \boldsymbol{r}') - \frac{6NkT}{R^2}\left(\frac{\boldsymbol{r}'}{1-\left(\frac{r'}{R}\right)^2}\right) - 2kT\nabla' \ln\psi + \frac{2q^2\boldsymbol{r}'}{\varepsilon r'^3} = 0 \qquad (1)$$

where $\boldsymbol{r}'$ is the (dimensional) end-to-end vector for the dumbbell, $R = Na$ is the maximum length of the dumbbell where N is the number of subunits of length a in the chain, kT is the Boltzmann temperature, ζ_0 the Stokes' law friction coefficient for the undeformed dumbbell, γ' the magnitude of the velocity gradient, and Γ the transpose of the (dimensionless) velocity gradient tensor. The first term represents the "frictional" interaction between solvent and macromolecule, the second the effect of conformational diffusion toward equilibrium (modeled as the effect of a nonlinear, elastic spring), the third the smoothed effects of Brownian diffusion in which ψ is the configurational probability density function, and the fourth, and last, the effects of the effective charge q assigned to the two beads.

It may be noted that the nonlinear elastic dumbbell model in the form of Eq. (1) exhibits a conformation-dependent relaxation time. Near equilibrium, with q suitably small, the relaxation time is $\theta = \zeta_0 R^2/6NkT$, namely the Zimm value for a non-free-draining coil. The inclusion of conformation-dependent friction allows the relaxation time to increase from θ to $\theta\sqrt{N}$ as the end-to-end dimension is increased (due either to Coulombic repulsion associated with increased q in the rest state, or to flow-induced expansion). The molecular weight dependence of θ is $\theta \sim (\mathrm{MW})^{3/2}$, while $\theta\sqrt{N} \sim (\mathrm{MW})^2$, and the inclusion of conformation-dependent friction is thus seen as affording the possibility of a transition from a non-free-draining to free-draining "coil" as the polymer molecule expands. Finally, in the limit of sufficiently large q, where the dumbbell is locked into a fully expanded configuration even in the absence of flow, the only relaxation process in the model is rotational Brownian motion and the characteristic relaxation time shifts to $\theta N^{3/2} \sim (\mathrm{MW})^3$.

We will use eq. (1) to determine the flow-induced changes of conformation for the same class of two-dimensional, linear flows that were considered earlier for the case $q = 0$ by Fuller and Leal, i.e.

$$\Gamma = \begin{pmatrix} 0 & 1 & 0 \\ \lambda & 0 & 0 \\ 0 & 0 & 0 \end{pmatrix}. \qquad (2)$$

The specific type of two-dimensional flow depends on the magnitude of the parameter λ. The complete class of linear, two-dimensional flows is encompassed for λ in the range $-1 \leqq \lambda \leqq 1$ with -1 being a purely rotational flow, $+1$ being the pure "hyperbolic" straining flow and $\lambda = 0$ being simple shear flow. The motivation for considering this class of motions is primarily that they can be simulated quite accurately in the four-roll (and two-roll) mill, thus providing a basis for comparison of model predictions with measurements of flow-induced birefringence (or other properties), cf. Fuller and Leal [2, 16], as a function of flow strength $\gamma'\sqrt{\lambda}$ and flow type λ. It may be noted that the response of the dumbbell in uniaxial elongation was also studied. However, the results were very similar to those for planar extensional flow ($\lambda = 1$) and will not be considered here in detail (the interested reader may refer to Dunlap [25]).

In order to complete the statement of the model, eq. (1) for the rate of change of the end-to-end vector must be combined with the continuity equation

$$\frac{\partial\psi}{\partial t'} + \nabla' \cdot (\dot{\boldsymbol{r}}'\psi) = 0 \qquad (3)$$

representing conservation of configurational probability. Thus, substituting (1) into (3) and introducing the usual dimensionless variables $\boldsymbol{r} = \boldsymbol{r}'/R$, $t = t'/\theta$, and $\gamma = \gamma'\theta$, where θ is the Zimm relaxation time $\zeta_0 R^2/6NkT$, we obtain the dimensionless dumbbell diffusion equation

$$\frac{\partial\psi}{\partial t} = \nabla \cdot \left\{\frac{1}{\sqrt{N}r}\left[\frac{1}{1-r^2} - \frac{E}{3Nr^3}\right]\boldsymbol{r}\psi\right\} - \gamma\Gamma : \nabla(\boldsymbol{r}\psi) + \frac{1}{3N^{3/2}}\nabla \cdot \left(\frac{1}{\boldsymbol{r}}\nabla\psi\right). \qquad (4)$$

The magnitude of the new term which arises from Coulombic repulsion between the beads is characterized by the dimensionless "charge density" parameter

$$E = \frac{q^2}{\varepsilon kTR} \qquad (5)$$

which can be viewed as a dimensionless measure of the charge per unit length of the polymer, or as the ratio of electrostatic to thermal energy. Not surprisingly, a

similar parameter appears widely in theories of polyelectrolyte solutions (see e.g. the review by Manning [17]). Its applicability to real solutions has been amply demonstrated by Kowblansky and Zema [19] who have used a charge density parameter to correlate intrinsic viscosity [18] and diffusion data [19] for a number of polyelectrolyte solutions. In the present study, we will consider the solution of eq. (4) – or rather, of moment equations derived from (4) – for a number of values for E. In order to relate the predicted behavior in strong flows to experimental observation, an independent estimate of the effective charge q (or, equivalently, the parameter E) is necessary. As noted earlier, we propose using a value of the effective charge (or, equivalently, the parameter E), which yields the correct prediction for the equilibrium coil expansion for the particular solvent/polyelectrolyte/counter-ion system. The degree of coil expansion at equilibrium can be inferred experimentally from either light scattering spectroscopy or intrinsic shear viscosity measurements.

It is not necessary to solve the diffusion equation (4) directly. Instead, we can use the diffusion equation to derive an equation for the second moments of the distribution function, $\langle \boldsymbol{rr} \rangle$. From these moments, the stress tensor and birefringence for the solution can be calculated directly [2]. The moment equation is obtained by simply multiplying (3) by $\boldsymbol{rr}$ and then integrating over the configuration space, assuming that ψ goes to zero exponentially at the limits of integration. The result is

$$\frac{d\langle \boldsymbol{rr} \rangle}{dt} = \chi \boldsymbol{\Gamma} \cdot \langle \boldsymbol{rr} \rangle + \chi \langle \boldsymbol{rr} \rangle \cdot \boldsymbol{\Gamma}^{\mathrm{T}} - \left\langle \frac{2}{\sqrt{N}r} \left(\frac{1}{1-r^2} - \frac{E}{3Nr^3} + \frac{1}{3Nr^2} \right) \boldsymbol{rr} \right\rangle + \frac{2}{3N^{3/2}} \left\langle \frac{1}{r} \right\rangle \boldsymbol{I}. \tag{6}$$

There are two differences between eq. (6) and the moment equations used by Fuller and Leal [1], in addition to the presence of the Coulombic force. First, we have included explicitly the factor of two which multiplies each of the forces except the friction force in the equation of motion (1). Fuller and Leal essentially absorbed this factor into their dimensionless velocity gradient α which means that putting $\alpha = \chi/2$ will allow a direct comparison with their results. The other difference is the presence of the term $1/3Nr^2$ on the right-hand side of eq. (6). This arises from the Brownian force with variable friction, but did not appear in the moment equations of Fuller and Leal because these authors preaveraged the nonlinear spring and conformation-dependent friction expressions in eq. (4) prior to derivation of the moment equations. Eq. (6) does not make this preaveraging assumption and is strictly correct. As might be expected, given the nature of the preaveraging approximation, the new term has little effect on the dumbbell when it is in a highly stretched state, but it does change both the equilibrium behavior and the onset behavior in strong flows. The resulting differences from the results of Fuller and Leal will be described in the next section.

Because of the nonlinear spring, the charge force, and the variable friction coefficient, higher order moments appear in eq. (6). Although the full configuration space diffusion eq. (4) could be solved, it is much preferable to deal with the moment equations, and this requires use of the preaveraging approximation which can now be used legitimately once (6) has been derived. The preaveraging approximation is very accurate whenever the distribution friction is strongly peaked, approaching a delta function in the neighborhood of the expected configuration of the dumbbell (see Tanner [20]). This is the case for dumbbells with nonlinear springs which are elongated to 50% or more of their maximum length. This almost always occurs in the strong flows we are interested in and also occurs at equilibrium for large enough values of the charge parameter, E. When the preaveraging approximation is applied, eq. (6) becomes a set of nonlinear ordinary differential equations which are easily solved numerically for unsteady flows or for transients due to the initiation or cessation of a steady flow. Steady solutions for the second moments of the distribution function can be solved largely analytically. The results are presented in the next section, beginning with the equilibrium configuration in the absence of flow.

3. Results

3.1 Equilibrium configuration

We begin by considering the predicted effect of Coulombic repulsion on the equilibrium coil dimensions. It should, of course, be recognized that much more sophisticated models than the simple dumbbell have been developed for polyelectrolytes in ionic solvents in an attempt to describe equilibrium thermodynamic and near-equilibrium transport properties. One might expect a direct comparison with these theories to provide predictions of the dependence of E on added salt concentration, degree of ionization, and ion binding (or equivalently, provide a more complicated and detailed expression for the electrostatic force between the beads). However, the goal of our work is not to describe equilibrium properties as such, but rather to develop a model which gives at least a qualitatively correct description of the large *departures* from

equilibrium configurations that can develop in strong flows. The primary interest in the predicted equilibrium properties for our model is as a possible basis, independent of the strong flow birefringence experiments which we are currently carrying out, to estimate the effective charge density parameter, E, for a given polymer/solvent combination.

The equilibrium root-mean-square end-to-end dimension for the dumbbell model can be obtained easily from the moment eq. (6) with $\gamma \equiv 0$ and $\hat{c}\langle \boldsymbol{rr} \rangle / \hat{c}t \equiv 0$. The result is the cubic equation

$$(3N+2)\langle r^2\rangle^{3/2} + E\langle r^2\rangle - 2\langle r^2\rangle^{1/2} - E = 0 . \qquad (7)$$

Precisely the same result is obtained for the most probable end-to-end distance by first calculating the equilibrium distribution function from the diffusion equation (4) with γ and $\hat{c}\psi/\hat{c}t$ equal to zero, and then solving for r such that $\hat{c}\psi_{eq}/\hat{c}r = 0$. Thus, insofar as the equilibrium coil dimensions are concerned, the preaveraging approximation (which corresponds to the assumption of a delta function configurational distribution) does not introduce significant error for any value of E. This is not surprising in view of the highly peaked form of the actual equilibrium probability density function

$$\psi_{eq} = \frac{1}{J_{eq}}[1 - r^2]^{3N-2} \exp(-3E/r) \qquad (8)$$

which is shown for various values of E and $N = 100$ in figure 1. This distribution function becomes more highly peaked as N increases. It may be noted that previous comparisons of theory and predictions for flow-induced birefringence of nonionic polymers (for example, polystyrene in Arochlor) would suggest that each statistical subunit contains about 30 monomer units [2]. Thus, depending upon the precise molecular weight of a monomer unit and the number of monomer units in a statistical subunit, a polymer molecule with $N = 100$ subunits corresponds approximately to a molecular weight of $O(10^5)$, while $N = 1000$ is equivalent to a molecular weight of $O(10^6)$.

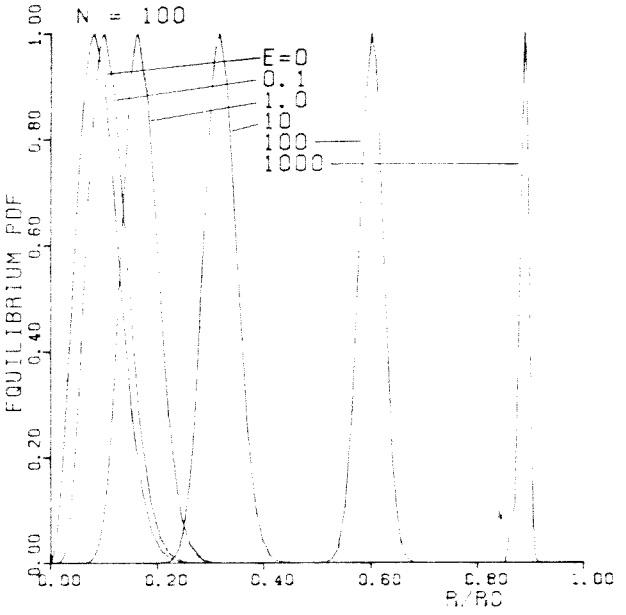

Fig. 1. Equilibrium probability density function of the charged dumbbell for $N = 100$ and $E = 0$, 0.1, 1.0, 10.0, 100.0 and 1000

The variation of the rms dimension of the dumbbell as a function of the charge density parameter E is shown for various values of N in figure 2. Evidently for sufficiently large E, the charge repulsion can drastically increase the equilibrium "coil" dimensions, in extreme cases causing the dumbbell to approach full extension. It is possible to estimate the actual charge density of a polyelectrolyte if the number and average spacing of the charged groups is known. Indeed, typical values range from zero to three for monovalent vinyl polyelectrolytes [18]. However, in view of the fact that point charges at the ends of the dumbbell are intended to

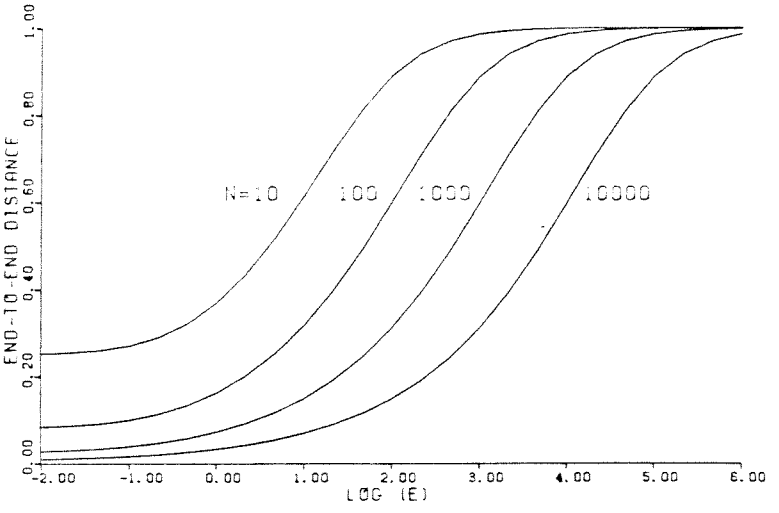

Fig. 2. Equilibrium end-to-end distance vs. the effective charge density parameter, E for $N = 10$, 100, 1000 and 10000

replace the complete charge distribution, considerably larger values may be expected for the effective charge density in our model [21]. At any rate, an a priori estimate of the charge density parameter, E, for the dumbbell model is not practical, as indicated previously, and E must therefore be determined by comparison between some measurable macroscopic property and model prediction.

One possibility, as already noted, is to use an experimental measurement of the equilibrium coil expansion to obtain an estimate for E. For this purpose, it is convenient to express the predicted equilibrium configuration in terms of the so-called expansion factor α defined as

$$\alpha^2 = \langle r^2 \rangle / \langle r^2 \rangle_0 \tag{9}$$

where $\langle r^2 \rangle_0$ is the equilibrium coil dimension in the absence of any Coulombic repulsion. This expansion factor can be determined directly via dynamic light scattering measurements of diffusion coefficients. Results for the equilibrium expansion coefficient α from the current model are plotted in figure 3 as a function of E and N. It may be noted here that expansion factors are also sometimes determined from measured changes in the intrinsic shear viscosity according to the formula $\alpha_\eta^3 = [\eta]/[\eta]_0$, and in general, the result may be somewhat different from that determined by measuring the radius of gyration. However, for the model considered here $\alpha_\eta \equiv \alpha$.

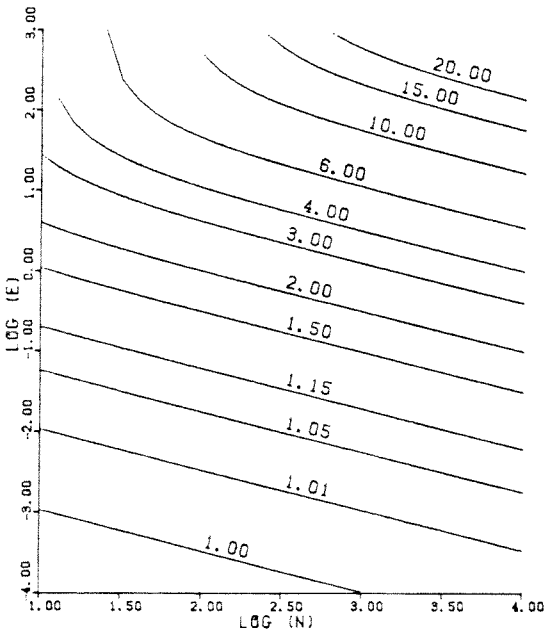

Fig. 3. Electrostatic expansion factor vs. E and N (from eq. (10))

An analytic relationship can be obtained for α as a function of E and N by using the solution of eq. (8) for $\langle r^2 \rangle$ and noting that $\langle r^2 \rangle_0 = 2/(3N+2)$. The result is

$$2\sqrt{2}\,(3N+2)^{1/2}\frac{\alpha^3-\alpha}{(3N+2-2\alpha^2)} = E\,. \tag{10}$$

For $\alpha \ll N$, this equation reduces to the simpler form [21],

$$\alpha^3 - \alpha = \frac{E}{2}\left(\frac{3N}{2}\right)^{1/2}$$

for which the term "third power" type coil expansion has been coined [5].

It should be noted that α appears, for $\alpha \ll N$, to be a function of $E\sqrt{N}$ rather than E alone. Hence the problem of specifying E from coil-expansion measurements is somewhat complicated since both E and N for a particular solvent and polyelectrolyte may be expected to vary with the concentration of added salt. In the case of nonionic polymers, Fuller and Leal [2] used the high strain-rate saturation value of the flow-induced birefringence to obtain an independent estimate for N. The same procedure can be followed here, in principle. The other independent model parameter θ can also be estimated from dynamic light scattering methods as outlined by Fuller and Leal [2]. The problem of obtaining independent estimates for the three model parameters, θ, E and N for real polyelectrolyte/solvent/counter-ion systems will be discussed in more detail in our forthcoming experimental investigation of dilute polyelectrolyte solutions [22].

3.2 *Steady flow behavior*

We turn now to the predicted behavior of the charged dumbbell model for steady flows. Previous investigations of polyelectrolyte solutions have considered only the behavior in simple shear flows (i.e. the special case $\lambda = 0$ of the general flow field, given in eq. (2), which we study here). At steady state, the moment eqs. (7) are solved easily for arbitrary λ with the results

$$\begin{aligned}
\langle x^2 \rangle &= \frac{1}{6N^{3/2}rf}\left(2 + \frac{\gamma^2(1+\lambda)}{f^2 - \gamma^2\lambda}\right),\\
\langle y^2 \rangle &= \frac{1}{6N^{3/2}rf}\left(2 + \frac{\gamma^2\lambda(1+\lambda)}{f^2 - \gamma^2\lambda}\right),\\
\langle xy \rangle &= \frac{1}{6N^{3/2}r}\,\frac{\gamma(1+\lambda)}{f^2 - \gamma^2\lambda},\\
\langle z^2 \rangle &= \frac{1}{3N^{3/2}rf},\\
\langle r^2 \rangle &= \frac{1}{6N^{3/2}rf}\left(6 + \frac{\gamma^2(1+\lambda)^2}{f^2 - \gamma^2\lambda}\right),
\end{aligned} \tag{11}$$

where

$$f = \frac{1}{\sqrt{N}r}\left(\frac{1}{1-r^2} - \frac{E}{3Nr^3} + \frac{1}{3Nr^2}\right).$$

The end-to-end distance $\langle r^2 \rangle$ at several values of E is plotted in figure 4 as a function of the velocity gradient γ for λ in the range $0 \leqq \lambda \leqq 1$, and $N = 1000$.

The results for $E = 0$ in figure 4 were described qualitatively by Fuller and Leal [1]. However, due to the modifications in the moment equation, described previously, there are some quantitative differences between the results in figure 4 and those obtained by Fuller and Leal. In particular, the equilibrium coil radius for $E = 0$ is $2/(3N + 2)$ for the present correct version of the moment equation instead of $1/(N + 1)$ in their case. Thus, for any large N, the radius in the coiled state is slightly smaller for the present model, the effective bead friction coefficient is reduced, and a larger magnitude of the velocity gradient is required, for any flow type λ, for significant departure of the end-to-end distance from equilibrium. The most striking feature in figure 4, which was also obtained by Fuller and Leal [1], is the existence of multiple solutions for some range of γ and $\lambda > 0$. In this regime, three steady states are possible, but the middle one is unstable. Thus, the predicted behavior, say for $\lambda = 0.1$ and $E = 0$, is a range of γ where a macromolecule initially in the equilibrium coil configuration will remain only slightly "deformed" until a critical "onset" value of $\gamma = \gamma_{onset}$ (~ 1.7 for the case $\lambda = 0.1$ and $E = 0$ considered in figure 4) is reached, at which there is a discontinuous transition to the upper branch of stable solutions which correspond to an almost fully extended state. A polymer molecule in the extended state, on the other hand, can be maintained in a highly stretched state down to a value of $\gamma = \gamma_{recoil}$ which is considerably lower than γ_{onset}. This hysteresis in end-to-end distance has extremely important implications for the behavior of dilute solutions of flexible, coiled polymers (as discussed earlier by Fuller and Leal [1], and by Leal, Fuller and Olbricht [23] for the well-known "drag reduction" phenomenon), and persists down to flows which are only very slightly more extensional in character ($\lambda \sim 0.001$) than simple shear flow ($\lambda = 0$). The explanation for these effects in the model is the fact that the bead friction coefficient is very much larger in the extended state than it is for coiled, near-equilibrium configurations. As a consequence, the intrinsic timescale characteristic of the model is much larger, $t_c \sim \theta\sqrt{N}$, in the extended state than it is in the near-equilibrium states corresponding to the lower branch of stable solutions in figure 4, where $t_c \sim \theta$.

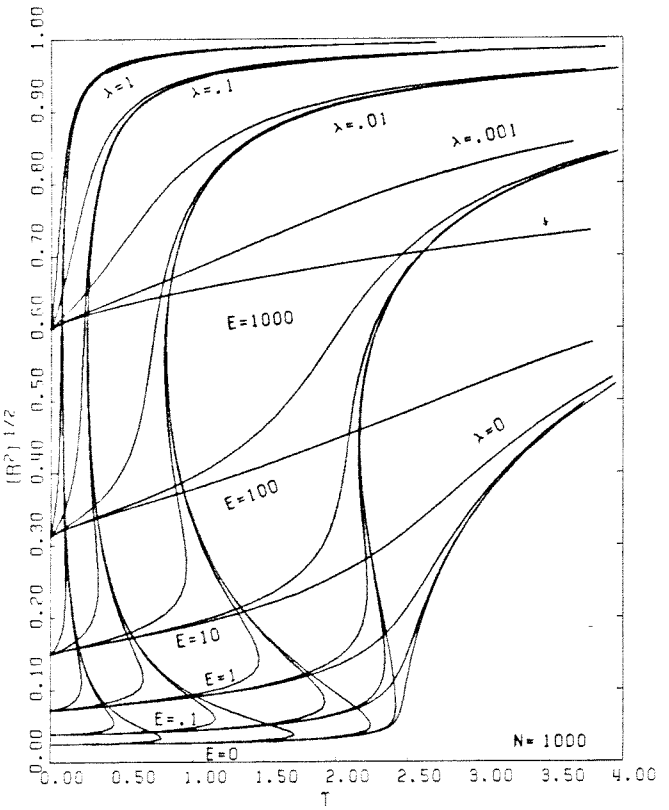

Fig. 4. End-to-end distance vs. velocity gradient for various flow types (λ) and for values of the charge density parameter, $E = 0, 0.1, 1.0, 10, 100$ and 1000, and for $N = 1000$

The interesting new results from the present work concern the effect of electrostatic charge repulsion on the features outlined above for $E = 0$. These results are illustrated in figure 4 for $E = 0.1$, 1.0, 10.0, 100 and 1000. For relatively weak Coulombic repulsion ($E \leqq 1$), the qualitative behavior is the same as that described above for the nonionic case, $E = 0$. That is, there is still a predicted critical onset point for extension to a fully extended configuration, and the end-to-end dimension still shows the hysteresis effect. However, it should be noted that the critical velocity gradient, γ_{onset}, is shifted dramatically to lower values for all values of λ. This is a consequence of the increase in coil dimension in the rest state, coupled with the assumption of an increasing bead friction coefficient with increase of end-to-end dimension in the dumbbell. Since the Coulombic repulsion increases the rest state end-to-end dimension, the bead friction factor is increased and the velocity gradient necessary for the coil stretch transition is decreased. Once the dumbbell reaches about 20% of its full extension, however, the effect of the Coulombic repulsion for $E = 0.1$ and 1 is completely negligible and the predicted end-to-end dimension vs. velocity gradient curves are identical. This means that the critical

velocity gradient for the transition from a stretched state back to the near-equilibrium coil is unchanged from the case $E = 0$, and the magnitude of the hysteresis effect is diminished (i.e. the difference between γ'_{onset} and γ'_{recoil} is reduced by increase of E). It should be noted that the shift in onset point with E for these cases is entirely a consequence of the existence of conformation dependent friction in the model. For example, the effects of E on coil expansion predicted by the dumbbell model with a nonlinear spring, but only constant bead friction, are shown in figure 5. It is evident that there is some "smoothing" of the transition to a stretched configuration over a wider range of velocity gradient, as E is increased, but no change in the "mean" onset point (and, of course, the hysteresis effect is entirely eliminated). Hence, experimental confirmation of the predicted decrease in the critical velocity gradient for onset of the coil-stretch transition as the polyelectrolyte expands would constitute a sensitive and convincing verification of the validity of the conformation-dependent friction concept in the dumbbell model. Such experimental verification appears to exist in the published work of Miles, Tanaka and Keller [14]. These authors report critical strain rates for onset of birefringence in a "cross-slit" flow device which increase with increasing NaCl concentration in 1000 PPM solutions of sodium-polystyrene sulfonate in water. In addition, the critical strain-rates were found to decrease as $1/(MW)^2$ at low salt concentrations, but as $1/(MW)^{1.5}$ with additional added salt. Measurements at lower polymer concentrations will be reported by Dunlap, Wang and Leal [22].

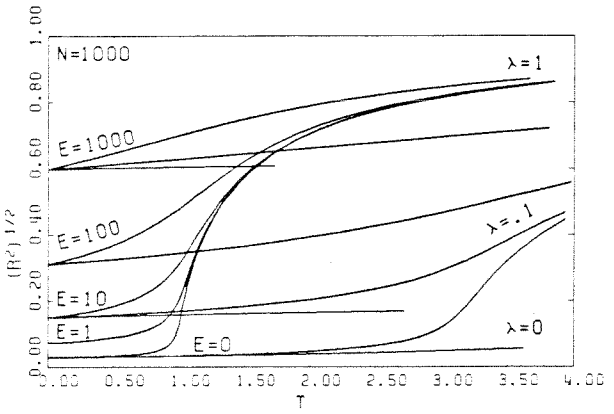

Fig. 5. End-to-end distance vs. velocity gradient for various values of λ and E when the bead friction coefficient is kept constant

If it is assumed that onset of the coil-stretch transition shoulder occur when $t_c \gamma'_{onset}$ = constant, where t_c is a characteristic relaxation time for the polymer/solvent combination, then the observed shift in onset point for birefringence can be interpreted as an increase in t_c. This appears to be consistent with the molecular weight dependence of the onset strain rates reported by Miles et al. [14], and it is the point of view which they adopted. It may be recalled that the relaxation time for the dumbbell model undergoes a transition from θ to $\theta\sqrt{N}$ with increasing end-to-end extension. This reflects the increase in conformation-dependent friction as the mean-square end-to-end distance $\langle r^2 \rangle$ is increased from $O(1/N)$ to $O(1)$. Indeed, the decrease in γ'_{onset} (or increase in t_c) with increasing charge repulsion should be approximately proportional to the increase in end-to-end distance according to our model, and therefore to the expansion factor α (if α is not large), because the friction increases in proportion to α. The

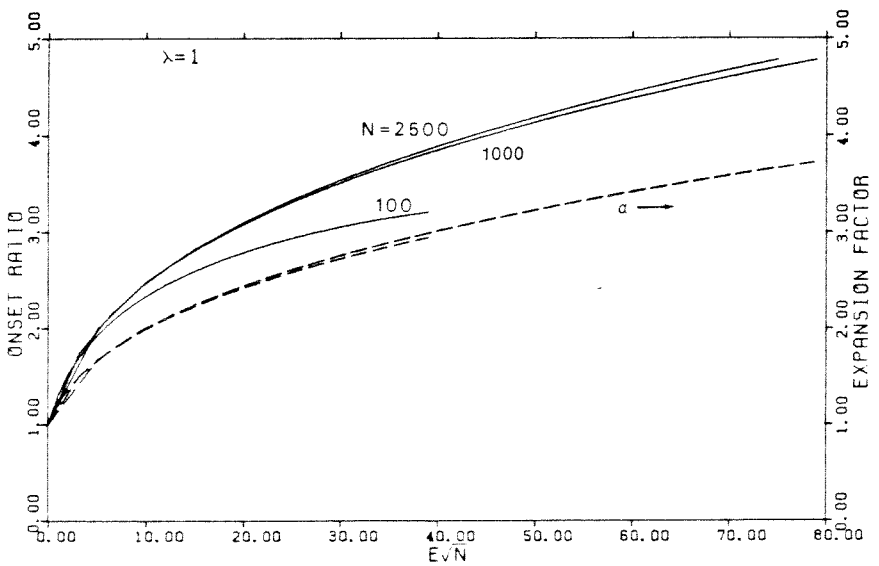

Fig. 6. Shift in onset point due to Coulombic repulsion for various N; comparison with expansion factor α (---). The onset ratio is the ratio of γ'_{onset} at a given value of E to γ'_{onset} with $E = 0$

extent to which this approximation is valid can be seen in figure 6 where we have compared the dependence of α and $(\dot{\gamma}'_{onset}/\dot{\gamma}'_{onset,E=0})^{-1}$ on $E/\sqrt{N}$ for several values of N. For sufficiently large N, the expansion factor should depend only on $E/\sqrt{N}$. The dependence of the onset ratio on N is somewhat more complicated, but the basic correspondence between the onset ratio and α is clear.

For the larger values of E illustrated in figure 4, the effects are similar in nature, but much more dramatic in detail. As the rest state end-to-end dimension continues to increase with increase of E, the onset velocity gradient continues to decrease until finally, for the largest values of E there is only a monotonic increase in end-to-end distance with velocity gradient. For $E = 1000$, the dumbbell becomes more nearly a slightly extensible "rod-like" particle and the effect on the flow is primarily a reflection of orientation of a nearly "rigid" particle.

In addition to end-to-end dimensions, we have also calculated the rheological properties predicted by the model for steady shear and planar elongational flows using the standard form

$$\sigma = n\langle \boldsymbol{F}_{connector}\boldsymbol{r}'\rangle$$

for the additional stress due to n dumbbells per unit volume (less an isotropic contribution). In the dumbbell with $E = 0$, the only contribution to the effective "connector" force between beads is due to the presence of the spring. For $E \neq 0$, on the other hand, the force transmitted between beads by the Coulombic repulsion must also be included so that,

$$\frac{\sigma}{3kTn} = N\left\langle\left[\frac{1}{1-r^2} - \frac{E}{3Nr^3}\right]\boldsymbol{rr}\right\rangle.$$

Thus, with the pre-averaging approximation

$$\frac{\sigma}{3kTn} = N\left[\frac{1}{1-r^2} - \frac{E}{3Nr^3}\right]\langle\boldsymbol{rr}\rangle. \tag{12}$$

The expression for the stress obtained in this simple way is precisely equivalent to that obtained by summing the contributions due to the mechanical spring and the Maxwell stress to account for the ionic contributions [24], including those contributions from the counterion charge cloud in the solvent (these being reflected indirectly through the effective charge assigned to the beads).

The steady shear viscosity is shown in figure 7 for $N = 1000$ and various values of E. The expected increase in the zero shear-rate viscosity due to increased coil expansion with increase of E is clearly evident. For very large E, the solution is strictly shear-thinning,

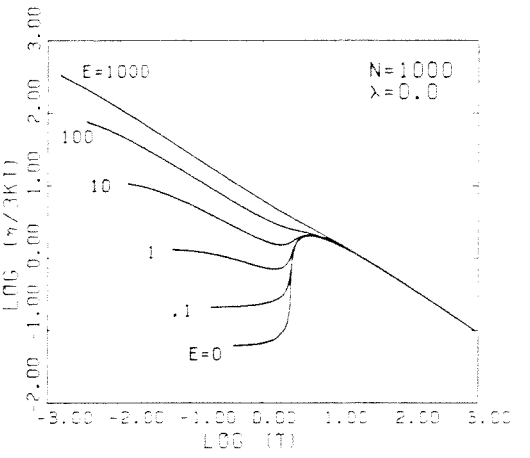

Fig. 7. Steady shear viscosity for $N = 1000$ and various values of E

again reflecting the transition toward an extended, rigid rod. The increase in shear viscosity to a maximum value for E between 0 and 10 was also found by previous investigators [1, 25], and is a consequence of the increase in bead friction with increased dumbbell extension. Although this prediction is probably at odds with reality, very few experimental studies of truly dilute solutions are available and at least one of these purports to measure a similar peak in viscosity [26]. It may be noted here that a recent study of an anisotropic dumbbell model shows that the predicted maximum is probably due to an oversimplistic fluid mechanical description of the polymer, which can be removed by inclusion of "strain inefficiency" of rotation in the hydrodynamic description of the dumbbell [28]. At any rate, we are more concerned here with adequate representation of dilute solution behavior in "strong flows" and this aspect of the model behavior is unchanged by the modifications of the model which would remove the shear-thickening of shear viscosity. We report the shear viscosity result primarily for completeness in the present paper. It may be noted that the first normal stress difference exhibits the same qualitative behavior as the shear stress in simple shear flow. The second normal stress difference is zero.

Of greater interest in the present context is the elongational viscosity ($\bar{\eta} \equiv \sigma_{xy}/\dot{\gamma}$) in the planar extensional flow given by eq. (2) with $\lambda = 1$. This result is shown in figure 8 for $N = 1000$ and $0 \leqq E \leqq 1000$. The elongational viscosity for any given value of the extension rate $\dot{\gamma}$ is increased by the Coulombic repulsion between beads, and this reflects the increased degree of extension which the dumbbell exhibits. This includes the limiting case $\dot{\gamma} \to 0$, where the elongational viscosity is just two times the predicted shear viscosity (as is

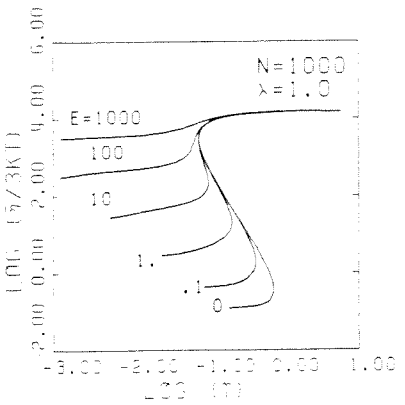

Fig. 8. Planar elongational viscosity for $N = 1000$ and various values of E

also true for a Newtonian fluid at all extension rates). The shape of the curves in figure 8 is a direct reflection of the dependence of end-to-end dimension on the velocity gradient, and shows all of the same features including multiple steady values and a hysteresis for some intermediate range of $\dot{\gamma}$. The high extension rate limiting value of $\bar{\eta}$ is, of course, common for all values of E since it is the value for full extension and alignment of the dumbbell with the principle strain axis of the flow. There is not yet a clear consensus, from experimental studies, of the expected asymptotic behavior of $\bar{\eta}$, even for more concentrated polymer solutions. No data directly relevant to dilute solutions is available. However, indirect indications of viscosity in extensional flow are possible from such sources as pressure drop/flow rate relationships for dilute polymer solutions in a porous media.

The data of Durst, Haas and Kaczmar [6] are particularly relevant. They have examined porous media flow of dilute solutions of hydrolyzed polyacrylamide (HPAM). The effects of charge density, degree of ionization, added salt, and solvent viscosity on the non-Newtonian pressure drop behavior were reported. Their results are in qualitative agreement with our model predictions. For nonionic PAM there is an onset of non-Newtonian behavior (increased pressure drop) at a critical flow rate which seems to coincide with $\dot{\gamma}'\theta \sim O(1)$. This same behavior was observed for HPAM with low charge density, low degree of ionization, or very high salt concentration. Each of these cases corresponds to our charge density parameter E being very small. The increased pressure drop is believed to be related to the extensional viscosity which dominates the effects of the shear viscosity when the polymer chains are greatly stretched out by the flow. Their data for moderate salt concentrations shows a shift in onset behavior to lower flow rates and no significant departures from Newtonian behavior for flow rates less than the onset, in agreement with our model predictions for $E \sim 0.1$ to 1. The highly charged HPAM in solutions of low ionic strength showed departure from Newtonian behavior even at the lowest flow rates used in the experiments, as is also observed for the model with very large values of E. A very similar qualitative correspondence can be observed between the charged dumbbell predictions and the drag reduction data for polyelectrolyte solutions of Virk [8]. A more quantitative test of the predictions of this model in strong flows will require data from a well-characterized flow experiment, with polydispersity taken into account. To accomplish this, we are currently measuring flow birefringence of well characterized samples of Na-polystyrene sulfonate in four- and two-roll mills which simulate quite well the flow field described by eq. (2).

3.3 *Transient behavior*

The nonlinear dumbbell has been previously shown to predict a stress overshoot during startup from rest of simple shear flow [25], both in the shear stress and the first normal stress difference. The presence of charges on the beads enhances the overshoot dramatically as shown in figure 9 for $N = 1000$, $\dot{\gamma} = 1$ and 10, and several values of E. For $\dot{\gamma} = 1$ the uncharged dumbbell ($E = 0$) shows no overshoot at all, but there is a significant overshoot for $E \geqq 1$. For some values of E, such as $E = 10$, there are also oscillations prior to the final steady state. For large values of E and high shear rates the stress overshoot reaches a level comparable to the

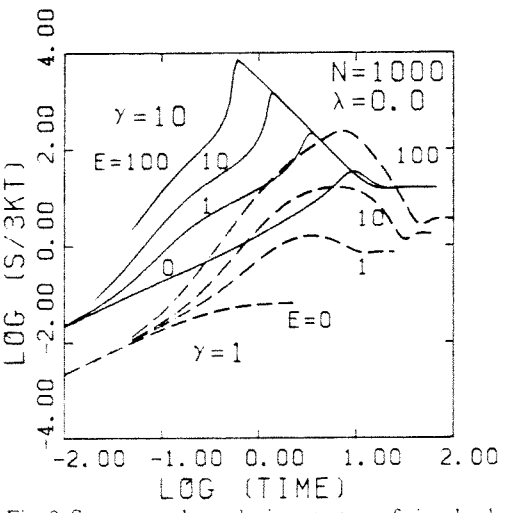

Fig. 9. Stress overshoot during startup of simple shear flow for $N = 1000$. Solid curves are for $\dot{\gamma} = 10$ and several values of E. Dashed curves are for $\dot{\gamma} = 1$ and several values of E

stress in extensional flow. The mechanism for the predicted overshoot is that the partially extended polymer is rotated through the orientation where it makes its maximum contribution to the stress prior to achieving its steady state orientation and extension. The larger the extension when the orientation of maximum stress is achieved, the larger the overshoot. In view of the weak extension due to the shear flow, the extension due to increased E has a strong effect on the magnitude of the stress overshoot. Unfortunately, there is currently a lack of appropriate experimental data for dilute polymer solutions with which to compare these predictions.

No overshoot is predicted or expected at inception of extensional flow, since the orientation of maximum stress contribution is also the axis of asymptotic orientation for large times. Typical results for the elongational viscosity in startup of planar extensional flow are shown in figure 10 for $N = 100$, $E = 1.0$ and various strain rates, γ. The effect of increasing the charge parameter is to reduce the time required to reach steady state at a given elongation rate. Figure 11 plots the time required for the charged dumbbell to reach 90% of its steady state end-to-end distance vs. strain rate for various values of E. As shown previously by Fuller and Leal [1], there is a great increase in the time required near γ_{onset} for $E = 0$. This same behavior occurs for any value of E for which the hysteresis is also observed. This peak occurs because at the onset point, two steady state configurations exist which are far removed from one another. In both states, the spring force and frictional force are balanced, leaving Brownian diffusion as the only mechanism for reaching

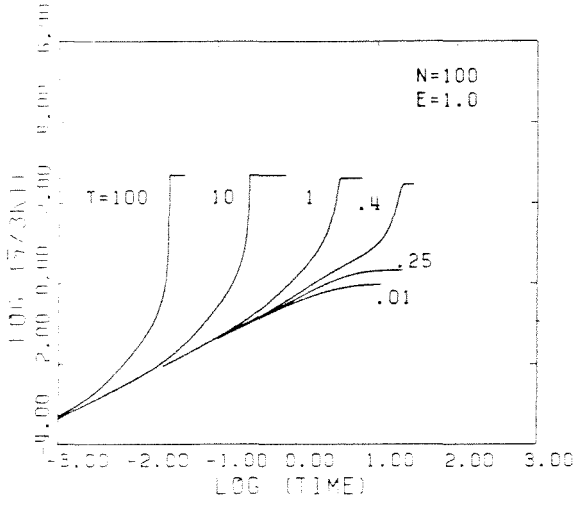

Fig. 10. Growth of elongational viscosity with time on startup of planar extension for $N = 100$, $E = 1.0$, and several values of the velocity gradient

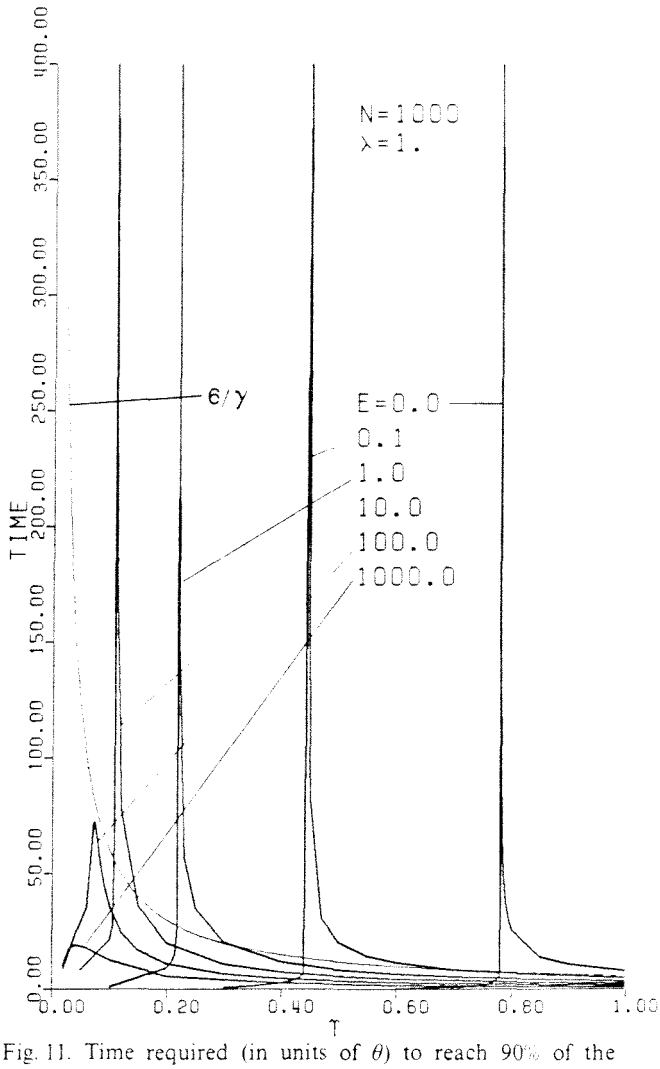

Fig. 11. Time required (in units of θ) to reach 90% of the steady state end-to-end distance for planar extensional flow for various values of E and $N = 1000$

the more extended steady state configuration, and this occurs on a much slower time scale than convection by the flow. When E is large enough to eliminate the hysteresis effect or for $\gamma > \gamma_{onset}$, frictional forces dominate, and the required time to steady state is proportional to $1/\gamma$.

It is apparent that for a polymer to be significantly extended requires not only a sufficiently strong flow, but also a sufficient transit time in that flow. The transit time is always finite in experimentally realizable extensional flows (except at a stagnation "point"). In general, the maximum time that a polymer molecule will be subjected to the extensional flow is

$$t_{max} = t^*/\gamma \tag{13}$$

where the proportionality constant t^* depends on the flow type, λ, and the geometry of the flow device. The

curve $t_{max} = 6/\dot{\gamma}$ has been plotted in figure 11. This value of t^* corresponds to the transit times actually observed in the four-roll mill for $\lambda = 1$ near the stagnation point [2]. This curve typically intersects the peaks of the dumbbell curves in figure 11, implying that the dumbbell will fail to reach its steady state configuration only for shear rates near $\dot{\gamma}_{onset}$. Thus, the finite transit time of a real flow affects the onset of the coil-stretch transition. In particular, the discontinuous transition to an extended configuration seen in the steady state behavior will be smoothed out over a range of shear rates when only a finite time is allowed for the dumbbell to extend. If t^* is small enough that the t_{max} curve remains below the dumbbell curve for $\dot{\gamma} \gg \dot{\gamma}_{onset}$, the dumbbell will have insufficient time to approach steady state extensions no matter how large the strain rate. Flows having such small transit times will not produce large departures from Newtonian behavior for dilute polymer solutions, even though the velocity gradients would be large enough to produce such departures at steady state.

4. Conclusions

We have considered the charged dumbbell model first introduced by King and Eisenberg as a model for polyelectrolytes in a dilute solution, and included a nonlinear spring and variable friction factor in order to study its behavior in "strong" flows. The variable friction factor results in a dramatic onset to an almost fully extended configuration (the coil-stretch transition) at a critical value of the velocity gradient which depends on flow type, λ. The onset point shifts to lower velocity gradients as Coulombic repulsion in the dumbbell is increased. This coincides with an increase in the rest state dimensions and an increase in the intrinsic viscosity. For very strong states of repulsion, the model behavior becomes that of a slightly extensible rigid dumbbell, with an effect in flow similar to that observed for highly extended or rigid macromolecules or fibers.

These results are in qualitative agreement with data on drag reduction in turbulent flow [8] and pressure drop vs. flow rate data in porous media flow [6]. These data for dilute solutions show an order of magnitude departure from Newtonian behavior at a critical flow rate which depends on salt concentration or charge density in a way consistent with the present model. Comparisons of a more quantitative nature for well-defined two-dimensional flows (in a four-roll mill) are currently being carried out. We intend to assess the ability of the model to predict strong flow behavior using values of E estimated from independent measurements of equilibrium coil expansion via light scattering spectroscopy.

Acknowledgment

This research was supported by the Office of Naval Research.

References

1. Fuller GG, Leal LG (1981) J Non-Newtonian Fluid Mech 8:271
2. Fuller GG, Leal LG (1980) Rheol Acta 19:580
3. De Gennes PG (1974) J Chem Phys 60:5030
4. Hinch EJ (1974) Proc Symp Polym Lubrification, Brest
5. Nagasawa M (1975) J Polym Sci: Symp No 49:1
6. Durst F, Haas R, Kaczmar BU (1981) J Appl Polym Sci 26:3125
7. Ouibrahim A, Fruman DH (1980) J Non-Newtonian Fluid Mech 7:315
8. Virk PS (1975) Nature 253:109
9. King M, Eisenberg A (1972) J Chem Phys 57:482
10. Nakajima H, Wada Y (1974) Reports Prog Polym Phys Japan 17:51
11. Fujimori S, Nakajima H, Wada Y, Doi M (1975) J Polym Sci: Polym Phys Ed 13:2135
12. Okamoto H, Nakajima H, Wada Y (1974) J Polym Sci: Polym Phys Ed 12:2177
13. Rosser RW, Nemoto N, Schrag JL, Ferry JD (1978) J Polym Sci: Polym Phys Ed 16:1031
14. Miles MJ, Tanaka K, Keller A (1983) Polymer 24:1081
15. Warner HR (1972) Ind Eng Chem Fund 11:375
16. Fuller GG, Leal LG (1981) J Polym Sci: Polym Phys Ed 19:557
17. Manning GS (1972) Ann Rev Phys Chem 23:117
18. Kowblansky M Zema P (1981) Macromolecules 14:1451
19. Kowblansky M, Zema P (1982) Macromolecules 15:788
20. Tanner RI (1975) Trans Soc Rheol 19:37
21. Katchalsky A, Kunzle O, Kuhn W (1950) J Polym Sci 5:283
22. Dunlap PN, Wang CJ, Leal LG (1984) to appear
23. Leal LG, Fuller GG, Olbricht WL (1980) Prog Astro Aero 72:351
24. Russel WB (1979) J Fluid Mech 92:401
25. Tanner RI (1975) Trans Soc Rheol 19:557
26. Burow SP, Peterlin A, Turner DT (1965) Polymer 6:35
27. Dunlap PN (1984) PhD Thesis, California Institute of Technology
28. Phan-Thien N, Manero O, Leal LG (1984) Rheol Acta 23:151

(Received July 19, 1983)

Authors' address:

Dr. P. N. Dunlap, Prof. L. G. Leal
Department of Chemical Engineering
California Institute of Technology
Pasadena, CA 91125 (USA)

CHAPTER III.

An Experimental Study of Dilute Polyelectrolyte Solutions in Strong Flows

An Experimental Study of Dilute Polyelectrolyte Solutions in Strong Flows

by

P. N. Dunlap and L. G. Leal

Department of Chemical Engineering
California Institute of Technology
Pasadena, California 91125

and

C.-H. Wang

Department of Chemistry
University of Utah
Salt Lake City, Utah 84112

Abstract: Flow-induced changes in the conformation of polymer molecules in dilute polyelectrolyte solutions were studied, using birefringence techniques, as a function of molecular weight and added salt concentration in laminar, two-dimensional extensional flows produced in four- and two-roll mills. Of particular interest is the so-called coil-stretch transition. It is shown that the electrostatic expansion of the polyelectrolyte has a dramatic effect on the onset shear rate for the coil-stretch transition and also on the shape of the flow birefringence versus shear rate curves during the stretching process. A reasonable description of the coil-stretch transition and its dependence on equilibrium configuration is obtained theoretically using a charged dumbbell model with conformation-dependent bead friction. Being dependent on the longest relaxation time of the polymer, and therefore not too sensitive to intramolecular details, the dumbbell model can be applied in two ways: either using a charge force to expand its rest state, or reducing N, the number of Kuhn segments, in proportion to the increase in relaxation time of the expanded polyelectrolyte.

1. INTRODUCTION

Dilute solutions of flexible, linear polymer molecules are well-known to exhibit dramatic non-Newtonian effects in flows which induce a transition from the coiled equilibrium configuration to a highly extended and oriented configuration. Examples of such effects include increased pressure drops in porous media,[1] converging channels,[2] and orifice flows,[3] and drag reduction in turbulent pipe flows.[4] Recent experimental studies in this lab have concentrated on measuring this coil-stretch transition process in well-defined extensional flows,[5,6] and on determining the resulting effects of the polymer on the flow fields.[6] Theoretical studies have aimed at predicting the details of the coil-stretch process in the same flows using dumbbell models.[7–9] These studies have shown that for high molecular weight, flexible linear polymers, the coil-stretch transition does occur in the way predicted by theory,[10,11] with an onset shear rate, γ_c, that is $O(1/\tau)$, where τ is the longest relaxation time of the polymer. The nonlinear elastic dumbbell model gives quantitative predictions of flow birefringence versus shear rate in steady extensional flows provided account is taken of the effects of polydispersity and of finite residence times in the extensional flow region of the flow device.[5,6]

Polyelectrolytes in high ionic strength solutions also exist in a compact coiled configuration, and thus can be expected to show the same type of strong flow behavior as nonionic polymers. However, in solutions of lower ionic strength the electrostatic repulsion between the charged groups on the polyelectrolyte chain expand (and *elongate*) the equilibrium coil. This electrostatic expansion causes a change in the hydrodynamic interaction between solvent and polymer, and therefore a change in the relaxation time and the onset behavior of the coil-stretch transition. The change in hydrodynamics of the polyelectrolyte is clearly evident in the molecular weight (M_w) dependence of the intrinsic viscosity ($[\eta]$).[12–14] At high ionic strengths, the coil is relatively impermeable to flowing solvent and this

results in so-called non-free-draining hydrodynamics, with $[\eta] \sim M_w^{.5}$. At intermediate ionic strengths, "good solvent" behavior is found with $[\eta] \sim M_w^{.8}$. At very low ionic strengths, the hydrodynamic interaction between the expanded coil and the solvent is enhanced enough that the polymer exhibits so-called free-draining behavior, with $[\eta] \sim M_w$. The transition in hydrodynamic interaction with the solvent affects the relaxation time of the polymer in an analogous way since τ is related to $[\eta]$ according to $\tau = [\eta]\eta_s M_w/RT$ with η_s the solvent viscosity, R the universal gas constant, and T the temperature. The shift in the molecular weight dependence of the relaxation time has been inferred by Miles *et al.*[15] by estimating τ as the inverse of the onset shear rate for the coil-stretch transition in a two-dimensional extensional flow device.

The transition from non-free-draining to free-draining behavior can also be detected in flow through packed beds,[16] in orifice flows,[17] and in drag reduction experiments.[18] In these situations, the change in hydrodynamic behavior is indicated by a distinct shift in the conditions for onset of non-Newtonian effects. As the equilibrium coil dimensions increase due to electrostatic expansion, the onset point for the coil-stretch transition shifts to lower shear rates. In the free-draining limit, the distinct onset point often disappears altogether as conformation changes are easily induced at all shear rates by simple re-orientation of the expanded coil which now adopts an elongated shape in the rest state.

In the present work, we report the results of flow birefringence measurements in dilute solutions of sodium polystyrenesulfonate (NaPSS) in glycerol with a range of added salt concentrations. We have investigated the entire range of linear two-dimensional extensional flows and simple shear flow as produced in four- and two-roll mills and a cylindrical Couette device, respectively. Independent data on the equilibrium expansion of NaPSS as a function of salt concentration have been obtained by quasi-elastic light-scattering spectroscopy and intrinsic viscosity measurements.

The influence of the polymer on the extensional flow fields was determined by direct measurement of the velocity gradient fields.

The details of the *local* conformation changes that are responsible for the observed *overall* electrostatic expansion of the polyelectrolyte *in equilibrium* have been widely studied theoretically. The theories giving the best comparisons with experiment describe two contributions to the total electrostatic expansion.[19,20] One is the increased rigidity of the polyelectrolyte, which is characterized by an increase in the persistence length or the Kuhn segment length due to short range electrostatic forces between neighboring charges on the polymer backbone. The other contribution is due to a change in excluded volume as a result of long range electrostatic forces between charges on more widely separated segments of the polyelectrolyte. Though one experimental study[21] has suggested that the excluded-volume effect may be dominant in a flexible linear polyelectrolyte (using classical light scattering), dynamic experiments of the type reported here (including intrinsic viscosity measurements, flow birefringence, and diffusivity measurements via quasi-elastic light scattering) are sensitive mainly to the *overall* conformational and hydrodynamic features of the polyelectrolyte, and cannot provide detailed information on the nature of electrostatic interactions in the polyelectrolytes. Specifically, in the present studies, one cannot unambiguously distinguish the effects of increased rigidity on the coil-stretch transition from the effects of excluded-volume interactions. Therefore, the predictions of the charged dumbbell model[8] are compared with the flow birefringence data using two different approaches to choosing the model parameters. One approach corresponds to assuming that the measured equilibrium expansion is due only to an increase in the persistence length. The other approach corresponds to assuming that only electrostatic excluded-volume expansion occurs. Predictions of the model using both approaches are then compared with the flow birefringence data.

2. EXPERIMENTAL DETAILS

2.1 Materials

Two sodium polystyrenesulfonate (NaPSS) samples were used in this study. The first sample, PSS1, was obtained from Pressure Chemical Company. The reported M_w was 1.2×10^6, and the parent polystyrene had a polydispersity ratio of $M_w/M_n \leq 1.1$. The second sample, PSS4, was generously provided by Dr. D. Brown of the National Bureau of Standards. Its M_w was 4.16×10^6, and it had an estimated polydispersity ratio of 1.3. The synthesis and characterization of the PSS4 sample have been described in the literature.[22] Both of these samples were dried over anhydrous $CaCl_2$ to remove the absorbed water content which was found to be about 10% by weight.

The solvent, glycerol, was obtained from Sigma Chemical and distilled to remove its ~3% water content. The resulting increase in the solvent viscosity was desired for two reasons. First, it increased the relaxation times of the solutions and therefore brought the coil-stretch transition into a more accessible range of shear rates. Second, it increased the stability[23] of the flow devices and reduced the three-dimensionality of the flow due to the top and bottom of the flow device.[6,23] In preparing our solutions, the NaPSS was initially dissolved in a small amount of water, and this NaPSS/water solution was then diluted with the glycerol to 100 ppm PSS^- by weight for PSS1 and 89 ppm PSS^- for PSS4. The resulting solvent contained about 0.25% water and had a viscosity, η_s, of ~14 p.

Flow birefringence data will be presented for seven different polymer/solvent combinations. The available equilibrium data for these solutions are given in Table I. The various salt concentrations were obtained by adding measured amounts of NaCl to the two original "no-salt" solutions (#1 and 4). The salt molarities reported include all the Na^+ from the polymer, which is .00068 M for the PSS1 solutions and .00061 M for the PSS4 solutions. During all the studies, the solutions were sealed or

handled in a dry atmosphere to minimize the absorption of water which can reduce the viscosity of glycerol drastically and make interpretation of the results difficult if it is present in indeterminate amounts. The equilibrium data include intrinsic viscosity ($[\eta]$) measurements and light-scattering measurements of hydrodynamic radii (R_h). These data provide expansion factors (α) which are ratios of the length scale of the polyelectrolyte rest state relative to its size in an "uncharged" state. The uncharged state is assumed to occur in the solutions with the highest salt concentration in calculating α and will be identified by the subscript "0." The usual definitions[24] are used,

$$\alpha_R = \frac{R_h}{R_{h0}} \quad \text{and} \quad \alpha_\eta^3 = \frac{[\eta]}{[\eta]_0}. \tag{1}$$

That these different "measures" of the coil size usually[24,25] give different expansion factors can also be seen from Table I.

TABLE I. Equilibrium Data for NaPSS Solutions[a]

		Light Scattering		Intrinsic Viscosity			Birefringence	
#	Solution	R_h (Å)	α_R	$[\eta]$ ($\frac{cc}{gm}$)	α_η	τ_η (s)	τ_{FB} (s)	α_{FB}
1	PSS1[c]–No Salt	824	4.7	2000	3.1	0.632	1.3	5.1
2	.005 M	282	1.6	–	–	–	0.05	1.7
3	.1 M	176	1.0	70[b]	1.0	0.026	0.011	1.0
4	PSS4[d]–No Salt	1610	6.4	5300	5.8	4.52	1.2	4.8
5	.004 M	–	–	–	–	–	0.09	2.0
6	.04 M	400	1.6	–	–	–	0.035	1.5
7	.4 M	250[b]	1.0	27[b]	1.0	0.035	0.011	1.0

[a] 20.0°C [b] $[Na^+]$=1 M

[c] 100 ppm PSS^-, $[Na^+]$ includes .00068 M from polymer

[d] 89 ppm PSS^-, $[Na^+]$ includes .00061 M from polymer

The intrinsic viscosity measurements also provide an estimate of the relaxation time of the polymer using the Zimm formula,[26] $\tau_\eta = 0.422[\eta]\eta_s M_w/RT$. The relaxation times ($\tau_{FB}$) and expansion factors (α_{FB}) in Table I were estimated from the flow birefringence data and will be discussed later.

One interesting feature of the equilibrium data is the molecular weight dependence of R_h and η. In the no-salt solutions the scaling is as expected for "good solvent" behavior, $\eta \sim M_w^{.78}$. For the highest salt concentrations, the M_w dependence of R_h and τ_η is much less than expected even for Θ conditions, and the M_w dependence of $[\eta]$ is the inverse of that expected. As will be seen, the same trends appear in the flow birefringence data, the solution #7 giving much less birefringence than expected based on its molecular weight. Thus, the PSS4 molecules at high salt concentrations appear to be more compactly coiled than PSS1 molecules are. This may be an example of the unusual scaling behavior that has recently been predicted for polyelectrolytes.[27]

The equilibrium light-scattering measurements of R_h are described in more detail in the Appendix.

2.2 The Flow Devices

The four- and two-roll mills used in these experiments have been extensively described elsewhere.[5,6,28] They are intended to provide a close approximation to the idealized two-dimensional laminar strong flows used in most theoretical analyses of polymer dynamics. The general form for the velocity field for this class of flows is $\mathbf{v} = \gamma(y, \lambda x)$, where γ is the magnitude of the velocity gradient, and λ is a flow type parameter which ranges from -1 to 1. Pure rotational flow is $\lambda=-1$, simple shear flow is $\lambda=0$ and pure extensional flow is $\lambda=1$. Figure 1 shows the streamlines of these limiting, theoretical flows and how they can be obtained in our flow devices, in principle.

A cylindrical Couette flow device was built for simple shear flow experiments. The radius of the inner rotor is 3.361 cm, and the outer cylinder radius is 3.561 cm. The shear rates are found to be γ=16.75ω, where ω is the angular velocity of the inner cylinder.[29]

The velocity gradient fields in the four- and two-roll mills were characterized for these NaPSS solutions using homodyne light-scattering spectroscopy[28] (HLS). Extensive measurements to characterize the four- and two-roll mills which are used in the flow birefringence experiments are reported by Dunlap and Leal.[6] We used the same procedures in this work to determine the extent of any modification of the flow field due to the presence of the polymer. The incident light was from a Spectra-Physics 165 Argon ion laser at 488 nm. The scattering angles used were typically 20–60° outside the cell and 12–40° inside the flow cell due to refraction. The photomultiplier pulses were amplified and shaped by an Ortec amplifier/discriminator and counted and correlated by a BIC-2030 autocorrelator. The solvents were carefully filtered to improve the correlations. We used 0.091 μm PS latex spheres to seed the solutions. The resulting signals were typically of $\sim 10^5$ counts/s, and a very smooth correlation function could be obtained in just a few seconds. The half-height time of the correlation function was evaluated and its inverse used as a characteristic frequency proportional to the actual velocity gradient. The values reported are averages of several measurements. Standard deviations are typically 1% or less.

2.3 Flow Birefringence

The most direct and widely used experimental probe of the polymer behavior in flow seems to be the flow birefringence (FB) experiment.[30] It has been used to study various aspects of the coil-stretch transition in well-defined flows.[5,6,15,31] It can also be used to test predictions of polymer behavior from molecular theories. A schematic of our experimental setup is shown in Figure 2. The flow device can

be moved independently of the optics so that almost any position in the flow field can be studied. The same optics are easily realigned to do the HLS experiment described above. The relative orientations of the polarizer, analyzer, solution optic axes (indicative of the orientation of the elongated polymer molecules), and flow field are also shown in Figure 2. The intensity I measured by a laser power meter or photomultiplier tube is related to the incident intensity I_0, wavelength λ_0, the solution thickness d, the birefringence Δn, and the angle ϑ between the polarizer and the optic axis of the solution.

$$I = I_0 \sin^2 2\vartheta \sin^2 \frac{\pi d \Delta n}{\lambda_0} \tag{2}$$

By finding the position of maximum intensity, $\vartheta = 45°$, the orientation angle χ for the optic axes of the solution can be determined. This angle χ is defined to be consistent with the classical extinction angle from simple shear flow experiments.[30] For all flow types, χ is 45° at low shear rates and rapidly approaches the flow direction φ (the angle between the asymptotic streamline and the x-axis) as the polymer extends at higher shear rates.

The birefringence of the glycerol was measured independently, and its contribution was subtracted from the solution birefringence in order to determine a polymer contribution to the birefringence. The relations recommended by Philippoff[32] were used to subtract off the solvent contribution.

$$\begin{aligned} \Delta n_p^2 &= \Delta n^2 + \Delta n_s^2 - 2\Delta n_s \Delta n \sin 2\chi \\ \cos 2\chi_p &= \frac{\Delta n}{\Delta n_p} \cos 2\chi \end{aligned} \tag{3}$$

Here, the subscript p refers to the polymer, s to the solvent, and no subscript to the measured *solution* property. This relation assumes that the solvent orientation angle is always 45°. This was found to be true for glycerol. From measurements in two-roll mills, the birefringence of glycerol was found to be $\Delta n_s = 2.7 \times 10^{-10} \gamma(1 + \lambda)$.

The FB data for PSS1 will be seen to be considerably "noisier" than that for PSS4 though both exhibited comparable levels of birefringence. In the PSS1 experiments the flow cell had a full glass cover which supported the rollers and could develop considerable stress birefringence. This cover effect sometimes dominated the polymer FB at low and intermediate shear rates. The only way to deal with it was to make short measurements since the glass effect built up on a slower time scale than the polymer contribution to the FB. This problem of parasitic birefringence was later remedied by building a metal top (and bottom) plate with a small leaded glass window. Leaded glass was used because its stress-optical coefficient is much smaller than Pyrex or other typical glasses.[33] There is a significant improvement in the PSS4 data over the PSS1 data as a result.

All the experiments were carried out at $20.0 \pm .15°C$. However, FB is very sensitive to solvent viscosity, and since these temperature fluctuations result in about 5% variations in glycerol viscosity, this is another source of spread in the FB data. Furthermore, since the temperature changes are generally larger for the larger roller speeds, this tends to cause larger variations in the high shear rate FB data.

Mechanical degradation of the polymer was apparently not a problem in the present experiments, though direct evidence of degradation was found in our earlier studies of higher molecular weight polystyrene solutions.[6] To be certain that degradation was not significant, the FB experiments with solution #6 (which had been through two sets of experiments previously as solutions #5 and #4) were repeated with a freshly made PSS4 solution with .04 $\underline{M}$ $[Na^+]$. The FB results for the fresh solution were found to be essentially identical to those for solution #6. Thus, no significant degradation had occurred in the original solutions which were used repeatedly with different amounts of added salt.

2.4 Transient Flow Birefringence

It would be desirable to do startup and relaxation experiments in the four- and two-roll mills. Unfortunately, with the present apparatus transient experiments are too difficult and unreliable. The four separate motors and their clutches are not perfectly synchronized, and the FB is very localized (except in the solutions with no added salt), so that any shift in the stagnation point or center streamline due to inertia or unsymmetrical roller speeds can obscure the real behavior of the FB. Our transient experiments are therefore confined to simple shear flow.

The transient response of the PSS4 solutions to startup and cessation of the flow in the Couette device was recorded using the BIC-2030 correlator in a "multi-channel scaling mode." In this mode of operation, the 64 real-time data channels store sequentially the number of photon counts received during each of 64 consecutive sampling periods. This sweep is triggered by a TTL logic pulse which is generated when the clutch is engaged for startup experiments, and when the brake is applied for relaxation experiments. Any number of sweeps may be collected and added up by repeating the experiment without clearing the memory. In this way, random noise is averaged out, and the 64 channels contain an averaged transient response on top of a flat background from the averaged noise. In simple shear flow, 20 sweeps generally resulted in a very smooth response curve. At low birefringence levels, up to 40 sweeps were sometimes required.

The analysis of transient flow birefringence is based on the same equation (2) as the steady-state experiments. In the steady-state case, the angle χ can be determined by rotating the flow device to the position of maximum intensity, and then Δn can be determined from the measured intensity values. In the transient experiment, both the orientation of the solution optic axes and the magnitude of the birefringence are varying as a function of time. One way to determine both Δn and χ as a function of time is to *repeat* the experiment with two different orientations of

the polarizer and analyzer.[34] The simplest method is to rotate both polarizer and analyzer 45° for the second measurement. Then the equations for the two runs are

$$\begin{aligned} I_1 &= I_0 \sin^2 2\chi \sin^2 \frac{\pi d \Delta n}{\lambda_0} \\ I_2 &= I_0 \cos^2 2\chi \sin^2 \frac{\pi d \Delta n}{\lambda_0} \end{aligned} \tag{4}$$

where d is the solution depth and λ_0 the incident wavelength. The birefringence is obtained for a given instant in time by adding the two equations and the extinction angle by dividing. The two runs each consist of 64 numbers giving the average values of I_1 and I_2 at corresponding times. These are processed channel by channel using equations (4) to obtain the desired $\Delta n^+(t)$.

3. RESULTS

3.1 Flow Modification

The solutions we use in this work are very dilute solutions and well under the critical concentration, c^*, of 200–300 ppm that was previously estimated[6] as the minimum concentration for flow modification to occur for fully extended polystyrene with $M_w=2\times10^6$, which has the same contour length as PSS4. Thus, we do not expect much (if any) influence of the polymer on the flow for our present experiments. In fact, the *only* flow modification we observed was in the PSS4 solutions with no added salt (#4), the .004 M salt solution (#5), and the .04 M solution (#6). In each case, the flow modification occurred only at the upper limit of roller speeds attainable in the two-roll mills. In other words, the flow modification we observed with the polyelectrolyte only occurred in solutions with the most expanded rest states and at the shear rates most likely to have produced maximum extension of the polymer molecules. The data are plotted in Figure 3 as the measured velocity gradient versus the angular velocity of the rollers, ω. One measure of the degree of polymer stretch necessary to achieve a measurable effect on the flow is the so-called effective volume fraction, ϕ_{eff}, defined as the volume concentration of spheres circumscribed about the fully or partially extended polymer molecule. Simple theoretical arguments, based upon dumbbell model calculations, suggest that this parameter must be $O(1)$ at least for the polymer to significantly influence the solution rheology. Measurements with narrow molecular-weight distribution polystyrene, on the other hand, led to an estimate for a critical $\phi_{eff}\sim O(4000)$ to obtain a measurable decrease in the velocity gradient in the two- and four-roll mill experiments. The effective volume fraction at which flow modification occurs for the present polyelectrolyte solutions, assuming full extension of the PSS4 molecule at the highest flow rates, is $\phi_{eff}\sim1000$. This suggests that a high degree of overlap of the polymer domains is necessary for flow modification, but not as high as for

polystyrene.[6] The reason for the *difference* between the the polystyrene and the polystyrenesulfonate solutions is not clear to us at this time.

3.2 Flow Birefringence

Figure 4 shows the FB data obtained for 100 ppm PSS1 with 3 different amounts of added NaCl (solutions #1–3). A 50 ppm PSS1 solution was also measured and the FB was exactly half that of the 100 ppm solution for the case of no added salt, as one would expect for dilute solutions. The criterion of Odijk[35] can also be used to see if our solutions are truly dilute. Using his scaling laws we find that if the salt concentration is greater than .0002 M for 100 ppm PSS1 (and .0004 M for PSS4), then the solution should be considered dilute. These salt concentrations are well under the natural contribution from the polymer itself. Moreover, other diluteness criteria, such as $c[\eta] < 1$ and the volume fraction of circumscribed spheres based on the measured hydrodynamic radii at equilibrium, $\phi_{eff} < 1$, are satisfied by all the solutions. Thus, it appears that even the no-salt solutions are probably truly dilute.

For small amounts of added salt, the 50 ppm PSS1 solution gave identical FB results to the 100 ppm solution when the total $[Na^+]$ concentration was half that of the 100 ppm PSS1 solution. We were only able to pursue this type of comparison up to a salt concentration of .0075 M for the 50 ppm solution because the FB was too small to measure accurately for higher salt concentrations. However, this limited study of the effect of salt on polymer behavior as the concentrations of both are varied suggests that similar behavior is obtained for two solutions when the ratio of the added $[Na^+]$ to that contributed by the polymer (or equivalently, the number of Na^+ ions added per charge site on the polyelectrolyte) is the same.

The asymptotic value of the FB, Δn_∞, which corresponds to fully stretched and aligned polymer molecules was found to be 2.6×10^{-6} for 100 ppm PSS1. This is approximately the same as the values obtained for polystyrene (after correcting

for the difference in monomer weight). This suggests that the intrinsic optical anisotropy for NaPSS is about the same as for polystyrene, as one would expect from the similar molecular structure. The value of Δn_∞ also is in good agreement with asymptotic values obtained in electric birefringence measurements at high field strength.[36,37]

Figure 5 shows the flow birefringence data for the 89 ppm PSS4 solution with 4 different amounts of added salt (solutions #4–7). In both Figures 4 and 5, the FB data are plotted versus $\gamma\sqrt{\lambda}$, which causes the data from the entire range of flow types available ($.019 \leq \lambda \leq 1$) to collapse to a single curve for each solution. This is typical behavior for dilute polymer solutions, and is consistent with theoretical predictions based upon elastic dumbbell models.[5,6]

The two sets of data in Figures 4 and 5 demonstrate the dramatic effects of polyelectrolyte expansion in the equilibrium or rest state on the coil-stretch transition. The highest salt concentrations produce behavior like that of a typical flexible polymer. Unfortunately, the molecular weight and relaxation times of our samples at the highest salt levels are sufficiently small that the entire coil-stretch transition could not be achieved over the range of shear rates available. The PSS4 sample was expected to give results equivalent to a 2×10^6 M_w polystyrene (PS2).[6] Instead, less than half the FB is observed in solution #7 at a comparable shear rate (even after the correction for concentration and M_w differences). This is apparently because the PSS4 is much more compactly coiled in the .4 M salt than is polystyrene in Chlorowax LV (LV). In fact, the polystyrene in LV is estimated to be expanded from Θ conditions by about a factor of 1.2 while the data in Table I for solution #7 suggest the PSS4 is collapsed from Θ conditions by a factor of about .75. This implies a total linear expansion factor between the PSS4 and PS2 of 1.6. This is about the same amount of expansion as in PSS4 with only .04 M salt (#6) relative to the PSS4 solution with the highest salt concentration (#7). Therefore, it is

probably more appropriate to compare the PS2 data with solution #6 rather than with solution #7. Indeed, the FB data for solution #6 are much closer to that of PS2, but the onset is not as distinct and the transition is spread over a larger range of shear rates. This suggests either that the electrostatic expansion in PSS4 has a different effect on the hydrodynamic behavior of the polymer than the excluded-volume expansions in PS2, or that the molecular weight distribution is broader in PSS4 than in PS2. This second possibility seems more likely. Both PSS4 and PS2 were reported as having polydispersity ratios of 1.3. However, that of PSS4 was based on the parent polystyrene and the sulfonation process could have caused some crosslinking or chain breakage to occur, resulting in greater polydispersity. Also, it was found that model calculations for the PSS1 data fit much better when we used a larger polydispersity ratio than the value reported for the parent polystyrene.

As the salt concentration decreases in both PSS4 and PSS1 solutions, the FB occurs at much lower shear rates and loses any distinct "onset shear rate" behavior. In fact, the shape of the FB data at low salt concentrations is similar to that obtained with elongated rigid macromolecules[38] as they orient with the flow direction. Though the polyelectrolytes with low salt levels are still undergoing significant stretching due to the flow (from the equilibrium R_h in Table I to complete extension), and therefore are not really rigid, they are highly anisotropic at equilibrium because the expansion is greatest in the end-to-end direction. This anisotropy accounts for the similarity to rigid macromolecules in the shape of the low salt solution birefringence data. Another important aspect of the changing FB behavior with decreasing salt is the spatial extent of the birefringent region. At high and intermediate salt concentrations the FB is highly localized along the outgoing streamline of the flow, and this is similar to the behavior of non-ionic, flexible polymers like polystyrene. Only in this localized region are the residence times in the strong flow region of the two- and four-roll mills sufficiently long to stretch

the polymer. With the drastically expanded molecules in the "no-salt" solutions, however, significant orientation and stretching occurs everywhere in the flow with an accompanying decrease in the localization of the FB. Figure 6 illustrates these two extremes in behavior.

The shift in the coil-stretch behavior may be characterized by determining the onset shear rate,[15] or, for the shape of our data, the shear rate at which the FB reaches a certain arbitrary level. The inverse of this critical shear rate is a measure of the relaxation time, τ_{FB}, of the polymer in (or near) its equilibrium configuration. The values of τ_{FB} based on the shear rate at 20% of the asymptotic birefringence level are given in Table I. Similar data were reported for PSS1 in aqueous solutions by Miles *et al.*[15] Our τ_{FB} data can be adjusted for the difference in solvent viscosity by dividing by η_s and then compared directly with their relaxation times. The effects of using a solvent with a dielectric constant about half that of water can be seen. With no added salt, our relaxation times for PSS1 in glycerol (normalized) are about 1/10 of the values in water. The normalized relaxation times in glycerol remain less over the entire range of added salt concentrations studied. In water, there was a very dramatic 10-fold drop in the relaxation times over a narrow range of salt concentrations (at about .025 M).[15] A similar 10-fold drop in τ_{FB} is seen in glycerol but at a much lower salt concentration (.001 to .004 M). Thus, in glycerol, the polyelectrolyte is much more sensitive to very small amounts of added salt. At salt concentrations less than .025 M, the τ_{FB} for aqueous solutions was found by Miles *et al.*[15] to scale with M_w^2. This scaling law corresponds to $[\eta] \sim M_w$ which has also been observed for aqueous PSS solutions at low salt concentrations.[12] Though our τ_{FB} data for the no-salt solutions do not show this same scaling, the intrinsic viscosity data do scale with M_w[78]. We therefore believe that $\tau \sim M_w^{\sim 1.8}$ scaling should apply in our NaPSS in glycerol solutions with no added salt. This scaling law implies that the hydrodynamic interaction

between solvent and polymer is approaching the free-draining limit for the most expanded equilibrium states, as opposed to the non-free-draining behavior ($\tau \sim M_w^{1.5}$) previously observed in the scaling of polystyrene data.[5,6,39] We will see that this transition in the strength of polymer-solvent hydrodynamic interactions with the degree of equilibrium expansion is very important in attempts to *model* the coil-stretch process in polyelectrolytes.

3.3 Flow Birefringence Overshoots

Overshoots were observed in the FB, $\Delta n^+(t)$, during startup of simple shear flow in the Couette device for the two PSS4 solutions with lowest salt concentration (#4 and 5). Typical data for the solution without added salt (#4) at four shear rates are plotted in Figure 7. The data for solution #5 at three shear rates are plotted in Figure 8. Table II shows the maximum overshoot as a percentage of the steady-state value, Δn_{ss}, and the steady-state values as the ratio $\Delta n_{ss}/\Delta n_\infty$, where Δn_∞ is the asymptotic value attained for fully extended and aligned molecules.

The existence of measurable overshoots is a direct consequence of the expanded rest state of the polymer and the resulting approach to free-draining hydrodynamics. The straining component of the flow is much more effective in stretching the expanded polyelectrolytes than it is in stretching the compact non-free-draining coils at high salt concentrations (or the polystyrene solutions). Thus the polyelectrolyte is initially stretched in the principal strain direction. As it then reorients, approaching a steady-state orientation more closely aligned with the flow direction and away from the principal strain axis, the amount of extension also decreases to its steady-state value.

TABLE II. $\Delta n^+(t)$ Overshoots in Simple Shear[a]

#	γ (s^{-1})	$(\frac{\Delta n_{os}}{\Delta n_\infty})$	% ov.
1	3	0.23	7.5
2	12	0.37	14.8
3	44	0.47	23.6
4	146	0.61	24.5
5	88	0.13	22.
6	175	0.21	39.5
7	263	0.26	45.2

[a] Curves #1–4 are with no added salt

Curves #5–7 have .004 $\underline{M}$ $[Na^+]$

4. MODEL COMPARISONS

In dilute solutions, significant deviations from Newtonian flow behavior occur only as a result of a coil-stretch transition in the polymer conformation. A goal for modeling is thus to give at least a correct qualitative description of the coil-stretch (or stretch-coil) transition using a "molecular" model which is sufficiently simple to eventually be used for a complete fluid-mechanical description of a given flow. Since the *overall* conformation of the polymer determines the dynamics in strong flows, we adopt the elastic dumbbell framework[40] (in which the polymer conformation is represented by a single vector $\mathbf{r}$), but with spring and hydrodynamic friction forces designed to mimic the behavior of a polymer over the whole range of configurations from the equilibrium to highly stretched states. The essential characteristics of the spring force are that it increase linearly with $\mathbf{r}$ at small deformations from equilibrium, but then increase very rapidly as the full contour length, L, of the polymer is approached. The friction law must again describe the hydrodynamic interaction between the polymer and the solvent for any conformation of the polymer, from the equilibrium coil to the fully extended threadlike configuration.

From a hydrodynamics point of view, the most complete attempt at dumbbell modeling of dilute solutions to date is the anisotropic dumbbell model of Phan-Thien *et al.*[9] However, a proper description of steady, strong flow data can be achieved with the simpler isotropic version of the dumbbell model with a nonlinear (Warner) spring, and an isotropic, but conformation-dependent bead friction law as first proposed by de Gennes,[10] Hinch,[11] and others. We have previously shown[5,6] that predictions with this "isotropic" friction model are in excellent agreement with experimental data for strong flows ($\lambda \geq 0.2$) of dilute polystyrene solutions. Furthermore, a second key consequence of conformation-dependent friction has been verified by previous experimental work: namely, the existence of a relaxation time for the stretch→coil transition which greatly exceeds the "relaxation time" characteristic of the initial coil→stretch transition (due to an increased frictional "grip" on the polymer in its stretched state).[31] This feature cannot be predicted with models, such as the FENE dumbbell of Bird and coworkers,[40] which do not incorporate the concept of conformation-dependent friction. The more complicated model of Phan-Thien *et al.*[9] attempts to incorporate a "more realistic" hydrodynamic response including frictional anisotropy and "strain-inefficient" rotation as is characteristic of *rigid* particle hydrodynamics at low Reynolds number. The goal was to produce a model which would show improved behavior in flows nearer to simple shear flow ($\lambda < 0.2$) where there is nearly as much vorticity as strain. However, comparison with experimental data[6] shows that the modified dumbbell model of Phan-Thien *et al.* is really no better than the simple isotropic model of de Gennes[10] and Hinch[11] in strong extensional flows and still shows only fair to poor predictions in flows approaching simple shear flow. This is presumably because the *rigid* particle hydrodynamics (especially the "strain-inefficient" rotation) built into the model are not correct for flexible polymer coils.

In the present study, we therefore compare our data for polyelectrolytes in

strong flows (Figures 4 and 5) with predictions from the charged dumbbell model of Dunlap and Leal.[8] This model includes the Warner spring, and the isotropic, conformation-dependent friction law of the original deGennes-Hinch nonlinear dumbbell model. We will use the abbreviation VF to refer to this variable-friction model. In addition, the charged dumbbell has a Coulombic repulsive force between the beads which allows it to model the equilibrium electrostatic expansion of dilute polyelectrolyte solutions. No attempt is made to model the overshoot data for simple shear flow, because it is known (as explained above) that the existing conformation-dependent friction models do not do a good job even for steady flows that are too near to simple shear flow. It is also instructive to compare our data with predictions of the FENE dumbbell[40] with the Coulombic charge force,[8] which has the nonlinear spring but constant friction (CF).

The detailed development of the charged dumbbell model has been given elsewhere.[8] The only difference in the present calculations is that we have defined the relaxation time of the model to be $\tau_{db} = \varsigma_0/4\xi_0$ where ς_0 and ξ_0 are the friction and spring coefficients, respectively, at equilibrium. This makes τ_{db} half that of Reference 8 and 9, but is consistent with most other authors.[5,26,40,41]

4.1 "Steady-State" Extensional Flow Predictions

The predictions of birefringence versus shear rate were calculated for the charged dumbbell model, taking into account experimental conditions. In these calculations, the effect of the finite transit time of a polymer through the extensional flow region of the four- and two-roll mills was handled using the method of Fuller and Leal[5] (with l/D=.003). An assumed log-normal molecular weight distribution was also used to account for polydispersity. The molecular weight dependence of the relaxation time must be specified in order to assess the effects of polydispersity in the birefringence predictions.[5] For polyelectrolyte solutions, the relaxation time cannot be assumed to follow the $M_w^{1.5}$ behavior as with polystyrene.[5] We used exponents

of 1.5, 1.8 or 2.0 for high, medium and no added salt concentrations, respectively. It was actually found that the choice of exponent had only a small influence on the shape of the resulting predictions of birefringence versus shear rate.

The basic approach to modeling the FB data for polyelectrolytes was to obtain the three model parameters of the charged dumbbell model from independent measurements. The value of N (the number of statistical subunits) can be obtained from Δn_∞, as for polystyrene solutions, or estimated from the molecular structure and flexibility of the polymer in the uncharged (high-salt) limit. The appropriate values, from comparison with polystyrene modeling results,[6] are N=1200 and 360 for PSS4 and PSS1, respectively. The effective charge parameter E can be obtained from measured equilibrium expansion factors using the formula[8]

$$2\sqrt{2}(3N+2)^{\frac{1}{2}}\frac{\alpha^3-\alpha}{3N+2-2\alpha^2}=E \tag{5}$$

for the VF model, and

$$3(N+1)^{\frac{1}{2}}\frac{\alpha^3-\alpha}{N+1-\alpha^2}=E \tag{6}$$

for the CF model. The relaxation time should be τ_η (the Zimm time from Table I) divided by 2.214 for the CF model (*i.e.*, the charged dumbbell with constant friction) and by 4.067 for the VF model (*i.e.*, the charged dumbbell model with variable friction) as explained by Peterlin[41] and Dunlap and Leal.[6] The VF model predictions are the solid curves in Figures 9 and 10 for the PSS1 and PSS4 data, respectively. The dashed curves are the predictions of the CF version of the model. The values of the parameter E were obtained from equations (5) and (6) using expansion factors of 5, 1.6, and 1 for the three PSS1 solutions, and 5, 2, 1.5, and 1 for the four PSS4 solutions. As can be seen, the VF charged dumbbell model predictions compare quite well with the data (and could be made to compare even better by making small "adjustments" to the model parameters). However, it is apparent that even with the correct amount of equilibrium expansion, the CF model

does not predict the large shifts in the onset behavior of the coil-stretch transition, especially for the no-salt curves. This is because the CF model fails to model the increased hydrodynamic interaction between the solvent and polymer as the polymer expands. The VF model, on the other hand, correctly predicts the transition from non-free-draining behavior to free-draining behavior as the dumbbell either expands in the flow or is expanded by electrostatic repulsion at equilibrium.

The electrostatic expansion of the charged dumbbell model is essentially an excluded-volume type expansion (as opposed to backbone stiffening which would correspond to changing values of N with varying salt concentrations). The form of the charge force is very similar to the kind of force that appears in excluded-volume theories,[24] and the equations (5) and (6) are typical "third-power" type expansion relations as also appear in excluded-volume theories.[24] However, recent theories of polyelectrolyte expansion suggest that a local increase in rigidity of the backbone chain also contributes significantly to the expansion.[19,20] Since the relative contributions of stiffening and excluded volume to the electrostatic expansion cannot be determined *a priori*, it is of interest to also apply the dumbbell model in a way that assumes that *only* electrostatic stiffening occurs. In this approach, the measured expansion factors are assumed to relate *solely* to changes in N, the number of statistical subunits in the polymer. As the polymer becomes locally stiffer, the length of a statistical subunit increases, and thus, for a given M_w or contour length, the number of statistical subunits must decrease.

Making use of the so-called Peterlin excluded-volume parameter,[24] ϵ, the mean square end-to-end distance, $\langle r^2 \rangle$, of any polymer with contour length L and subunit length A can in principle be represented by

$$\langle r^2 \rangle = N^{1+\epsilon} A^2, \qquad L = NA. \tag{7}$$

The usual Gaussian or non-free-draining statistics are obtained with ϵ=0, "good-solvent" behavior with ϵ=0.2, and free-draining behavior with $\epsilon=\frac{1}{3}$. Non-zero values

of ϵ may be due to either excluded volume or rigidity of the chain. We are, of course, assuming that it is chain rigidity which causes the deviations from Gaussian behavior for this application. Holding L constant as A increases due to electrostatic stiffening of the polyelectrolyte backbone gives a linear expansion factor,

$$\alpha = \left(\frac{N}{N_0}\right)^{\frac{1}{2}(\epsilon-1)}, \tag{8}$$

where N_0 is a reference value which applies to the polymer in the high-salt limit where it is most flexible. The model relaxation time increases as the subunit length increases according to the equation

$$\tau_{db} \sim \alpha^3 = \left(\frac{N}{N_0}\right)^{\frac{3}{2}(\epsilon-1)}. \tag{9}$$

Using these equations and the same expansion factors as before we can calculate the appropriate values of N and τ_{db} for the seven solutions, choosing as reference values the values of N and τ_{db} used above for the highest salt concentrations. We have done this and compared model predictions (of both the CF and VF models) assuming $\epsilon = \frac{1}{3}$, 0.2, and 0, and E=0. We will describe the results but only show the actual plots for the case $\epsilon = \frac{1}{3}$. Two characteristics of the dumbbell model predictions (and the experimental data) can be easily discerned: the *onset* shear rate for the coil-stretch transition (or equivalently, the relaxation time) and the *shape* of the predicted curves. Equation (9) shows that the relaxation time (which determines the onset shear rate or initial slope of the FB data) is determined from α and is therefore independent of the choice of ϵ. On the other hand, the *shapes* of the predicted curves are dependent on the value of N used in the model and therefore strongly dependent on ϵ. In particular, for $N \geq 50$ both models predict a distinct onset point and "S"-shaped curves for the FB. Only for quite small values of N <20 do the predictions resemble the shapes of the FB curves for the no-salt solutions. Equation (9) implies that the larger the value of ϵ, for given values of α and N_0,

the smaller N will be. For the most expanded (no-salt) solutions, a value of ϵ of .2 to .3 was required to obtain values of N small enough that the FB predictions from the models had shapes resembling those of the data. In other words, the increased "draining" of the expanded (more rigid) polyelectrolytes must be explicitly included when applying the dumbbell model in this way in order to successfully model the no-salt data.

The model predictions, assuming that the expansion reduces N and increases τ according to equation (9) with $\epsilon = \frac{1}{3}$ and with the same values of α, N_0, and τ_0 (shifted by 2.214 for CF and 4.067 for VF), are compared with the PSS1 and PSS4 data in Figures 11 and 12, respectively. The VF predictions and CF predictions were found to be essentially identical (except for the factor of 2.214/4.067 difference in relaxation times). The relaxation times calculated from equation (9) using the experimental expansion factors are consistently too large in comparison with the data by a factor of 2–4. If the α are "rechosen" to give τ_{db} which fit the data better, we obtain α=3.6, 1.5, and 1 for the PSS1 solutions and 3.5, 1.6, 1.2, and 1 for the PSS4 solutions. These "best-fit" model predictions are the dashed curves in Figures 11 and 12. These values of α are a bit less than measured for these solutions (see Table I), but possibly within experimental error for most of the seven solutions.

To the extent that both of the above approaches to modeling the polyelectrolyte FB data seem to work, we conclude that in strong flows the polymer behavior is indeed *insensitive* to the *local* structure of the polymer (rigidity versus excluded-volume interactions). This supports the use of the dumbbell model for the prediction of the overall dynamics of polymers. On the other hand, it seems that the first approach (which assumes electrostatic excluded volume via the charged dumbbell) slightly *under*estimates the shift of the FB data at low salt concentrations from that of the high-salt solutions, while the second approach (which assumes local stiffening) slightly *over*estimates the same shifts in the data. This suggests that

the *local* behavior may indeed have *some* measurable effect on the data and that some combination of stiffening and excluded-volume expansion might indeed give an optimal comparison of the model with the data. Unfortunately, without very precise expansion data and some knowledge of the relative importance of the two effects, such modeling efforts at this point would involve arbitrary parameter choices, and therefore definite conclusions could not be drawn.

5. CONCLUSIONS

We have presented an experimental investigation of the coil-stretch behavior of polyelectrolytes in extensional flows as a function of molecular weight and added salt concentration. The data show the same qualitative behavior as that of Miles *et al.*[15] The dramatic shift in onset of the coil-stretch transition occurs at lower salt concentrations in our glycerol solutions than in their aqueous solutions because of the lower dielectric constant of glycerol. The data are useful for testing the charged dumbbell model.[8] From comparisons of the charged dumbbell model with the FB data we conclude that a variable friction coefficient (VF) is essential for reasonably quantitative comparisons with "steady-state" strong flow polyelectrolyte data. The VF works because it builds into the model a natural transition from non-free-draining to free-draining behavior as the dumbbell expands, just as the data show that real polyelectrolytes do.[12,15]

The charged dumbbell model essentially treats the polyelectrolyte expansion as electrostatic excluded volume. We have demonstrated that the data can also be modeled by assuming that the expansion is due to a local electrostatic stiffening, or increase in persistence length. This simply involves reducing the number of statistical subunits, N, and increasing the relaxation time using the equilibrium expansion data and appropriate scaling laws. The success of both fitting procedures supports a basic assumption of dumbbell modeling, that overall conformation behavior is most important in strong flows, as opposed to details of the local polymer structure. The details of the fits obtained by the two methods did however suggest that both stiffening and excluded-volume interactions do actually influence the FB data, although their relative importance could not be determined in the present context.

References

1. F. Durst, R. Haas, and W. Interthal, *Rheol. Acta*, **21,** 572 (1982).
2. E. W. Merrill and A. F. Horn, *Polym. Comm.*, **25,** 144 (1984).
3. G. Chauveteau, M. Moan, and A. Magueur, *J. Non-Newtonian Fluid Mech.*, **16,** 315 (1984).
4. A. V. Shenoy, *Coll. Polym. Sci.*, **262,** 319 (1984).
5. G. G. Fuller and L. G. Leal, *Rheol. Acta*, **19,** 580 (1980).
6. P. N. Dunlap and L. G. Leal, "Dilute Polystyrene Solutions in Extensional Flows: Birefringence and Flow Modification," *submitted to J. Non-Newtonian Fluid Mech.*, 1986.
7. G. G. Fuller and L. G. Leal, *J. Non-Newtonian Fluid Mech.*, **8,** 271 (1981).
8. P. N. Dunlap and L. G. Leal, *Rheol. Acta*, **23,** 238 (1984).
9. N. Phan-Thien, O. Manero, and L. G. Leal, *Rheol. Acta*, **23,** 151 (1984).
10. P. D. DeGennes, *J. Chem. Phys.*, **60,** 5030 (1974).
11. E. J. Hinch, *Phys. Fluids*, **20,** S22 (1977).
12. A. Takahashi, T. Kato, and M. Nagasawa, *J. Phys. Chem.*, **71,** 2001 (1967).
13. R. E. Harrington, *Biopolymers*, **17,** 919 (1978).
14. M. Tricot, *Macromolecules*, **17,** 1698 (1984).
15. M. J. Miles, K. Tanaka, and A. Keller, *Polymer*, **24,** 1081 (1983).
16. F. Durst, R. Haas, and B. U. Kaczmar, *J. Appl. Polym. Sci.*, **26,** 3125 (1981).
17. A. Oubrahim and D. H. Fruman, *J. Non-Newtonian Fluid Mech.*, **7,** 315 (1980).

18. P. S. Virk, *Nature*, **253,** 109 (1975).

19. M. Fixman and J. Skolnick, *Macromolecules*, **11,** 863 (1978).

20. T. Odijk and A. C. Houwaart, *J. Polym. Sci.: Polym. Phys. Ed.*, **16,** 627 (1978).

21. T. Kitano, A. Taguchi, I. Noda, and M. Nagasawa, *Macromolecules*, **13,** 57 (1980).

22. D. W. Brown and R. E. Lowry, *J. Polym. Sci.: Polym. Chem. Ed.*, **17,** 1039 (1979).

23. R. L. Lagnado, *Ph. D. Thesis*, California Institute of Technology, Pasadena, 1985.

24. H. Yamakawa, *Modern Theory of Polymer Solutions*, Harper & Row, New York, 1971.

25. M. Nagasawa, *J. Polym. Sci.:Symp. No. 49*, 1 (1975).

26. B. H. Zimm, *J. Chem. Phys.*, **24,** 269 (1956).

27. D. M. Soumpasis and K. H. Bennemann, *Macromolecules*, **14,** 50 (1981).

28. G. G. Fuller, J. M. Rallison, R. L. Schmidt, and L. G. Leal, *J. Fluid Mech.*, **100,** 555 (1980).

29. H. G. Jerrard, *J. Appl. Phys.*, **21,** 1007 (1950).

30. V. N. Tsvetkov, V. E. Eskin, and S. Y. Frenkel, *Structure of Macromolecules in Solution, Vol. 3, trans. by* C. Crane-Robinson, National Lending Library for Science and Technology, Boston, 1971.

31. M. J. Miles and A. Keller, *Polymer*, **21,** 1295 (1980).

32. W. Philippoff, *Proc. IV Int. Cong. on Rheol., Part 2, ed.* E. H. Lee, Interscience, New York, p. 343 (1980).

33. W. Balmforth, *J. Soc. Glass Tech.*, **29,** 111 (1945).

34. K. Osaki, N. Bessho, T. Kojimoto, and M. Kurata, *J. Rheol.*, **23,** 457 (1979).

35. T. Odijk, *Macromolecules*, **12,** 688 (1979).

36. M. Tricot and C. Houssier, *Macromolecules*, **15,** 854 (1982).

37. K. Kikuchi and K. Yoshioka, *J. Phys. Chem.*, **77,** 2101 (1973).

38. A. Peterlin and P. Munk, in *Physical Methods of Chemistry, eds.* A. Weissberger and B. Rossiter, **1**(IIIC),271, John Wiley & Sons, New York, 1972.

39. C. J. Farrell, A. Keller, M. J. Miles, and D. P. Pope, *Polymer*, **21,** 1292 (1980).

40. R. B. Bird, O. Hassager, R. C. Armstrong, and C. F. Curtiss, *Dynamics of Polymeric Liquids: Vol. 2, Kinetic Theory*, John Wiley & Sons, New York, 1977.

41. A. Peterlin, *J. Chem. Phys.*, **39,** 224 (1963).

Figure Captions

Figure 1. Streamlines of the various idealized, linear two-dimensional flows and how they are obtained in four- and two-roll mills.

Figure 2. Relative orientations of the polarizer, analyzer, flow field, and polymer and angle definitions in the flow birefringence experiment.

Figure 3. Measured values of γ in 89 ppm PSS4 solutions with no added salt, .004 M Na^+, and with .04 M Na^+ concentration plotted versus the angular velocity of the rollers. The straight line represents the linear dependence on roller speed found in Newtonian fluids.

Figure 4. Flow birefringence versus eigenvalue ($\gamma\sqrt{\lambda}$) data for 100 ppm PSS1 in glycerol at 3 concentrations of Na^+; .00068 M (no added salt), .005 M, and .1 M.

Figure 5. Flow birefringence versus eigenvalue ($\gamma\sqrt{\lambda}$) data for 89 ppm PSS4 in glycerol at 4 concentrations of Na^+; .00061 M (no added salt), .004 M, .04 M, and .4 M.

Figure 6. Photographs of typical birefringence fields in the four-roll mill (λ=1) for *Top:* flexible coiled equilibrium shape as in nonionic polymers or polyelectolytes with added salt; and *Bottom:* polyelectrolytes with greatly expanded rest state (no added salt).

Figure 7. Flow birefringence versus time of the 89 ppm PSS4 solution with no added salt during startup of simple shear flow at several shear rates.

Figure 8. Flow birefringence versus time of the 89 ppm PSS4 solution with .004 M Na^+ concentration during startup of simple shear flow at several shear rates.

Figure 9. Comparison of PSS1 flow birefringence data with the predictions of the charged dumbbell model with variable friction coefficient (solid curves) and with constant friction coefficient (dashed curves). The coordinates are $\Delta n/\Delta n_\infty$ vs. $\gamma\sqrt{\lambda}$.

Figure 10. Comparison of PSS4 flow birefringence data with the predictions of the charged dumbbell model with variable friction coefficient (solid curves) and with constant friction coefficient (dashed curves). The coordinates are $\Delta n/\Delta n_\infty$ vs. $\gamma\sqrt{\lambda}$.

Figure 11. Comparison of PSS1 flow birefringence data with the predictions of the dumbbell model with constant friction coefficient and no charge. The solid curves were obtained with N_0=360, $\tau_0 = \tau_\eta/2.214$ for the .1 M solution and the other parameters from equation (9) with α=1.6 and 5. The dashed curves use α=1.5 and 3.6 for better fits. The coordinates are $\Delta n/\Delta n_\infty$ vs. $\gamma\sqrt{\lambda}$.

Figure 12. Comparison of PSS4 flow birefringence data with the predictions of the dumbbell model with constant friction coefficient and no charge. The solid curves were obtained with N_0=1200, $\tau_0 = \tau_\eta/2.214$ for the .4 M solution and the other parameters from equation (9) with α=1.2, 2.0 and 5. The dashed curves use α=1.2, 1.6 and 3.5 for better fits. The coordinates are $\Delta n/\Delta n_\infty$ vs. $\gamma\sqrt{\lambda}$.

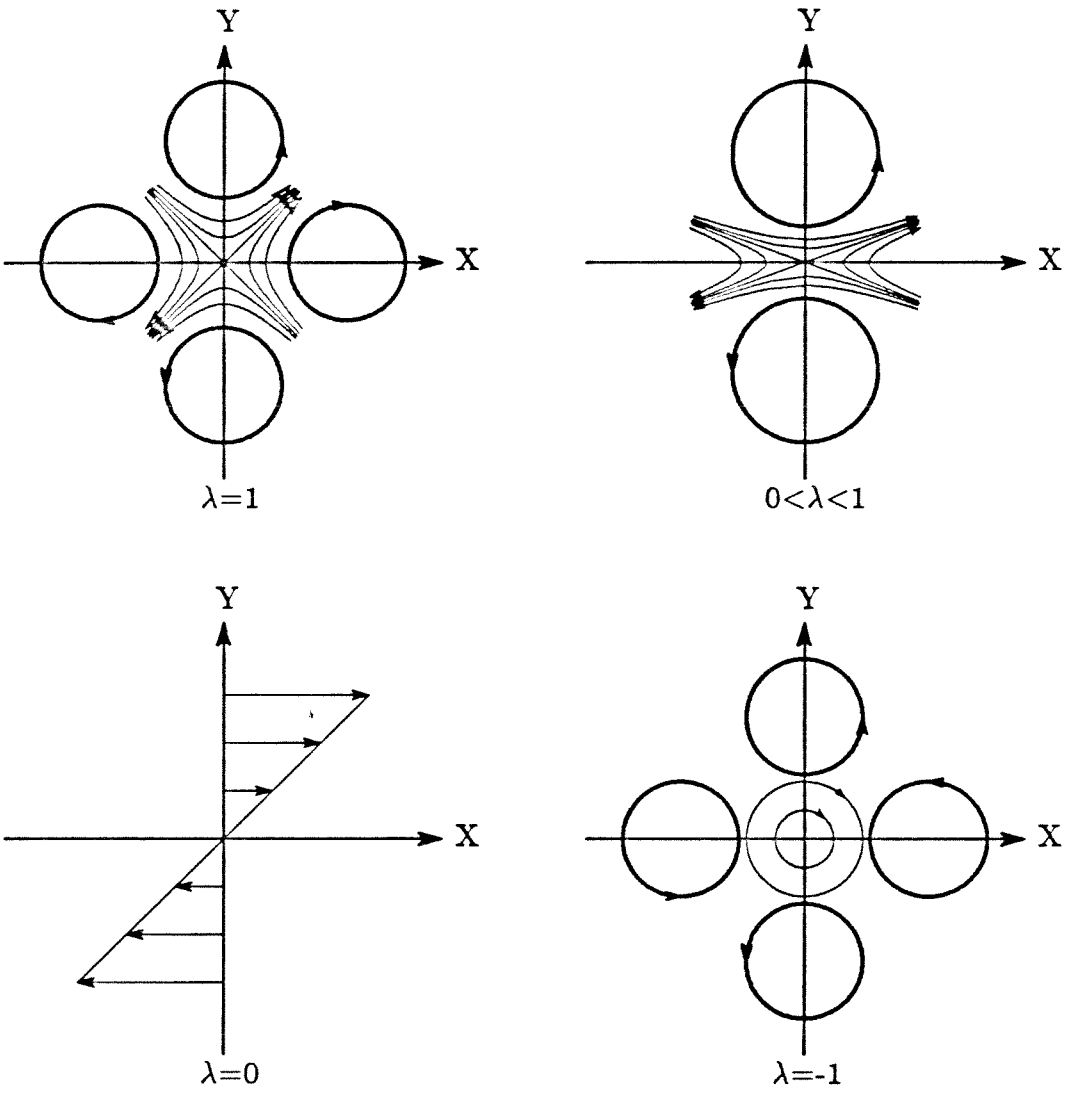

Figure 1.

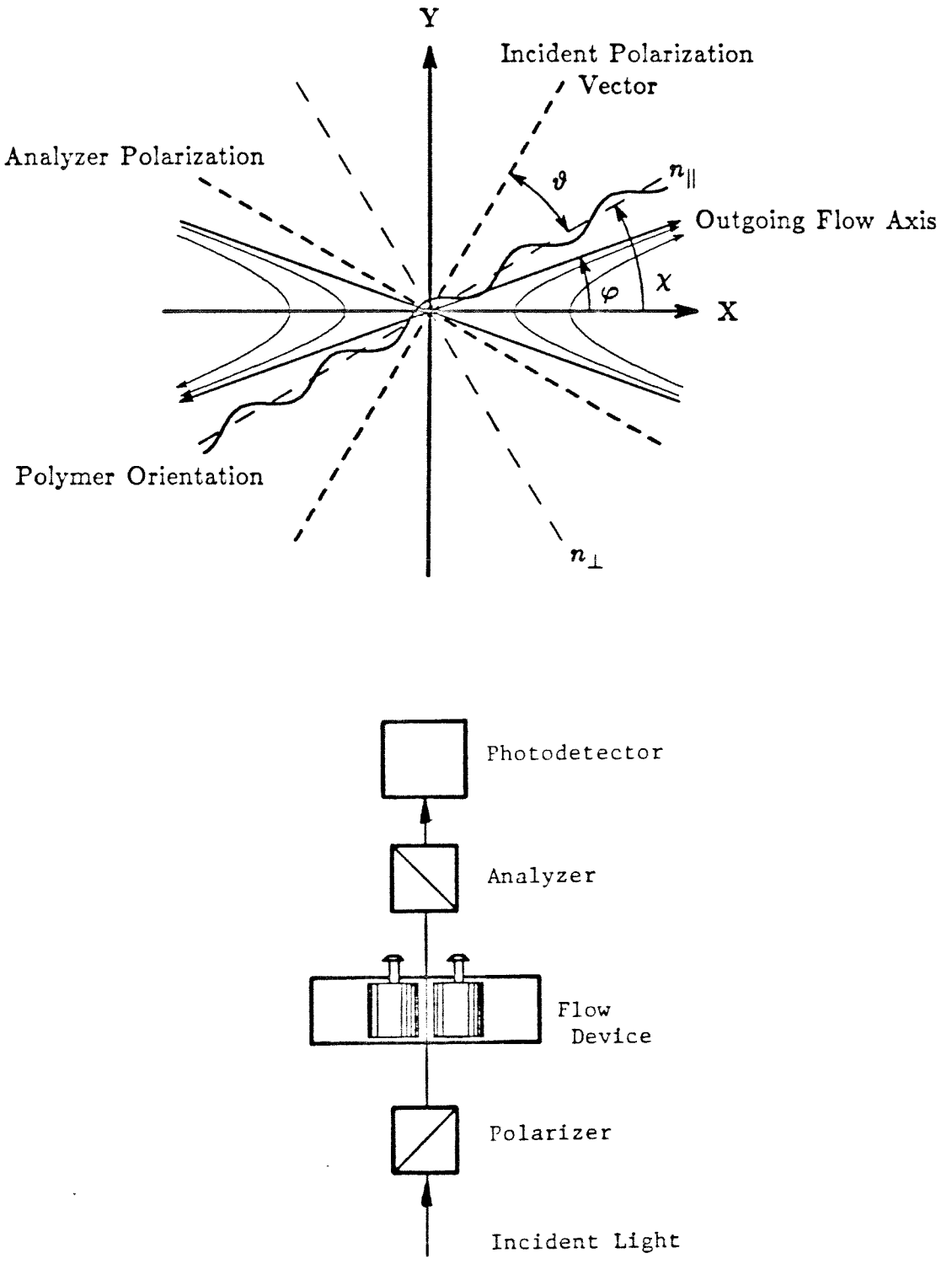
Y
Incident Polarization
Vector
Analyzer Polarization
ϑ
$n_{\parallel}$
Outgoing Flow Axis
φ
χ
X
Polymer Orientation
$n_{\perp}$
Photodetector
Analyzer
Flow
Device
Polarizer
Incident Light

Figure 2.

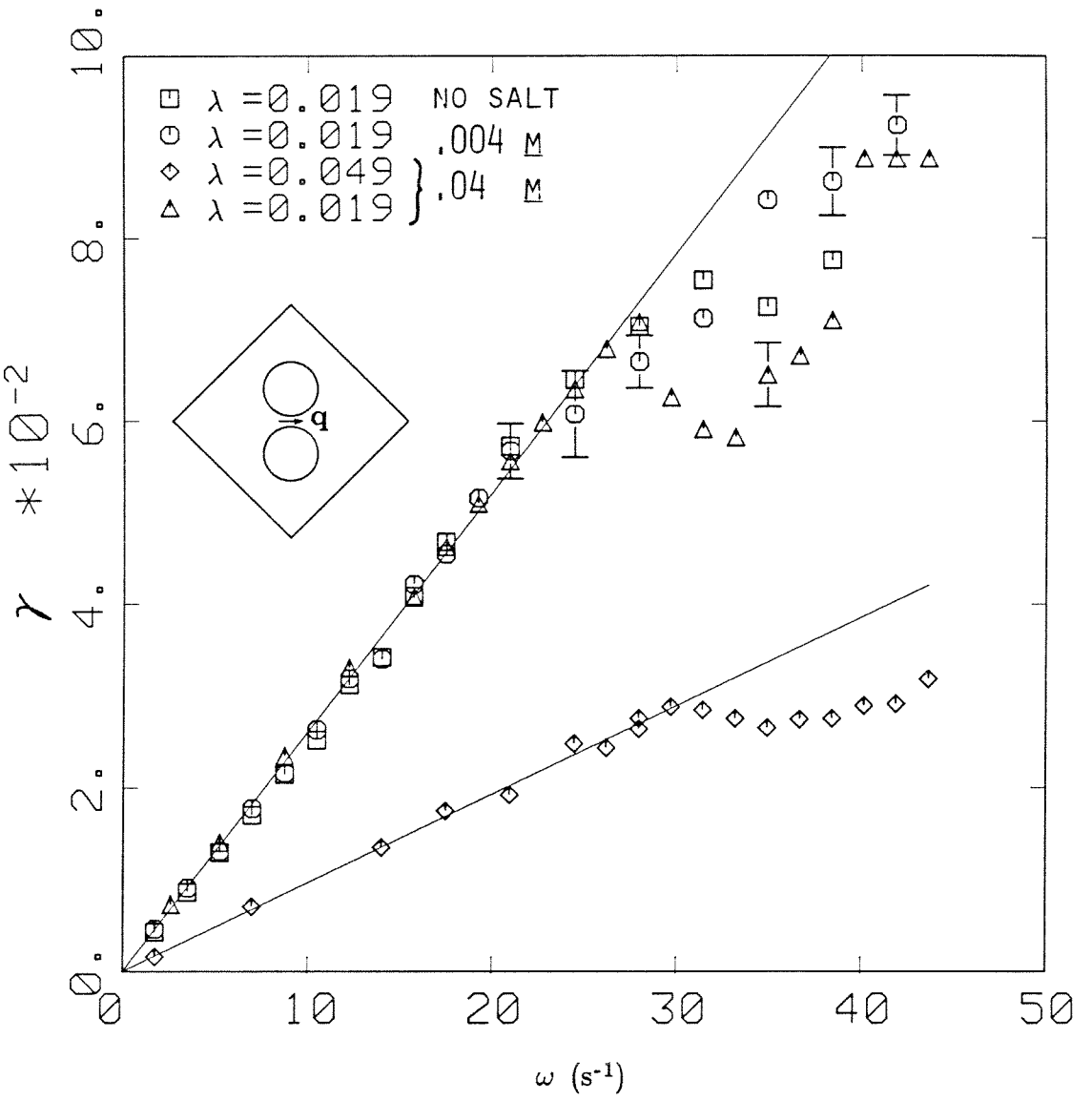
λ =0.019 NO SALT
λ =0.019 .004 M
λ =0.049 .04 M
λ =0.019 .04 M
q
γ *10^-2
0.
2.
4.
6.
8.
10.
0
10
20
30
40
50
ω (s^-1)

Figure 3.

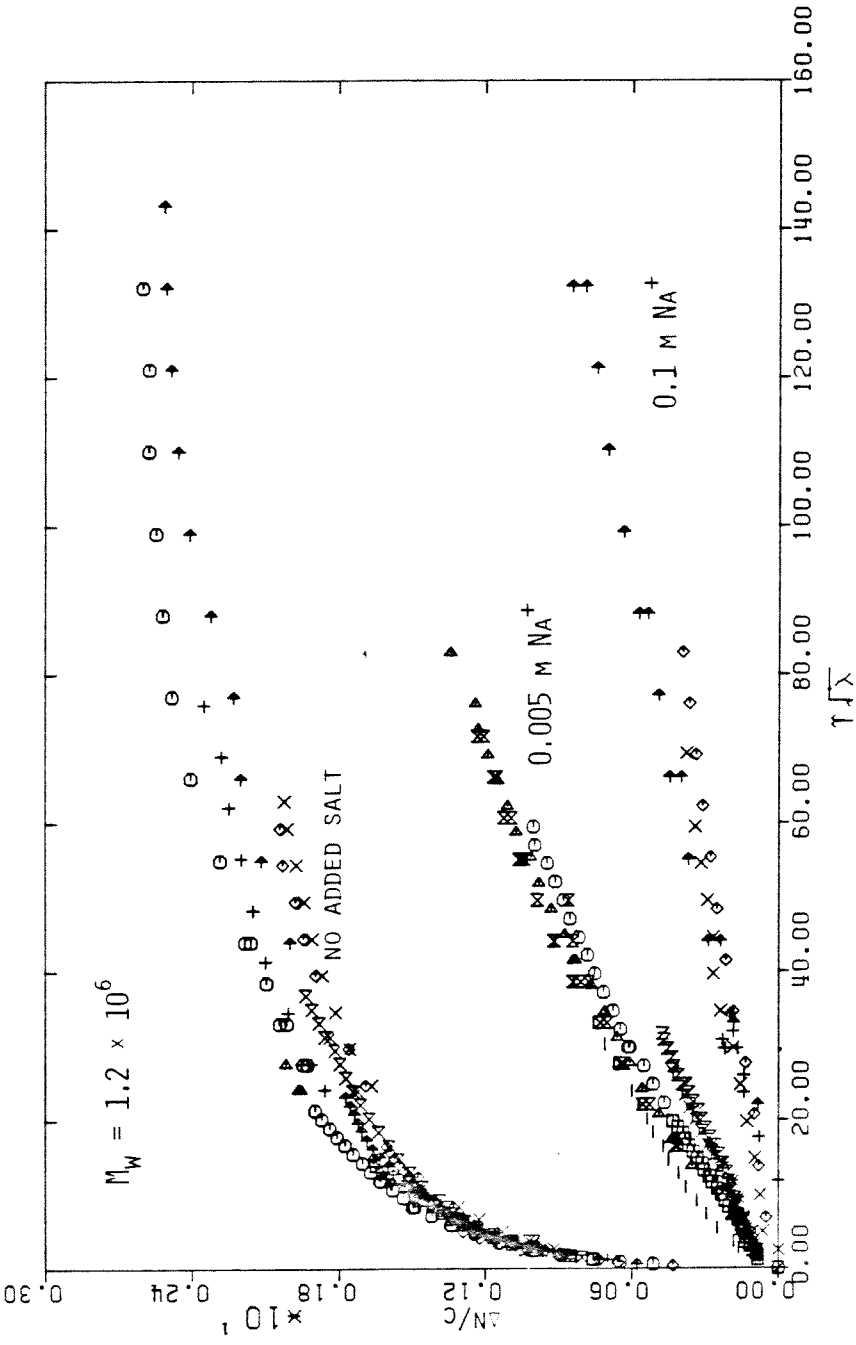

NAPSS IN GLYCEROL

Figure 4.

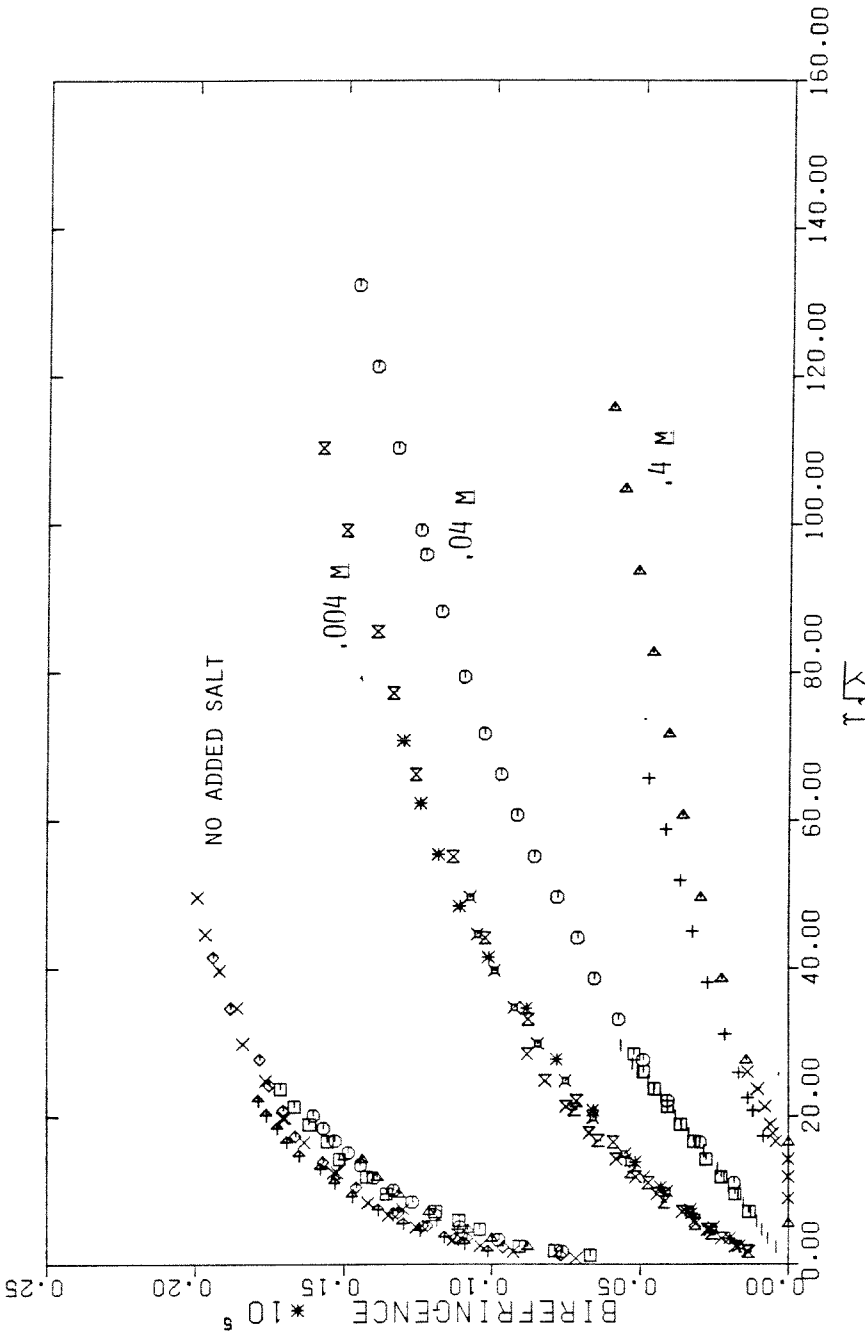
NAPSS4 IN GLYCEROL
BIREFRINGENCE *10 5
0.00
0.05
0.10
0.15
0.20
0.25
0.00
20.00
40.00
60.00
80.00
100.00
120.00
140.00
160.00
√τ
NO ADDED SALT
.004 M
.04 M
.4 M

Figure 5.

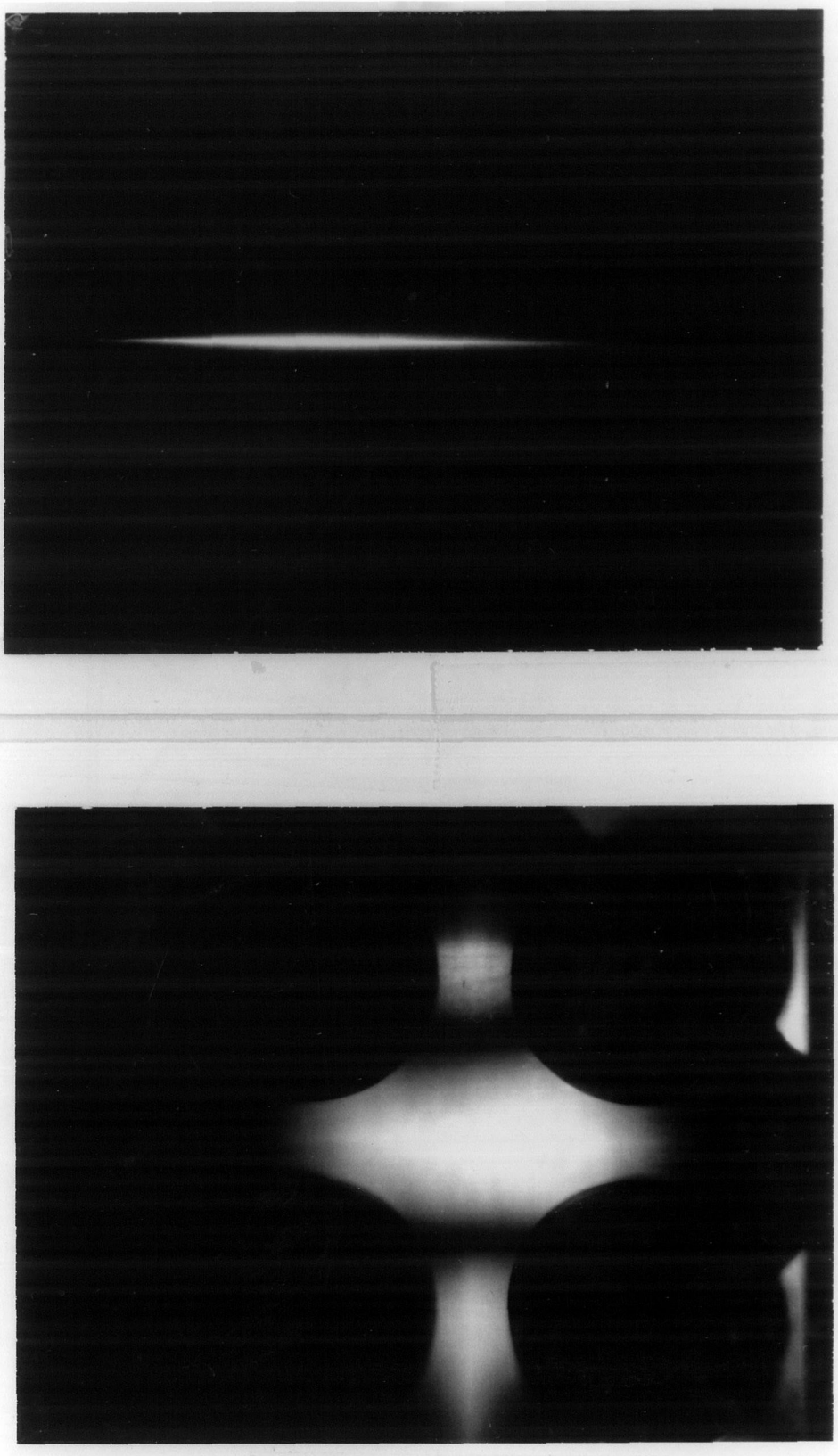

Figure 6.

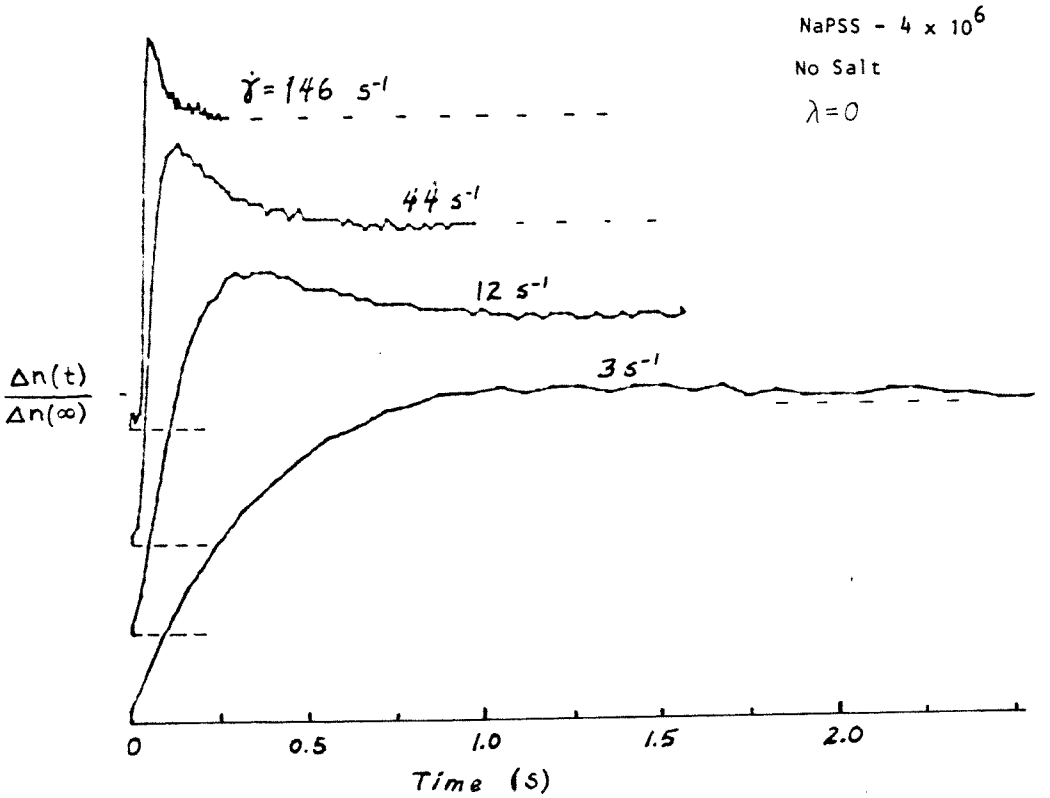
NaPSS - 4 x 10^6
No Salt
λ=0
γ̇=146 s⁻¹
44 s⁻¹
12 s⁻¹
3 s⁻¹
Δn(t)/Δn(∞)
0
0.5
1.0
1.5
2.0
Time (s)

Figure 7.

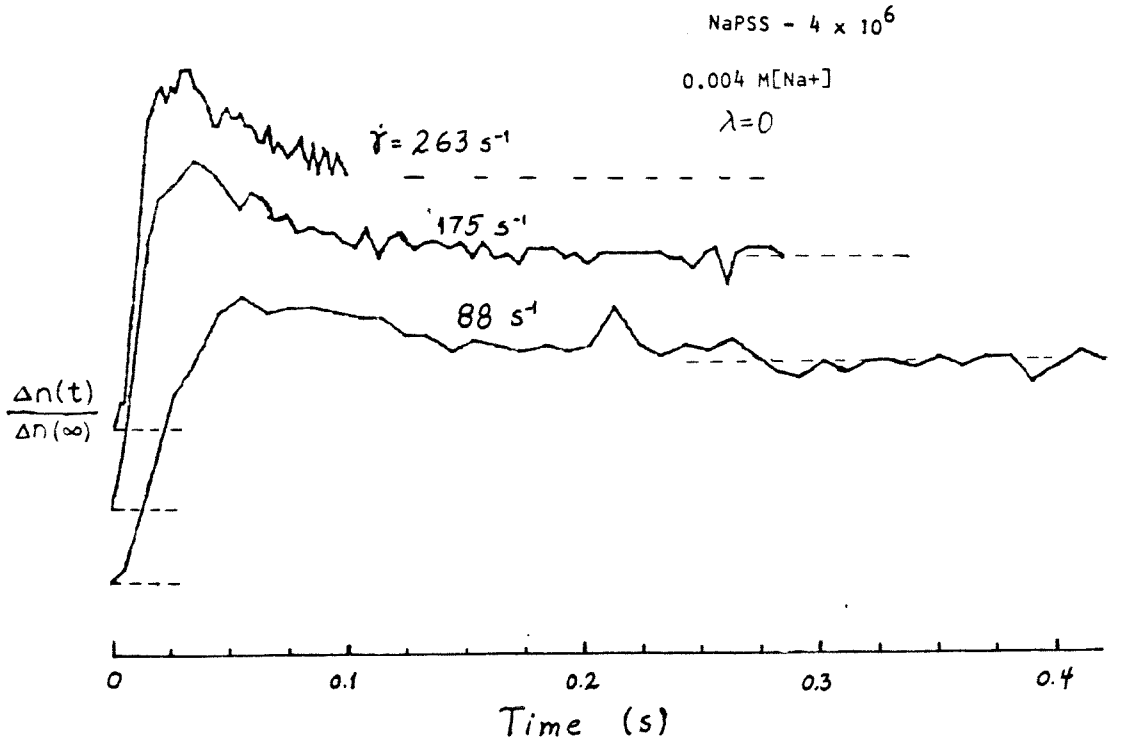
NaPSS - 4 x 10^6
0.004 M[Na+]
λ=0
γ̇ = 263 s⁻¹
175 s⁻¹
88 s⁻¹
Δn(t) / Δn(∞)
0
0.1
0.2
0.3
0.4
Time (s)

Figure 8.

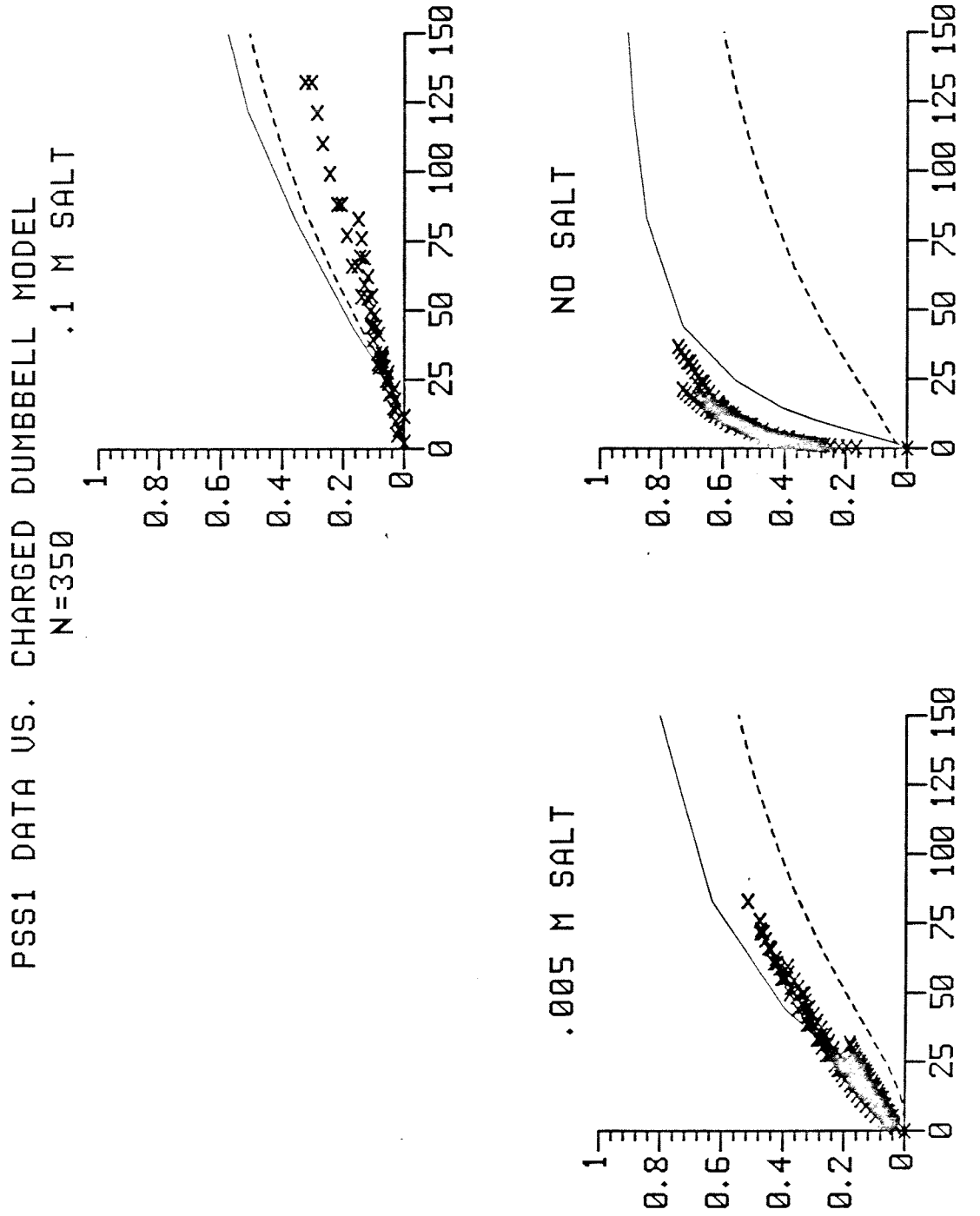
PSS1 DATA VS. CHARGED DUMBBELL MODEL
N=350
.1 M SALT
NO SALT
.005 M SALT
0
0.2
0.4
0.6
0.8
1
0
25
50
75
100
125
150

Figure 9.

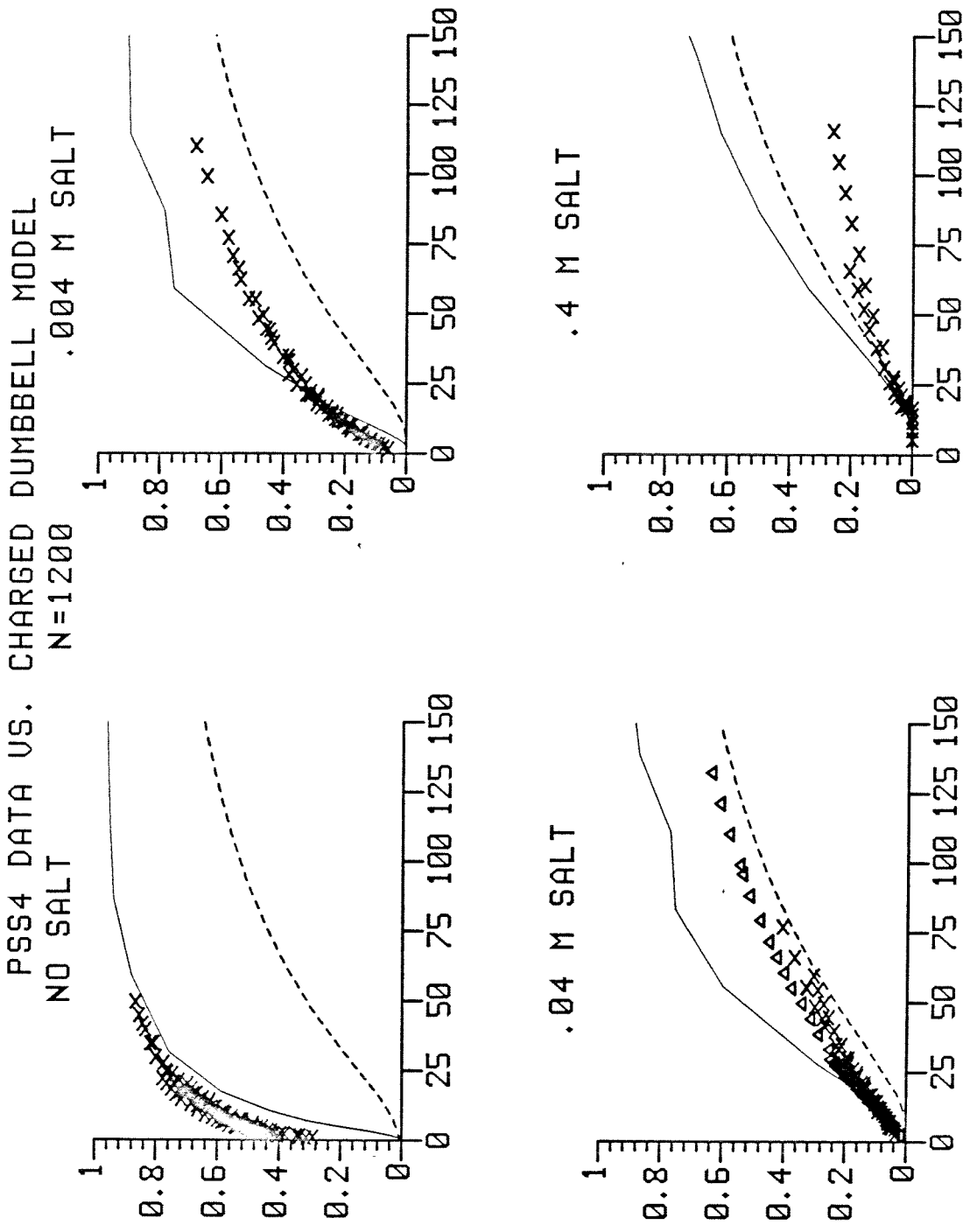
PSS4 DATA VS. CHARGED DUMBBELL MODEL
NO SALT
N=1200
.004 M SALT
.04 M SALT
.4 M SALT
0
0.2
0.4
0.6
0.8
1
0
25
50
75
100
125
150

Figure 10.

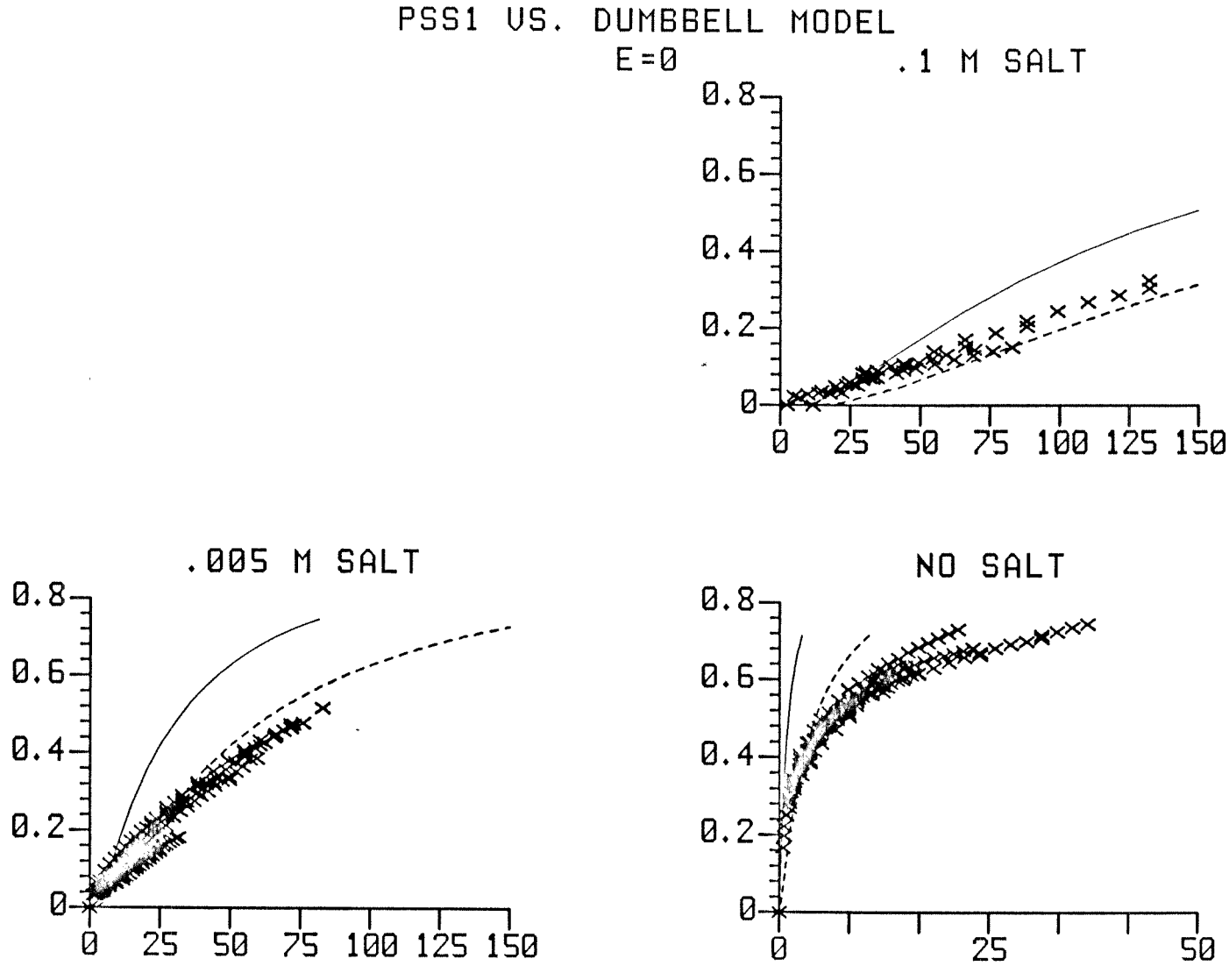
PSS1 VS. DUMBBELL MODEL
E=0
.1 M SALT
.005 M SALT
NO SALT
0.8
0.6
0.4
0.2
0
0 25 50 75 100 125 150
0 25 50

Figure 11.

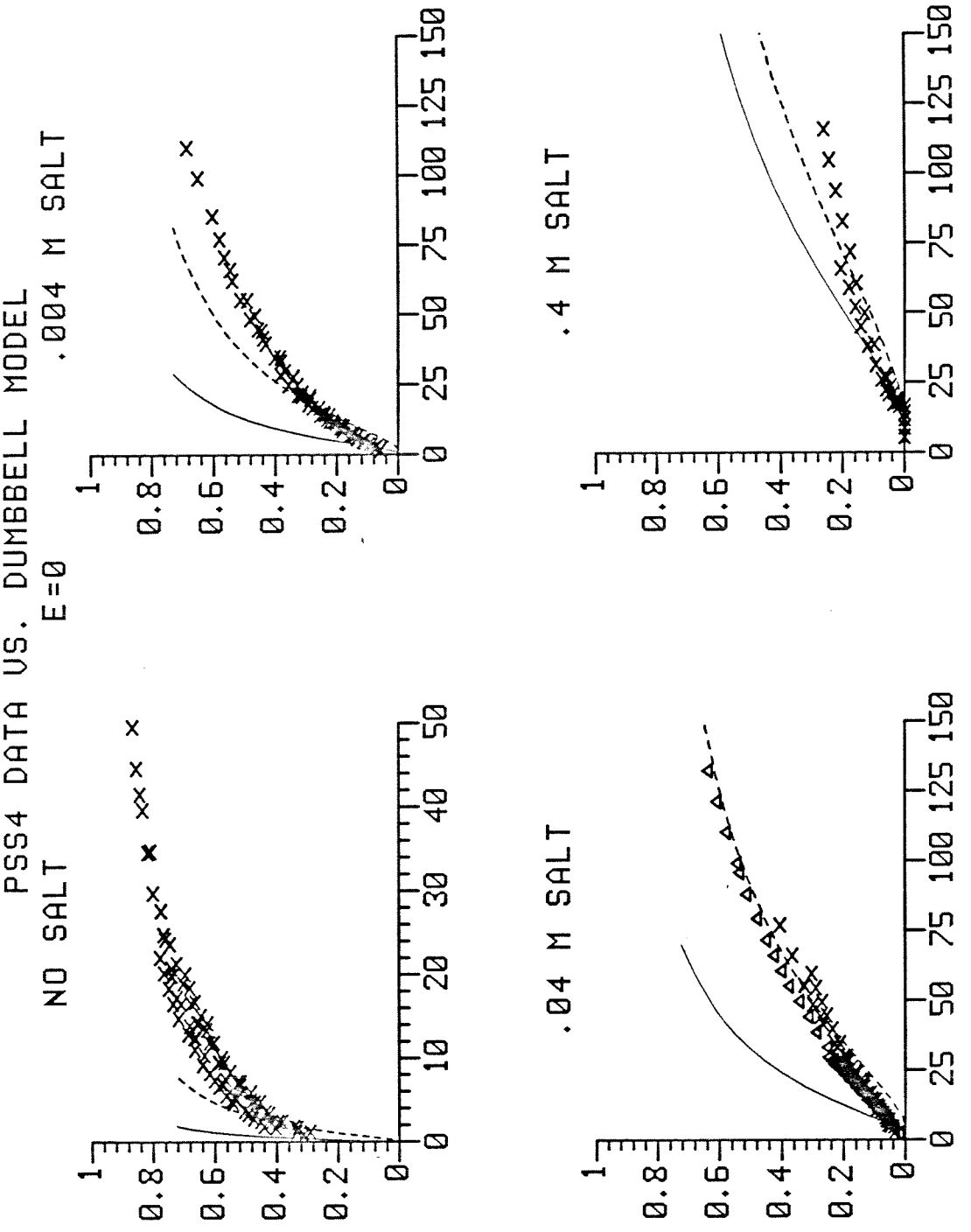
PSS4 DATA VS. DUMBBELL MODEL
NO SALT
E=0
.004 M SALT
.04 M SALT
.4 M SALT
0
0.2
0.4
0.6
0.8
1
0 10 20 30 40 50
0 25 50 75 100 125 150

Figure 12.

APPENDIX.

Quasi-Elastic Light Scattering of Polyelectrolyte Solutions

The equilibrium hydrodynamic radius for PSS1 in glycerol as a function of added salt concentration and polymer concentration was measured using quasi-elastic light-scattering spectroscopy.[1] These PSS1 measurements were performed by Binyao Li under the direction of C.-H. Wang at the University of Utah. A small amount of water was used to dissolve the PSS before adding it to the glycerol. The resulting glycerol solutions contained about 0.25% water. All solutions were filtered with Alpha Metrical membrane filters (pore size 0.45 μm) and then sealed in Pyrex tubes before being used in the light-scattering experiment.

The light-scattering apparatus consists of an argon-ion laser (Spectra-Physics 164) operated at 488 nm, and a Brookhaven Instrument BI2020 correlator to process the homodyne correlation function of the scattered light. The laser intensity was maintained at 300 mW. Before carrying out measurements on PSS solutions, the optical system was calibrated with polystyrene in cyclohexane solutions at different scattering angles, θ, to ensure that the q^2 dependence appropriate for a diffusion process was obtained. All experiments were carried out at 20°C.

The homodyne correlation function $G_2(t)$ obtained from the correlator is given by the functional form

$$G_2(t) = A(1 + B|g^{(1)}(t)|^2) \tag{1}$$

where A is the baseline, and B is related to the characteristics of the optical elements used in the experiment. The B value is treated as a fitting parameter. For all the correlation functions obtained, the measured baseline agrees with the calculated baseline to better than 0.06%.

The quantity $g^{(1)}(t)$ reflects the physical properties of the scattering medium. It is proportional to the time correlation function of the concentration fluctuation of the PSS in glycerol solution; *i.e.*, $g^{(1)}(t) \sim \langle \delta c(\mathbf{q},t)\delta c^*(\mathbf{q})\rangle$. For a monodisperse

polymer sample, this expression is given by

$$\langle \delta c(\mathbf{q},t)\delta c^*(\mathbf{q})\rangle = \langle |\delta c(\mathbf{q})|^2\rangle \exp\{-Dq^2t\} \tag{2}$$

where D is the mutual diffusion coefficient of the polymer and is related to the hydrodynamic radius, R_h, by the Stokes-Einstein equation

$$D = \frac{kT}{6\pi\eta_s R_h} \tag{3}$$

where η_s is the solvent viscosity and kT the Boltzmann temperature.

For polyelectrolytes in solution with no added salt, the charges located on the polymer chain are not screened out. The resulting expansion of the hydrodynamic radius causes polydispersity effects to be exaggerated and $g^{(1)}(t)$ is found to deviate from the single exponential shape of equation (3). Instead of equation (3), $g^{(1)}(t)$ should be described by

$$g^{(1)}(t) \sim \int f(R_h)\exp\{-D(R_h)q^2t\}\,4\pi R_h^2\,\mathrm{d}R_h \tag{4}$$

where $f(R_h)$ is the distribution function of hydrodynamic radii.

The deviation from the exponential behavior can conveniently be measured by fitting the cumulant expansion[1] to $g^{(1)}(t)$

$$g^{(1)}(t) \sim \exp\left\{-\overline{\Gamma}t + \tfrac{1}{2}\frac{\mu_2}{\overline{\Gamma}^2}t^2 + \cdots\right\} \tag{5}$$

where $\overline{\Gamma}$ is the first cumulant, μ_2 is the second cumulant, and $\mu_2/\overline{\Gamma}^2$ is a measure of the polydispersity. The results of a two-cumulant fit to the $g^{(1)}(t)$ for various samples are given in Table I. Note that both the mean relaxation time, $\langle\tau\rangle = \overline{\Gamma}^{-1}$, and the polydispersity factor, $\mu_2/\overline{\Gamma}^2$, decrease with increasing salt concentration. These results suggest that as the polymer chain decreases in size with increasing salt concentration, it also assumes a more uniform size.

TABLE I. Results of Two-Cumulant Fit to PSS1 Data.

Sample	c_p (ppm)	[Na^+]	$\overline{\Gamma}^{-1}$ (s)	$\mu_2/\overline{\Gamma}^2$	$\langle\frac{1}{R_h}\rangle^{-1}$ (Å)
1	50	0.00034	0.29±0.04	0.34	420±60
2	50	0.001	0.18±0.03	0.30	261±40
3	50	0.002	0.15±0.02	0.32	217±25
4	50	0.003	0.12±0.01	0.27	174±15
5	50	0.004	0.12±0.01	0.28	174±15
6	50	0.005	0.13±0.01	0.20	189±15
7	50	0.01	0.12±0.01	0.25	174±15
8	100	0.00068	0.29±0.03	0.37	419±50
9	200	0.00136	0.32±0.03	0.40	462±50
10	300	0.00204	0.18±0.02	0.27	260±30

The quantity $\overline{\Gamma}^{-1}$ is related to the mean hydrodynamic radius by

$$\begin{aligned}\langle\tau\rangle^{-1} = \overline{\Gamma} &= q^2 \int D(R_h)\, f(R_h)\, 4\pi R_h^2\, \mathrm{d}R_h \\ &= q^2\langle D\rangle = \frac{q^2 kt}{6\pi\eta_s}\left\langle\frac{1}{R_h}\right\rangle.\end{aligned} \tag{6}$$

Note that $\overline{\Gamma}$ is proportional to $\langle\frac{1}{R_h}\rangle$, so that the measure of the mean hydrodynamic radius obtained is the reciprocal of this quantity. The $\langle\frac{1}{R_h}\rangle^{-1}$ values measured for PSS at various salt and polymer concentrations are given in Table I. At the natural [Na^+] concentration (.00034 M for 50 ppm PSS^-) $\langle\frac{1}{R_h}\rangle^{-1}$ is 420±60 Å, and it decreases to 174±60 Å as the salt concentration is increased to a total [Na^+] of .003 M. The mean hydrodynamic radius remains constant at higher salt concentration, at least within experimental error. Increasing the concentration of PSS1 from 50 to 200 ppm does not change the mean size of the polymer chain, suggesting that the solution is truly dilute. As has been seen, the flow birefringence results suggest that the coil dimensions continue to decrease until the salt concentration is very

high $O(1\ \underline{\mathrm{M}})$. It would thus be desirable to extend these light-scattering studies to a much greater salt concentration.

The two-cumulant fit to the observed time correlation function is not satisfactory because of the poor quality of the fit. The fit is considerably improved if the empirical Williams-Watts (WW) function,[2] given by $\exp\{-(t/\tau_0)^\beta\}$, is used to approximate the data. The fitting parameters from the WW fits for the various solutions are given in Table II. In the WW equation, τ_0 is the natural relaxation time and β a measure of the deviation from the single exponential behaviour (which corresponds to β=1). The mean relaxation time is given by

$$\langle\tau\rangle = \int_0^\infty \mathrm{d}t\, \exp\{-(t/\tau_0)^\beta\} = \tau_0 \frac{\Gamma(1/\beta)}{\beta}$$

which, in terms of equation (6), gives

$$\begin{aligned}\langle\tau\rangle &= \frac{6\pi\eta_s}{q^2kT}\int f(R_h)\, R_h\, 4\pi R_h^2\, \mathrm{d}R_h \\ &= \frac{6\pi\eta_s}{q^2kT}\langle R_h\rangle.\end{aligned} \tag{7}$$

Note that, in contrast to the parameter $\overline{\Gamma}$ obtained from the cumulant fit, the $\langle\tau\rangle$ value obtained from the WW fit is directly proportional to $\langle R_h\rangle$, and thus probably better represents the actual size of the expanded polyelectrolytes.

A few light-scattering measurements were also made on some solutions of PSS4 in glycerol at Caltech. Only the two-cumulant analysis was carried out with the correlation functions from these solutions, and these results are given in Table III. Though these results are limited they show that the higher molecular weight sample behaves similarly to the lower one.

TABLE II. Results of Williams–Watts Fit to PSS1 Data.

Sample	c_p (ppm)	$[Na^+]$	τ_0 (s)	β	$\langle\tau\rangle$ (s)	$\langle R_h\rangle$ (Å)
1	50	0.00034	0.29±0.05	0.55	0.57±0.08	824±110
2	50	0.001	0.19±0.04	0.63	0.28±0.06	406± 80
3	50	0.002	0.14±0.02	0.51	0.22±0.03	319± 60
4	50	0.003	0.12±0.01	0.62	0.17±0.02	247± 30
5	50	0.004	0.12±0.01	0.71	0.15±0.02	217± 30
6	50	0.005	0.14±0.02	0.83	0.15±0.03	217± 40
7	50	0.01	0.13±0.02	0.71	0.16±0.03	232± 40
8	100	0.00068	0.24±0.05	0.43	0.64±0.09	925±130
9	200	0.00136	0.39±0.05	0.59	0.60±0.08	866±120
10	300	0.00204	0.14±0.02	0.49	0.29±0.03	619± 40

TABLE III. Results of Two-Cumulant Fit to PSS4 Data.

Sample	c_p (ppm)	$[Na^+]$	$\overline{\Gamma}^{-1}$ (s)	$\mu_2/\overline{\Gamma}^2$	$\langle\frac{1}{R_h}\rangle^{-1}$ (Å)
1	5	0.00003	0.83 ±0.10	0.99±0.13	1100±130
2	100	0.00061	1.23 ±0.14	0.68±0.13	1610±180
3	100	0.004	0.158±0.012	0.39±0.11	280± 20
4	100	0.04	0.40 ±0.06	0.38±0.04	430± 60
5	100	0.2	0.243±0.017	0.27±0.12	261± 18
6	100	1.0	0.318±0.032	0.41±0.08	250± 25

References

1. B. J. Berne and R. Pecora, *Dynamic Light Scattering*, John Wiley & Sons, New York, 1976.

2. J. A. Bucaro, H. D. Dordy, and R. D. Corsaro, *J. Appl. Phys.*, **46,** 74 (1975).